

Pyrolysis of asphaltenes in an atmospheric entrained flow reactor: A study on gasification reactivity and properties of chars

by
Nirlipt Mahapatra

A thesis submitted in partial fulfillment of the requirements for the degree of

**Master of Science
in
Chemical Engineering**

Department of Chemical and Materials Engineering
University of Alberta

©Nirlipt Mahapatra, 2014

Abstract

Solvent deasphalting, followed by asphaltenes gasification, has been recommended as a favorable alternative to coker based upgrading processes. However, very limited work has been carried out on pyrolysis and gasification of asphaltenes, at entrained flow conditions. The present work aims at addressing this gap. Chars were prepared in an atmospheric entrained flow reactor, at different process conditions. Several characterization techniques viz. SEM, EDX, XRD, FTIR, ICP-MS, TGA etc. were used to identify the changes in morphology, structure and properties of chars. Individual char particles were observed as having hollow structures, with porous walls. Effect of pyrolysis temperature, was observed to be much more prominent, than the effect of residence time (between 5-12s). Global gasification reactivity of different chars, was compared at a fixed temperature and concentration of CO₂ and steam. Chars obtained at higher temperatures exhibited lower H/C ratio, and had lower content of heteroatoms. Graphitization of chars was observed at higher temperatures. Consequently, chars obtained at higher operating temperatures, demonstrated lower gasification reactivity. Vanadium and nickel present in asphaltenes, accumulated in chars. Kinetic parameters for pyrolysis, and heterogeneous char steam/CO₂ reactions were estimated. Gasification reactions were observed, to be 5-6 orders of magnitude, slower than pyrolysis reactions. Temperature, velocity profile and residence time for particles in the DTF were also estimated by mathematical models (COMSOL Multiphysics®).

Preface

Some parts of this thesis, primarily from Chapters 3, 4, and 5 have been submitted to the journal Fuel as N. Mahapatra, V. Kurian, B. Wang, F. Martens and R. Gupta, “Pyrolysis of asphaltenes in an atmospheric entrained flow reactor: A study on char characterization” . The drop tube experiments were performed in the experimental setup designed by Dr. Farshid Vejahati, incorporating modifications for handling asphaltenes. Experiments in the drop tube furnace were conducted with collaboration of Vinoj Kurian, involving collection of soot. We also worked together for modification of the DTF setup, and a few common experimental characterizations. Sample preparation for SEM and SEM/EDX experiments were conducted by Gayle Hatchard. XRD/XRF experiments were performed by Shiraz Merali. CHNS and ICP-MS analysis of chars was performed in the Department of Chemistry, and the Department of Earth and Atmospheric Sciences by the respective laboratory technicians. I was responsible for conducting the experiments, data analysis; and manuscript composition and preparation.

To my parents and sister

Acknowledgements

I would like to extend my thanks and deep gratitude to my supervisor Dr. Rajender Gupta for his invaluable guidance, support and motivation throughout the course of my studies.

I gratefully thank Dr. Frans Martens for his valuable comments, throughout the course of my project. I would like to specially thank Vinoj Kurian for collaborating during the drop tube furnace experiments.

I greatly appreciate the help and assistance of Dr. Ben Wang, Seyyedali Hosseini and Dr. Moshfiqur Rahman during the course of my project.

I would also like to thank the members of my examining committee: Dr. Vinay Prasad and Dr. Leijun Li for reviewing my thesis.

Special thanks are extended to Gayle Hatchard and Shiraz Merali for their help and technical suggestions.

I gratefully acknowledge the financial support for this research from Nexen Energy ULC., Canadian Centre for Clean Coal/Carbon and Mineral Processing Technologies (C⁵MPT), Helmholtz Alberta Initiative (HAI) and Natural Sciences and Engineering Research Council of Canada (NSERC).

I would also like to appreciate the help of all the technicians and staff of the Department of Chemical and Materials Engineering, for their services during the course of my work.

Finally, I would like to thank my parents and sister for their tremendous support and encouragement, which allowed me to pursue my studies.

Contents

1	Introduction	1
1.1	Overview of Albertan oil sands and bitumen	1
1.2	Overview of gasification	3
1.2.1	Gasification Theory	4
1.2.2	Gasification Technologies	6
1.3	Motivation	7
1.4	Thesis outline	9
1.5	Objectives	10
2	Literature Review	11
2.1	Asphaltenes	11
2.1.1	Significance of asphaltenes	12
2.1.2	Composition and properties of asphaltenes	14
2.1.3	Structure of asphaltenes	16
2.2	Review of related work on gasification	20
2.2.1	Gasification of liquid feedstock	20
2.2.2	Gasification of oil sands coke	24
2.3	Literature review of work on char characterization	26
2.3.1	Similar work on char characterization	27
2.3.2	Significance of char crystallinity	28
2.3.3	Significance of active surface area	29
2.4	Brief review of work on gasification kinetics	32
2.5	Review of work on pyrolysis of asphaltenes	34

3	Experimental Section	38
3.1	Feed Preparation	38
3.2	Char Preparation	39
3.3	Characterization of asphaltenes and chars	42
3.4	Experiments for estimation of gasification reactivity and kinetics of chars	45
3.5	Experiments for estimation of pyrolysis kinetics of asphaltenes	47
4	Results and Discussions	48
4.1	Characterization of asphaltenes	48
4.2	Yield and composition of chars	50
4.2.1	Yield of chars	50
4.2.2	Proximate and ultimate analysis of chars	51
4.2.3	Thermal analysis of chars	54
4.2.4	Determination of functional groups in chars	54
4.2.5	X-ray diffraction pattern of chars	56
4.2.6	Mineral matter in chars	57
4.3	Morphological changes in chars	59
4.4	Reactivity of chars	61
4.5	Kinetics of asphaltenes pyrolysis	63
4.6	Estimation of char gasification kinetics	66
4.6.1	Char CO ₂ gasification kinetics	66
4.6.2	Char steam gasification kinetics	69
4.6.3	Comparison between pyrolysis and gasification kinetics	69
5	Conclusions and Recommendations for Future Research	71
5.1	Conclusions	71
5.2	Recommendations for Future Research	73
	References	75

Appendix	88
A-1 Mathematical modeling of the DTF	88
A-1.1 Steady state temperature and velocity profile of the DTF . .	88
A-1.2 Estimation of residence time of particles in the DTF	90
A-2 Calibration of the drop tube furnace	93
A-3 Additional Experiments	94
A-3.1 Preliminary study on the effect of feed size on char quality .	94
A-3.2 Test for repeatability	95
A-3.3 Preliminary studies on char surface area and particle size distribution	96

List of Tables

1.1	Properties of Athabasca bitumen vs. conventional crude oil	3
2.1	Gasification of liquid feedstock	20
3.1	Operating conditions at which char samples were collected	41
4.1	Proximate and ultimate analysis of asphaltenes	48
4.2	Ultimate analysis of asphaltenes chars prepared in the DTF at vary- ing operating conditions	53
4.3	Content of vanadium and nickel in asphaltenes and its chars	58
4.4	Values of $n \ln P + \ln A$ and $-E_a/R$ for different conversion levels of 1000°C Char CO ₂ interaction	68
4.5	Values of n and $\ln A - E_a/RT$ for different conversion levels for 1000°C Char CO ₂ interaction	68
4.6	Comparison between pyrolysis kinetics and gasification kinetics . . .	70
A-1	Test for repeatability	96
A-2	Pore diameter of char samples using low pressure mercury porosime- try	97

List of Figures

1.1	Integration of solvent deasphalting and gasification at OPTI Canada Inc. / Nexen Energy ULC. Long Lake integrated bitumen recovery and upgrading project	8
3.1	Asphaltenes feed (a) raw asphaltenes (b) crushed asphaltenes	39
3.2	(a) Feeder probe for feeding solid asphaltenes (b) Collection probe and cyclone	42
3.3	Schematic diagram of the entrained flow pyrolysis setup	43
3.4	Diffuser arrangement in TA Instruments SDT Q600 TGA	46
4.1	EDX mapping of asphaltenes	49
4.2	TGA and DTG curves for asphaltenes in inert atmosphere (heating rate 10 °C/min)	49
4.3	Yield of asphaltenes chars prepared in the DTF at varying operating conditions	51
4.4	H/C ratio (wt. /wt.) and S/C ratio (wt./wt.) of asphaltenes chars prepared in the DTF at varying operating conditions	52
4.5	Content of volatile matter in asphaltenes chars prepared in the DTF at varying operating conditions	52
4.6	DTG curves for asphaltenes chars in inert atmosphere (heating rate 50 °C/min)	54
4.7	FTIR spectra of asphaltenes and its chars	55
4.8	X-ray diffraction pattern of asphaltenes and its chars obtained at different operating temperatures	56

4.9	X-ray diffraction pattern of asphaltenes and its chars obtained at different residence times	57
4.10	EDX Mapping of 1200 °C Char (300X magnification)	58
4.11	SE SEM image of chars obtained at different operating temperatures (similar magnifications 500X)	59
4.12	SE SEM image of chars obtained at different residence times (similar magnifications 500X)	60
4.13	(a) cross section BSE SEM of 1200°C char (1000X) (b) SE SEM of soot on surface of char (25,000X)	61
4.14	TGA and DTG curves for global char gasification reactivity (a) Chars obtained at different operating temperatures with 20% steam (b) Chars obtained at different residence times with 20% steam (c) Chars obtained at different operating temperatures with 100% CO ₂ (d) Chars obtained at different residence times with 100% CO ₂	62
4.15	Mass loss curves for pulverized asphaltenes at different heating rates	65
4.16	ln k vs -1/RT for pyrolysis at different heating rates	65
4.17	Plot of ln(r) vs 1/T for 1000°C char 100% CO ₂ interaction at 40% conversion	67
4.18	Plot of ln(r) vs ln(P) for 1000°C char CO ₂ interaction at 950°C and 40% conversion	67
4.19	Plot of ln(r) vs 1/T for 1000°C char 20% steam interaction at 50% conversion	69
4.20	Plot of ln(r) vs ln(P) for 1000°C char steam interaction at 950°C and 50% conversion	70
A-1	Reynolds number for 7 SLPM flow of nitrogen and wall temperature of 1200°C in the DTF	88
A-2	Steady state velocity profile for 7 SLPM flow of nitrogen and wall temperature of 1200°C in the DTF	89
A-3	Steady state temperature profile for 7 SLPM flow of nitrogen and wall temperature of 1200°C in the DTF	90

A-4	Variation of residence time with particle size and density for 7 SLPM flow of nitrogen and 1200°C temperature in the DTF	92
A-5	Experimental setup for calibrating the DTF	93
A-6	Variation of temperature along the length of the DTF	94
A-7	Secondary electron SEM image of asphaltenes chars prepared with different feed sizes at 500X magnification a) <53 μm b) 53-106 μm c) 106-150 μm and d) 150-212 μm	95
A-8	Percentage of volatile matter in chars obtained from different feed sizes of asphaltenes	96
A-9	N ₂ adsorption isotherm for 1400°C char	97

Chapter 1

Introduction

1.1 Overview of Albertan oil sands and bitumen

The International Energy Outlook 2013 report by the U.S. Energy Information Administration predicts that the global energy consumption would increase from 553 EJ (1 EJ = 10^{18} J) in 2010 to 865 EJ in 2040. Liquid fuels, coal and natural gas would continue to supply more than 75 percent of the global energy consumption. Technological advancement and increase in crude oil prices could make production viable in complicated deposits viz. oil sands of Canada. [1] As of 2013, Canada has the third largest proven reserves of crude oil in the world and is the fifth largest crude oil producing country [2]. Oil sands are primarily obtained in Athabasca, Peace River and Cold Lake regions of northern Alberta and account for 56 percent of the total crude oil produced in Canada. Canadian Association of Petroleum Producers (CAPP) predicts that the production of crude oil from oil sands would register a threefold increase in volume and account for 77 percent of the total production by 2030. [3]

Oil sands were first reported in the year 1778 by Peter Pond, a fur trader of the Hudson Bay Company. He observed native Indians using bitumen, which had been washed out, for water proofing their canoes. However, commercial oil sands exploration technologies, are relatively recent and can be dated back to early 1950s. Nature and composition of bitumen derived from oil sands does not vary significantly with geographic location. Oil sands generally occur as black putty like mat-

ter at room temperature. The associated sand particles are fine grained ($<1000 \mu\text{m}$) and are primarily composed of quartz particles mixed with clay. Each sand particle is enveloped in water, with a bitumen film around it. [4] Several theories have been proposed for the origin of oil sands. It is now widely accepted that oil sands were formed from biodegradation and migration of conventional crude oil during the Cretaceous period [5, 6]. Depth of occurrence of oil sands deposits determines the method for extracting bitumen. *Open pit* or *surface mining* is used to recover bitumen from shallow deposits. *In situ* techniques including *cyclic steam stimulation (CSS)* and *steam assisted gravity drainage (SAGD)* are employed for deposits occurring at greater depths. It is estimated that 80 percent of the remaining deposits can only be extracted by in situ techniques [3].

Bitumen, derived from oil sands has lower API gravity, higher viscosity and higher content of sulfur, nitrogen, oxygen and heavy metals than conventional crude oil and needs to be upgraded before being used as feedstock in a conventional refinery, as well as, for facilitating better transportation [7–9]. Oil sands bitumen from Alberta is much more viscous than similar deposits of extra heavy oil from Orinoco belt of Venezuela and is completely immobile in the deposits. Properties of bitumen are more or less similar to extra heavy oil; however, it tends to be denser and more viscous. Typically extra heavy oil has an API gravity, less than 10. Natural bitumen has a viscosity higher than 10,000 cP. The boiling range of oil sands bitumen is comparable to that of atmospheric residue fraction. There are hardly any components in bitumen which boil below 350°C . Athabasca bitumen has a pour point between 50°C to 100°C which makes it solid at room temperature. The deposits of oil sands bitumen are presently considered as unconventional reserves. [8, 9]

Table 1.1 shows a comparison of the properties of Athabasca oil sands bitumen with conventional crude oil (adapted from the work of [9]). It can be clearly seen that bitumen has higher percentage of heteroatoms, mineral matter and degree of unsaturation than conventional crude oil. The government of the United States offers a more pertinent definition of bitumen. It is described as a highly viscous

Table 1.1: Properties of Athabasca bitumen vs. conventional crude oil

Property	Bitumen (°C)	Crude oil (s)
Specific Gravity	1.03	0.85-0.90
Viscosity (cP at 38°C)	750,000	<200
Viscosity (cP at 100°C)	11,300	<200
Pour Point (°C)	>10.0	-29.0
Carbon (wt. %)	83.0	86.0
Hydrogen (wt. %)	10.6	13.5
Nitrogen (wt. %)	0.5	0.2
Oxygen (wt. %)	0.9	<0.5
Sulfur (wt. %)	4.9	<2.0
Ash (wt. %)	0.8	0.0
Nickel (ppm)	250.0	<10.0
Vanadium (ppm)	100.0	<10.0
Pentane Asphaltenes (wt. %)	17.0	<10.0
CCR (wt. %)	14.0	<10.0
Resins (wt. %)	34.0	<20.0
Aromatics (wt. %)	34.0	>30.0
Saturates (wt. %)	15.0	>30.0

(adapted from [9])

hydrocarbon which cannot be recovered from its natural state by using conventional recovery techniques, as well as, currently employed enhanced recovery techniques. [9] Challenges of bitumen extraction and upgrading have been described extensively in literature and have not been touched upon in great detail in the present work.

1.2 Overview of gasification

Gasification can be historically described as any conversion of carbonaceous material to gaseous products with a usable heating value. It can be dated back to supply of town gas, during the 19th century. The process of gasification during those days typically involved pyrolysis and devolatilization of coal. During the early 20th century gasification started evolving and began to include water gas and partial oxidation processes generating carbon monoxide and hydrogen. [10]

Syngas, produced from gasification of coal, petroleum coke, biomass or heavy oil, is primarily used for production of ammonia and methanol. Hydrogen and carbon monoxide are also being separated from the syngas and are used as feedstock to various other industries. Fischer-Tropsch process has been used on a commercial scale, since the 1950s for production of synthetic fuels from coal gasification. Integrated gasification combined cycle (IGCC), which involves fuelling a combustion turbine, in a combined cycle power plant using syngas, from gasification of coal or other carbonaceous matter, is gaining greater attention due to its better efficiency and lower environmental impact. Researchers have also made an interesting observation that gasification could act as a bridge between present day conventional utilization of fossil fuels and a completely sustainable future. [10]

1.2.1 Gasification Theory

Gasification can be primarily divided into - *pyrolysis or devolatilization, gas phase reactions* and *char gas reactions*. Pyrolysis is the first step in any gasification process. Typically, it occurs at temperatures between 350 °C and 800 °C involving fast heating of fuel particles. The rate of heating has a significant effect on pyrolysis. Temperature, particle size and partial pressure of gasifying agent also affect the pyrolysis process. At low heating rates gasification reactions occur after pyrolysis is complete, since low temperatures do not favour partial oxidation reactions. However, at very high heating rates, as in an entrained flow gasifier, pyrolysis and gasification reactions can occur simultaneously. [10]

Gas phase reactions can be divided into cracking, reforming, combustion and CO shift reactions [10]. Pyrolysis of organic matter produces different types of volatile matter including tar, liquid and gaseous hydrocarbons, and gases like CH₄, CO₂, H₂, H₂O, H₂S etc. [11] In a gasifying environment, where oxidizing gases are present in limited quantities, the volatiles are not completely oxidized. Extensive kinetic data for oxidation of volatiles is not available; however, it is certain that rate of reaction is significantly higher than char gas reactions. [10]

Heterogeneous char gas interactions are the slowest and govern the overall rate of gasification. Gasification processes generally occur at very high temperatures between 800 °C and 1800 °C depending on the nature of feedstock. At such high temperatures, the reaction rates are very high and thermodynamic equilibrium models considering pure carbon and gaseous components can accurately predict the resulting components from gasification of any carbonaceous feedstock. These models are sufficiently accurate for entrained flow gasification systems above 850 °C. The major char gas reactions are as follows: [10]

- Combustion reactions
 - $C + 1/2O_2 \rightarrow CO$ ($\Delta H = -111 \text{ MJ/kmol}$)
 - $CO + 1/2O_2 \rightarrow CO_2$ ($\Delta H = -283 \text{ MJ/kmol}$)
 - $H_2 + 1/2O_2 \rightarrow H_2O$ ($\Delta H = -242 \text{ MJ/kmol}$)
- Boudouard reaction
 - $C + CO_2 \leftrightarrow 2CO$ ($\Delta H = +172 \text{ MJ/kmol}$)
- Water gas shift reaction
 - $H_2O + C \leftrightarrow H_2 + CO$ ($\Delta H = +131 \text{ MJ/kmol}$)
- Methanation reaction
 - $C + 2H_2 \leftrightarrow CH_4$ ($\Delta H = -75 \text{ MJ/kmol}$)

Boudouard, water gas shift and methanation reactions can be reduced into the following two reactions when conversion of carbon is complete: [10]

- CO shift reaction
 - $CO + H_2O \leftrightarrow CO_2 + H_2$ ($\Delta H = -41 \text{ MJ/kmol}$)
- Steam methane reforming reaction
 - $CH_4 + H_2O \leftrightarrow CO + 3H_2$ ($\Delta H = -75 \text{ MJ/kmol}$)

1.2.2 Gasification Technologies

There are three major types of gasifiers *moving bed, fluidized bed* and *entrained flow gasifiers*. Moving bed gasifiers (also known as fixed bed gasifiers) have a bed of solid fuel particles moving under gravity, which is gasified using a counter current flow of gasifying agent. The hot synthesis gas helps in preheating and pyrolysing the fuel particles. Consumption of oxygen is very low in this process; however, the resulting syngas contains significant quantities of moisture and volatile matter. Temperature of the syngas is generally low in such type of gasifiers. Acceptability of fine particles in feed is limited in both dry ash, as well as, slagging type of moving bed gasifiers. Acceptable size of feed particles ranges between 0.25 inches to 2 inches. [10]

Fluidized bed gasifiers offer a better mixing of feed particles and gasifying agent, which helps in better heat and mass transfer. The maximum operating temperature for these types of gasifiers is limited by the softening temperature of ash. As ash softens it could agglomerate and hinder proper fluidization of the fuel particles. However, operating at lower temperatures significantly reduces the extent of carbon conversion. This type of gasifier is more suited to handling feedstock like low rank coal and biomass, which are more reactive and need to be gasified at lower temperatures. Dry ash and agglomerating type of fluid bed gasifiers are currently in operation. Again, the acceptable size of feed particles ranges between 0.25 inches to 2 inches. Exit temperature of syngas is higher than a moving bed gasifier. [10]

Entrained flow gasification is the preferred choice in most industrial and commercial operations. These gasifiers operate in co-current flow (either up-flow or down-flow) of gasifying agent. Typically, feed particles of sizes $<200 \mu\text{m}$ are used as it aids in better mass and heat transfer. This ensures efficient conversion within a short residence time, typical to entrained flow gasifiers. All entrained flow gasifiers operate at temperatures higher than the slagging temperature. These types of gasifiers are better suited to handling different grades of fuel. However, using very low

grades of fuel could increase the consumption of oxidant significantly. Very high carbon conversion can also be achieved in these types of gasifiers. These gasifiers also have an added advantage of being able to handle slurry feeds. [10]

1.3 Motivation

The present day significance of bitumen and oil sands has been presented distinctly in the earlier section describing Albertan oil sands and bitumen. Albertan bitumen from different sources has about 15 wt. % of asphaltenes. Asphaltenes are the heaviest solubility class of bitumen, which account for half of the total micro-carbon residue (MCR) content in whole bitumen, as well as, most of the sulfur, heteroatoms and mineral matter [12–14]. Removal of asphaltenes can significantly reduce problems associated with transportation, production and refining of crude oil [15]. Asphaltenes, as well as, oil sands coke have large quantities of vanadium, nickel [United States Environmental Protection Agency (U.S. EPA) regulated elements] and sulfur which prevents their direct combustion. Integrated gasification combined cycle (IGCC) is the only recommended technology for such type of fuels. [16, 17]

As discussed earlier, the properties of bitumen necessitate upgrading. The upgrading processes can be divided into two major classes. The first type involves fractionation followed by coking of the residue. Upgraded synthetic crude oil is then transported by pipelines. Properties of heavy crude oil are modified according to the specifications of the pipeline company. The second type involves partial upgrading of the bitumen during in situ recovery process. Partial thermal upgrading and dilution with an aromatic solvent are the usual procedures. Visbreaking, hydrovisbreaking and similar thermal cracking procedures are generally used. Blending with low viscosity paraffinic hydrocarbons, in order to reduce the overall viscosity, promotes precipitation of asphaltenes. Recently, solvent based upgrading processes are gaining increased acceptance. [9]

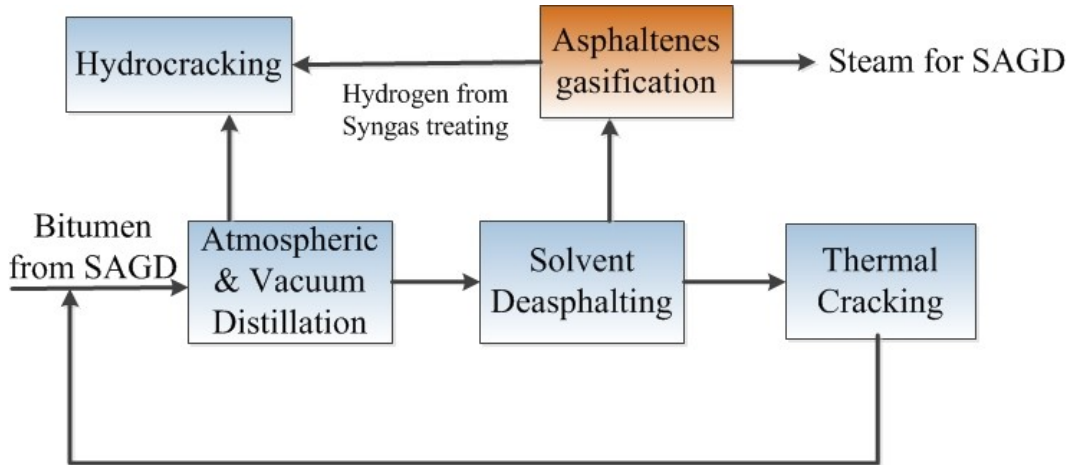


Figure 1.1: Integration of solvent deasphalting and gasification at OPTI Canada Inc. / Nexen Energy ULC. Long Lake integrated bitumen recovery and upgrading project

Integration of solvent deasphalting and gasification is a relatively recent approach (Fig. 1.1 adapted from Kerr et al. [18]). This process is currently in operation at the OPTI Canada Inc. / Nexen Energy ULC. Long Lake integrated bitumen recovery and upgrading project. Researchers have reported numerous advantages of this integrated approach. Firstly, asphaltenes are liquid at operating temperature; hence they are easier to handle than solid coke. Secondly, this process is more continuous than delayed coking based alternatives. Thirdly, the distillates and vacuum gas oil products are of higher quality as they are not produced from thermal cracking of asphaltenes. Finally, this process is more economical than coker based alternatives of similar scale. [18] Considering the numerous process advantages of this approach, it is essential to develop a better understanding of asphaltenes gasification process.

Considerable amount of literature on low heating rate pyrolysis and coking behaviour of asphaltenes exist [19–23]. However, very limited work has been reported on pyrolysis and gasification of asphaltenes at entrained flow gasification conditions. This study was undertaken to address these shortcomings and provide a better understanding of the gasification process by focussing on char - the primary intermediate in gasification.

1.4 Thesis outline

Organization of this thesis has been described in this section. In the first chapter, a brief overview of asphaltenes and bitumen has been presented. The significance of the current work has been outlined and the concept of gasification has been introduced. Objectives of the current work have been clearly outlined.

In the second chapter, work by various researchers, on related areas, have been presented. The relevance of asphaltenes has been discussed in sufficient detail, along with, extensive discussion on the structure and composition of asphaltenes. Better understanding of the pyrolysis process, necessitates thorough understanding of the structure of asphaltenes. Subsequently, work on gasification of liquid feedstock and oil sands coke has been discussed. Gasification of oil sands coke, which also happens to be a byproduct of bitumen processing, is more prevalent and could help in explaining certain aspects of asphaltenes gasification. Work on characterization of chars have been discussed in sufficient detail, touching upon the relevance of char crystallinity and active surface area. Thereafter, simple mathematical models for char gasification kinetics have been reported. Lastly, work on slow pyrolysis of asphaltenes has been presented. The behaviour of asphaltenes during slow pyrolysis is expected to shed light on the rapid pyrolysis in the drop tube furnace.

Experimental setup for preparation of chars, has been described in the third chapter. Preparation of asphaltenes feed has also been described. Subsequently, different experimental procedures for characterizing the chars have been described. Experiments for estimating the reactivity and kinetics have been described in detail.

The fourth chapter begins with the study on characterization of asphaltenes. This study is required in order to understand the properties of chars. Thereafter, extensive characterization of chars has been discussed. It is followed by a comparison of the reactivity of chars, prepared at different operating conditions. Subsequently, calculations on pyrolysis kinetics of asphaltenes, and gasification kinetics of chars

have been presented.

The last chapter compiles major findings of this work. Additional experimental, modeling and calibration data have been reported in the Appendix. Mathematical model for estimation of residence time of particles has also been presented. The mathematical model also describes the gas velocity and temperature distribution in the drop tube.

1.5 Objectives

Objective of the current work is to obtain a better understanding of the gasification process of asphaltenes, obtained from oil sands bitumen. Char, which happens to be a major intermediate in any gasification process, is prepared in an atmospheric entrained flow reactor or drop tube furnace (DTF) at different operating conditions. Behaviour of char plays a pivotal role in governing the overall gasification process. The following detailed investigations have been conducted:

- Morphological changes in chars obtained from the drop tube furnace (DTF) at different operating conditions
- Structural and compositional changes in chars obtained at different operating conditions
- Comparison of gasification reactivity of chars (with CO₂ and Steam) obtained at different operating conditions
- Effect of temperature and concentration on the gasification reactivity of chars and estimation of gasification kinetic parameters for char-CO₂ and char-steam interactions
- Estimation of kinetic parameters for pyrolysis of asphaltenes
- Mathematical modeling for particle flow in the DTF

Chapter 2

Literature Review

2.1 Asphaltenes

American Society for Testing and Materials defines asphaltenes as a petroleum-fraction that is soluble in specific aromatic solvents, but precipitates at higher dilutions with paraffinic hydrocarbons. Typically, the standard aromatic solvent is toluene and the paraffinic solvent for precipitation is heptane. [24] The standard ratio of feedstock to light hydrocarbon for precipitation of asphaltenes is 1:40 by volume [9,25]. Historically, asphaltenes were first reported by the French chemist, Boussingault [26] in 1837. [15,27] Solvent precipitation method for obtaining asphaltenes was introduced later, in the early 20th century, by the German chemist Marcusson [28]. He used petroleum naphtha to precipitate asphaltenes. [27] Initially naphtha/oil ratio of 10:1 was used to precipitate asphaltenes. During the period of World War II, it was identified that more precipitant would be required for complete precipitation of asphaltenes. 30-40 volumes of precipitant was suggested for 1 volume of oil. [27] Streiter [29] introduced n-pentane for precipitating petroleum asphaltenes in the year 1941, which remained as a standard precipitant till the 1980s. It was replaced by n-heptane which is being used as a standard precipitant till today. [27] Asphaltenes are black or dark brown in color and are usually solids at room temperature. Any non-polar solvent with a surface tension lower than 0.0025 N/m at 25 °C, viz. n-pentane, iso-pentane, n-heptane, liquefied petroleum gases, petroleum naphtha, petroleum ether etc., can be used to separate asphaltenes. Asphaltenes constituents are typically soluble in hydrocarbons with a

surface tension higher than 0.0025 N/m at 25 °C, like benzene, carbon disulfide, carbon tetrachloride and pyridine. [9] Describing asphaltenes completely in a single paragraph is very difficult, however, the following sub-sections would help in providing a better understanding of the concept of asphaltenes.

2.1.1 Significance of asphaltenes

Asphaltenes gained significance, primarily due to various issues associated with their presence. Heavier crude oil and bitumen have higher quantity of asphaltenes, which makes refining and upgrading operations more difficult. Researchers have effectively identified the problems faced during *downstream*, *upstream* and *mid-stream* processes due to the presence of asphaltenes. [15]

Upstream processes

Precipitation of asphaltenes during the upstream production of crude oil is an important issue in various parts of the world. The asphaltenes problem in Prinos Field, north Aegean sea; Hassi Messaoud field, Algeria; Ventura Avenue field, California and Lake Maracaibo, Venezuela have been studied extensively. Mechanical and chemical cleaning of the wells and surface equipment at frequent intervals was employed to prevent blockage. Asphaltenes deposition could also be minimized by varying the temperature and pressure of the produced fluids. Solvents were used in some cases to dissolve asphaltenes. Accurate mathematical model for coagulation and deposition of asphaltenes is not available and this hinders development of an effective solution. [30] Development of deposition models with good prediction accuracies has been restricted due to the complex nature of asphaltenes. In upstream operations, temperature and pressure at which asphaltenes precipitate holds more significance than the characteristics of precipitated asphaltenes. PC-SAFT model and modified OCCAM model are some of the recent models that have been proposed to predict the deposition of asphaltenes with certain degree of accuracy. [31, 32] Flory-Huggins equation, which is based on Gibbs mixing energy and

considers entropies, solubility parameters and volume fractions, is the basis of most of the deposition models. However, most models do not give very accurate results for different wells and more research needs to be conducted. [15]

Midstream processes

Deposition of asphaltenes during transportation, a mid-stream process, is gaining gradual significance. Very limited amount of work has been reported on this area. As temperature decreases the crude oil becomes more viscous. Precipitation tendency of asphaltenes tends to increase at lower temperatures. Heating of pipelines in-order to reduce precipitation is not economical. Again, with a decrease in the API gravity of crude oils, transportation is becoming increasingly difficult. With an increase in production of heavy oil in remote locations, the need for developing efficient transportation systems is gaining importance. Further research needs to be conducted in order to develop economically viable dispersants and drag reducing agents. [15]

Downstream processes

Asphaltenes have significant impact on downstream refining processes. The main culprit behind formation of deposits in refinery equipment are asphaltenes. Removing deposits from refinery equipment is a costly process. Asphaltenes also pose problems during thermal and catalytic hydro-processing of heavy feedstock. They tend to deposit on catalyst surface as coke precursors causing catalyst deactivation. Moreover, asphaltenes have significant quantities of mineral matter which could deactivate catalysts. Properties of asphaltenes are modified during hydro-treating process. At higher temperatures asphaltenes undergo thermal decomposition and asphaltene molecules with lower solubility are formed. Formation of more aliphatic maltenes at higher temperatures also helps in precipitation of more asphaltenes. [33] The major problems caused by asphaltenes during downstream refining process can be summarized primarily into poisoning of catalysts, deposition on process equip-

ment and delayed/fluidized bed coker which reduce refinery yield. [15]

2.1.2 Composition and properties of asphaltenes

The ultimate composition of asphaltenes obtained from different sources is more or less constant. However, variation in heteroatoms content is observed depending on the geological location, as well as, plant precursors. The H/C atomic ratio for asphaltenes is observed to vary over a small range ($1.15\% \pm 0.5\%$). This is quite interesting considering origin of asphaltenes from very different sources. Heteroatoms show a wider range of variation. Content of oxygen usually lies within 0.3% to 4.9%; sulfur between 0.3% and 10.3% and nitrogen between 0.6% and 3.3%. Oxygen content of asphaltenes can increase upon exposure to atmospheric oxygen. Content of sulfur also increases when asphaltenes come in direct contact with sulfur containing minerals. This can explain the observed greater variation in sulfur and oxygen content of asphaltenes. [9] Properties of asphaltenes also vary depending on the precipitant. The H/C ratio of n-heptane precipitated asphaltenes is lower than n-pentane precipitated asphaltenes, indicating greater aromaticity of the former. N/C, S/C and O/C tend to be higher for n-heptane precipitated asphaltenes. [34]

Asphaltenes can be fractionated using a mixture of polar and non-polar solvents in different ratios [9, 35]. The fact that asphaltenes can be fractionated reveals the highly complex nature of asphaltenes. In fact asphaltenes have been separated based on numerous properties other than solubility. These properties include polarity, temperature, pressure and molecular size to name a few. [9, 25, 36] About 23% sulfur, 1% nitrogen and 81% oxygen is lost during thermal treatment suggesting the presence of nitrogen and sulfur in aromatic form. [9] The elemental composition of asphaltenes has been discussed in greater detail in the later section describing structure of asphaltenes.

The major properties of asphaltenes can be divided into macroscopic and mi-

croscopic properties. Study of microscopic properties primarily deals with molecular weight and structural properties which have greater impact on downstream operations. Macroscopic properties generally concentrate on colloidal and thermodynamic properties of asphaltenes, which are primarily relevant to upstream operations. It is now known that molecular weight of asphaltene molecules is not a significant parameter for defining asphaltenes. Other parameters viz. presence of unpaired electrons, aliphatic chain lengths and polarity are needed to define the properties of asphaltenes. Asphaltene molecules usually self-associate to form asphaltenes colloids. [15]

Researchers have tried to predict the critical micelle concentration (CMC) of asphaltenes in various mixtures of solvents at certain temperatures. It has been reported that asphaltenes exhibit a very low value of CMC, indicating that asphaltenes exist as micelles even in dilute solutions. When asphaltenes are dissolved in a mixture of n-alkane and toluene, the CMC value shows a linear relation with the mixture Hildebrand solubility parameter. Addition of resins also tends to increase the CMC value. [37] However, unlike micelles the asphaltene aggregates do not grow in size with an increase in concentration. It could be due to the complex structure of asphaltene molecules, which might hinder proper packing. Conductivity and dielectric relaxation measurements suggest that asphaltene aggregates are formed primarily due to electron transfer. [38] Self association of asphaltene molecules has prevented effective determination of molecular weight. Accurate estimation of molecular weight would help in predicting the aggregation number, thermodynamics of self-association and also the empty volume fraction in an aggregate. Surface tension based methods are expected to provide a better result. [15] Flocculation and deposition models for asphaltenes are extensively researched and are beyond the scope of this work.

2.1.3 Structure of asphaltenes

This section is highly relevant to the present work. A better understanding of the structure of asphaltenes is required to identify and predict the behaviour of chars. The molecular structure of asphaltenes has been a subject of debate among researchers. Nellensteyn, in 1933 suggested that the nuclei of asphaltene micelles are composed of graphitic carbon [39]. Subsequently, in the year 1940, Pfeiffer and Saal suggested that asphaltenes could be primarily composed of highly aromatic hydrocarbons [40]. During the late 1950s, NMR and X-ray diffraction studies were used to predict the structure of asphaltenes. These studies concluded that asphaltenes are primarily composed of aromatic and aliphatic structures. Presence of naphthenic structures was not predicted. [41] During 1961, Yen and co-workers reported an investigation on the structure of petroleum asphaltenes using X-ray diffraction. The aromaticity values were predicted from areas of the X-ray bands after incorporating necessary corrections. They could reproduce the characteristic X-ray pattern of asphaltenes using a blend of carbon black (which consists of condensed aromatic sheets) and polyethylene. [42]

In 1967, Dickie and Yen reported a prediction of the structure of asphaltenes using different techniques, including X-ray diffraction, vapor pressure osmometry (VPO), ultracentrifugation, gel permeation chromatography (GPC) and mass spectrometry. Molecular weight of asphaltene molecules determined from VPO studies were approximately 2.5 times of the values determined using GPC. Interestingly, the predicted molecular weight of resins derived from the same sources was higher using GPC than VPO. They reported that three molecular weights are significant viz. unit sheet weight, stacked sheet weight (or particle weight) and molecular weight (association of two or more unit cells). In this model aromatic condensation was given significant importance. [43] Later, during 1977, Ignasiak and co-workers reported that Athabasca asphaltenes could be a polymer of sulfur. They predicted that alicyclic di-aromatic structures and alkyl substituents are held together by sulfide linkages. [44] A more recent and highly cited work by Strausz

and co-workers predicts the average weight of an asphaltene molecule as 6191 Daltons. They used ruthenium ion catalyzed oxidation (RICO), which is capable of selectively oxidizing aromatic carbon, while aliphatic carbon remains unaffected. Alkyl chains attached to the aromatic group are oxidized to carboxylic acids or dicarboxylic acids. NMR spectra of the products can reveal completion of the RICO reactions. The length of aliphatic hydrocarbon chains lies between C_1 and C_{27} , with a maxima at C_1 . C_3 bridged aliphatic chains are predominant. Maximum observed length of bridged hydrocarbons was C_{24} . Benzenepolycarboxylic acids were also reported in the products. Presence of these acids is a strong indicator of aromatic condensation. Functional groups were systematically identified from the yield data of different acids and CO_2 . Finally, the molecular structure of asphaltene was predicted as $C_{420}H_{496}N_6S_{14}O_4V$. [41]

More recently, Strausz and co-workers reported an improvement of the RICO procedure used to predict the structure of asphaltenes. They detected α -branched n-alkyl side chains with maximum length of C_{40} . Regular iso-prenoids (C_{15} - C_{20}), cheilanthanes (C_{20} - C_{28}), hopanes (C_{27} - C_{32}), steranes (C_{27} - C_{29}), pregnanes (C_{21} - C_{24}) and branched hydrocarbons producing hydroxy carboxylic acids were reported in the products. They also stated that these biomarkers attached to aromatic functional groups could have originated from secondary biotic sources. Friedel Crafts type of reactions could be responsible for incorporating these structures into asphaltenes. They strongly concluded that pericondensed aromatic rings had a minor role in the structure of asphaltenes. [45] A year later, Groenzin and Mullins reported that the molecular weight of asphaltene molecules from different sources varies between 500-1000 amu. Absorbance of the solutions was measured using UV-Visible-NIR spectrometer. Steady state fluorescence spectra of the samples were obtained using PTI fluorescence spectrometer. They concluded that asphaltene molecules are heterogeneous with a mean weight of 750 amu. Some molecules could possess heteroatoms, while a few molecules could have metals associated with them. They also reported that molecular weight of coal asphaltenes is lower than petroleum asphaltenes. [46]

Sheremata and co-workers used Monte Carlo method to represent the structure of Athabasca asphaltenes. Molecular weight of asphaltene molecule was determined by VPO using o-dichlorobenzene as the solvent. The temperature for this process was fixed at 130°C. NMR spectroscopy (using ^1H and ^{13}C) was used to identify the state of carbon. Naphthenic, aromatic and aliphatic structures could be effectively identified using both procedures. They assumed that all nitrogen and 60% of the total sulfur are associated with aromatic rings. Concentration of polyaromatic groups was optimized so that it could satisfy the NMR data. They reported that asphaltene molecules are composed of islands of aromatic clusters linked to each other by aliphatic chains and sulfur side linkages. They also expected the asphaltene structure to be flexible in solution. The predicted molecular weight of the asphaltene molecule was 4705 g/mol with a molecular formula $\text{C}_{318}\text{H}_{395}\text{N}_6\text{O}_6\text{S}_8\text{V}$. This model happens to be the first quantitative representation of archipelago model of asphaltenes. [47] Very recently, in the year 2010, Mullins proposed the modified Yen model for asphaltenes. The modified Yen model consists of three primary components viz. asphaltene molecules, asphaltene nano-aggregates and clusters of asphaltene nano-aggregates. He states that this model could settle different controversies regarding the structure and aggregation of asphaltenes. [48]

Sulfur in asphaltenes

Payzant and co-workers identified that sulfur occurs in two major forms in heavy petroleum fractions and bitumen - thiophenes (including benzothiophene, dibenzothiophene, substituted thiophene etc.) and aliphatic sulfides (including cyclic sulfides). [49] Waldo et al. reported from XANES (a form of X-ray absorption spectroscopy) analysis of asphaltenes that thiophenic form of sulfur is predominant. However, significant proportions of sulfidic sulfur also exist. They also stated that sulphoxide was the most predominant form of oxidized sulfur. [50] Later, Kasrai et al. also reported a similar finding. However, they reported the absence of any oxidized form of sulfur in bitumen. [51] Very recently, Siskin et al. have reported a sim-

ilar finding. They obtained the X-ray photoelectron spectroscopy (XPS) of finely ground asphaltenes from different sources. They reported that asphaltenes primarily contain aromatic sulfur (63-84%) and very less aliphatic sulfur (16-37%). [14] Researchers are generally in agreement regarding the form of sulfur present in asphaltenes.

Other heteroatoms in asphaltenes

Frakman et al. tried to identify the oxygen compounds occurring in Athabasca asphaltenes. Oxygen containing groups tend to be polar and can affect the behaviour of bitumen. Polar compounds are distributed unevenly in bitumen fractions. Asphaltenes have higher content of polar compounds than maltenes. They used chromatographic methods and mass spectrometry to identify the oxygen groups. Carbazoles, quinolones, porphyrins, different carboxylic acids, fluorenols, substituted fluorenones and multicyclic terpenoid sulfides and sulfoxides were identified in the maltenes fraction. Similar molecules were reported in the acetone extracted fraction of asphaltenes as that in resins. [52] Earlier, Ignasiak and co-workers had investigated the nature of oxygen compounds in asphaltenes. IR spectra of asphaltenes extracted with polar solvents revealed the presence of free OH, -NH and carbonyl groups. They also reported that oxygen is primarily present in the form of hydroxyl groups (about 75%). [53]

More recently, Siskin et al. also reported that asphaltenes contain very limited amount of elemental oxygen. Most of the oxygen occurs in the organic form. [14] Mitra-Kirtley et al. have tried to identify the different forms of nitrogen in asphaltenes using XANES. Most of the nitrogen occurs in aromatic form. Pyrrole and pyridine were reported as the most predominant structures in asphaltenes. Pyrrolic nitrogen was observed in higher quantities than pyridinic forms. Complex forms such as porphyrins and benzimidazole, which have both pyridinic and pyrrolic nitrogen groups could also be explained from XANES spectra. [54] By the year, 1969 it was also known that porphyrins contained about half of the transition met-

Table 2.1: Gasification of liquid feedstock

Number of reactors	124
Approximate feed rate (t/d)	42,000
Syngas production (MM Nm ³ /d)	124
Syngas for production of	
Ammonia (MM Nm ³ /d)	50.5
Methanol (MM Nm ³ /d)	15.3
Hydrogen (MM Nm ³ /d)	7.1
Power (MM Nm ³ /d)	34.3

(adapted from [10, 58])

als (primarily V and Ni) present in native crude oil or bitumen [55]. Researchers have also shown that trace metals - vanadium and nickel are present in porphyrinic and non-porphyrinic structures, which exhibit similar physical and chemical stabilities [56, 57].

2.2 Review of related work on gasification

2.2.1 Gasification of liquid feedstock

Higman et al. briefly describe different liquid feed gasification processes that are in operation. Syngas production from liquid feedstock was 124 million-Nm³/day from 124 reactors (SFA Pacific [58] data). Over 95% of liquid feedstock consists of refinery residues. [10] Table 2.1 (adapted from data of SFA Pacific [58] reported by Higman et al. [10]) shows the different applications of gasification of liquid feed stock. It can be clearly identified that power generation from syngas accounts for less than 30% of the total production.

It is known that gasification processes usually occur at very high temperatures and are non-catalytic in nature. This offers greater flexibility in handling different grades of liquid feed. However, some basic requirements need to be fulfilled. Firstly, the liquid feedstock should be free of any gaseous components. Presence of even small amounts of gaseous components can be detrimental to the gasifier. They could ignite near the burner causing damage. Secondly, the liquid feedstock should

be maintained within a viscosity range. Finally, ash content of the liquid feedstock needs to be estimated. This allows more efficient design of the syngas cooler, where deposition of ash is a major issue. [10]

Composition of the feedstock has a significant impact on product quality. C/H ratio of refinery residues can vary between 7 (kg/kg) for vacuum residue to 10 (kg/kg) for asphalts. Usually, feeds with higher C/H ratio produce syngas with higher content of carbon monoxide and lower content of hydrogen. This might be relevant to the industry where the syngas needs to be used. Sulfur content of petroleum residues used as a feedstock for gasification usually lies within 1% to 7%. Higher sulfur content does not have direct influence on gasification processes; however, it affects subsequent gas treatment operations. Lower sulfur content produces syngas with lower hydrogen sulfide/ carbon dioxide ratio and should be taken into account while designing the sulfur recovery unit. Moreover, sulfur is known to cause corrosion of the gasifier setup. However, corrosion is highly dependent on other parameters viz. temperature etc. and can be controlled by adjusting those parameters. Content of nitrogen in petroleum residues is usually lower than 0.6% and most of the nitrogen is organically associated with the oil. Higher content of nitrogen in feed usually results in increased concentration of HCN and ammonia in syngas. [10]

Minerals in petroleum residue affect the operation of gasifier. Higman et al. outlined the work of numerous authors on the effect of mineral matter in petroleum residue on the operation of gasifiers. Vanadium present in petroleum residues has undesirable side effects on the operation of gasifiers. Vanadium exists as vanadium pentoxide in an oxidizing atmosphere. V_2O_5 has a melting point of 690°C [59]. At operating temperatures, higher than 690°C , vanadium diffuses into the refractory linings and destroys the binder material. However, in reducing atmosphere vanadium exists as V_2O_3 which has a very high melting point of 1977°C and does not affect the refractory linings significantly. Vanadium is also known to cause fouling of economizer surfaces of conventional boilers. Moreover the problem increases

when soot from gasifier is mixed with carbon oil and is used to fire an auxiliary boiler. When the content of vanadium is as high as 700 mg/kg, frequent cleaning of the exposed surfaces is required. Additional problems have also been reported when the content of sodium is also high. In such cases sodium vanadate might be formed. It has a lower melting point and could deposit on the exposed surfaces of the gasification setup. [10]

Researchers have not assigned an upper limit for the content of nickel in liquid feedstock suitable for gasifiers. However, nickel has significant impact on subsequent gas treatment. Nickel carbonyls could be formed when nickel sulfides react with carbon monoxide under high pressure. Nickel sulfide can also react with water and air to form nickel sulfate. Sodium is usually present as sodium chloride or sodium hydroxide in petroleum feedstock. These salts usually deposit on heat exchanger surfaces raising the outlet temperature. Severe deposition could also cause a drop in pressure. Advisable limit for content of sodium in feedstock is 30 mg/kg. Fouling caused by sodium chloride can be reversed easily unlike other foulants. Usually, operating with sodium free feedstock reduces fouling and increases heat transfer. Sodium compounds have another major unpleasant effect on gasifiers. Most alkali metals including sodium are known to diffuse into the refractory lining of the reactor. They affect the crystal structure of alumina reducing its life. Usually, sodium is effectively removed in the efficient desalters and is not considered as a severe problem. 6-20 mg/kg of calcium is usually present in petroleum residues. Calcium could react with carbon dioxide to form carbonates. However, carbonates are not known to cause any significant problems. When significantly higher concentration of calcium is present they could be precipitated during quenching. Iron also behaves in a similar way as nickel forming carbonyls at a lower temperature. Content of silica typically varies between 20-50 mg/kg. They could cause problems like abrasion of liquid feed pump [60], affecting the flame pattern and SiO₂ - a reduced form of silica could be deposited on the refractory lining [61]. Chloride present in feedstock can cause fouling and corrosion. However, the extent of corrosion can be prevented by limiting the content of sodium chloride. [10]

Other parameters that are important during gasification of liquid feedstock are viscosity, pour point, flash point, ignition temperature and Conradson carbon content. Effective atomization of liquid feedstock at the burner depends on its viscosity. Steam heating is the preferred method required to achieve the desired viscosity. Failure during preheating could result in inefficient atomization which could lead to increase in soot production. Pour point is another important property that needs to be estimated. Temperatures lower than the pour point of liquid feed in the feed line could cause pumping issues. Density is another property that needs to be estimated. However, it does not impose any limitations on the design of gasifiers. Liquid feeds should not be preheated to temperatures greater than their flash point. Temperature of the feed before reaching the burner should ideally be less than the flash point. Ignition very close to the exit of the burner could damage the burner affecting the flame pattern and subsequent reactor failure. This problem is more prominent when feeds having different pour points are blended in order to reduce the viscosity of the heavier liquid. Preheating temperature needs to be carefully controlled in such cases. Estimation of the Conradson carbon content of the liquid feed along with knowledge of the C/H ratio could help in estimating the steam requirement. [10]

Ashizawa and co-workers have reported on the behaviour of extra-heavy oil in a research-scale gasifier. They considered OrimulsionTM as feedstock for their experiments. A pressurized (1.9 MPa) entrained flow gasifier with a fuel capacity of 2.4 t/d was used. The average residence time of particles in the gasifier was 12s. Composition of feed and products has been reported. With an increase in oxygen ratio they observed an increase in carbon conversion efficiency and reduction in cold gas efficiency and calorific value of product gas. Carbon conversion efficiency also increased with distance from the gasifier top. They observed that carbon conversion was strongly dominated by pyrolysis. Concentration of methane was observed to decrease near the gasifier outlet and the concentration of hydrogen increased. The concentration of product gases also approached values estimated from the water gas shift reaction (equilibrium based calculations). [62]

2.2.2 Gasification of oil sands coke

Gasification of oil sands coke is more popular than gasification of asphaltenes. Moreover, very limited work has been conducted on gasification of asphaltenes. Elemental and mineral composition of asphaltenes are not very different from oil sands coke. Therefore, understanding the gasification of oil sands coke could help us understand some aspects of asphaltenes gasification. In this section work of various researchers on gasification of oil sands coke has been discussed briefly.

In the year 1985, Furimsky estimated the reactivity of oil sands cokes using fixed and fluidized bed systems. As stated, this happens to be the first published work on gasification characteristics of coke derived from Athabasca bitumen. Operating temperature of the gasifiers was maintained between 830°C to 1010°C. The delayed coke sample had a carbon content of 83.7% (wt. /wt.); sulfur content of 5.7% (wt. /wt.) and hydrogen content of 3.7% (wt. /wt.). The fluid coke sample had a carbon content of 81.9% (wt. / wt.); sulfur content of 6.9% (wt. /wt.) and much lower H content of 1.6% (wt. /wt.). The coke samples had an ash content of 3.8% (wt. /wt.) and 7.1% (wt. /wt.) respectively. The ash was primarily composed of silica, alumina and iron oxide. He observed an increase in carbon conversion for both cokes with an increase in temperature. Although, the fluid coke had been subjected to greater heat treatment during the coking process, the observed bulk reactivity of fluid coke was higher than that of delayed coke. However, he observed that the reactivity per unit surface area of the delayed coke was higher than that of fluid coke. The observed overall carbon conversion varied between 37% and 55% for fluidized bed gasification and 30-50% after 60 minutes of experiment in fixed bed gasifier. He concludes by suggesting that reactivity of cokes was much lower than lignite coal and severe conditions would be required for better gasification. [63]

In the late 1980s, Watkinson et al. studied gasification of oil sands coke samples derived from different oil sands projects. The delayed coke sample had a carbon

content of 84.9% (wt. /wt.); sulfur content of 6% (wt. /wt.) and hydrogen content of 3.9% (wt. /wt.). The fluid coke sample had a carbon content of 79.5% (wt. / wt.); sulfur content of 7% (wt. /wt.) and much lower H content of 1.6% (wt. /wt.). Both the coke samples had very high heating values (order of 30 MJ/kg). They used a 0.3 m ID atmospheric pressure gasifier operated in either spouted or fluidized bed mode. The temperature of operation was around 950°C in both the modes. They observed 33-38 vol. % hydrogen and 22-28 vol. % CO with a feed rate of 20 kg/h of delayed coke to the spouted bed gasifier. Increase in carbon conversion was observed with an increase in temperature. However, they did not observe a very high conversion for the fluid coke gasified in the fluidized bed reactor with recycle of char. They suggest that for obtaining a conversion higher than 80%, temperature of the reactor should be more than 1000°C. Carbon conversion could also be increased by recycling the fines, as well as, using a potassium carbonate catalyst. They used dolomite beds to reduce the sulfur content of product gas. Finally, they also state that thermodynamic models could not provide an estimate of the equilibrium gas concentrations. However, the models were able to provide an approximate prediction of the gas heating values. [64]

In the year 1998, work on gasification of oil sands coke was effectively compiled by Furimsky. As the production of synthetic crude oil from oil sands increases, there would be an increase in the production of coke. Furimsky pointed out that the production of oil sands coke exceeded 6000 t/d during that period. All this coke could be utilized in an IGCC plant to produce 1000 MW of electricity. However, during that period most of the coke was either stockpiled (Syncrude) or combusted at site (Suncor). Syncrude coke had relevant particle size, high heating value and low ash content. The amount of electricity that could be produced from Syncrude coke would be sufficient for operating the plants and could also support nearby communities. However, low natural gas prices challenged commercial viability of the gasification process. Higher content of V and Ni also prevented combustion of the coke. IGCC technologies are highly preferred for feedstock containing high concentrations of sulfur [65]. A low reactivity of oil sands coke compared to coal

could also favour IGCC over other technologies viz. circulating fluidized bed combustion (CFBC) and pressurized fluidized bed combustion (PFBC). Moreover at temperatures below 1000°C, proper conversion cannot be achieved. Syncrude coke had an H/C ratio about 0.25, C content between 81-84%, sulfur about 6.5% and oxygen between 0.75-2.5% [66]. Suncor coke had about 84% C, 6% S and 1% O [67]. Moreover, the fluid ash fusion of coke samples was very high and entrained flow gasification could be the preferred technology. Finally he reviews the work of other researchers and concludes that the coke samples had a reactivity slightly higher than semi-anthracites and anthracites but lower than most grades of coal. He also suggests that entrained flow gasifiers are best suited for handling oil sands coke. [16]

Recently, in the year 2008, researchers tried to estimate the economics of bitumen coke gasification. They reported that bitumen coke gasification could produce hydrogen and electricity at prices comparable to natural gas and coal fed plants. The installation cost of a bitumen coke gasification plant could be higher, however, it might be compensated by the low cost of coke. [68] Very recently, in the year 2011, Karimi et al. reported on steam gasification kinetics of bitumen coke. They observed that potassium and sodium carbonates decreased the apparent activation energy of the gasification reactions. They used first order Langmuir-Hinshelwood type rate equations to describe the reactivity based on partial pressure of steam. The rate of initial gasification reactions varied linearly the predicted external surface area. It also increased with an increase in catalyst loading. They could also predict the rate at higher conversions using a shrinking core model. [69]

2.3 Literature review of work on char characterization

The importance of char has been described clearly in the earlier sections of this thesis. We already know that char gas reactions viz. Boudouard, water gas and hydrogenation reactions are the slowest step of any gasification process and hence govern

the overall rate of reaction [10]. This necessitates the study of char extensively. In the following section the characterization procedures used by various researchers has been presented. Most of the work on gasification has been conducted on coal and biomass. However, these chars are also primarily rich in carbon but have different proportions and types of mineral matter. The effect of reactor conditions on the properties of char has also been discussed. Models used for estimation of kinetic parameters have been discussed in a later section.

2.3.1 Similar work on char characterization

A highly cited work on characterization of biomass chars has been conducted by Cetin et al. They studied the effect of heating rate and pressure on the properties of biomass chars. Chars were prepared in various reactors including drop tube furnace (DTF), wire mesh reactor and tubular reactor. The wire mesh reactor could promote high heating rates of $500^{\circ}\text{C}/\text{s}$ and pressures up to 100 bar. The tubular reactor was used low heating rate experiments at atmospheric pressure. Very high heating rates of $10,000^{\circ}\text{C}/\text{s}$ at atmospheric pressure could be generated using the DTF. Size of feed particles was varied between $50\ \mu\text{m}$ and $200\ \mu\text{m}$. The chars were pyrolyzed in a flow of nitrogen. They measured the reactivity of char particles at different pressures using thermogravimetry. Change in structure of chars was investigated using SEM. X-ray diffraction technique was used to investigate changes in carbon structure. Total surface area of char particles was also estimated using nitrogen and carbon dioxide adsorption techniques. They observed that high heating rate chars consisted primarily of macropores. Increase in proportion of voids; decrease in the thickness of cell wall; and decrease in total surface area were observed with an increase in pressure. They also observed an increase in global gasification reactivity with an increase in heating rate. Increase in pyrolysis pressure was observed to decrease the reactivity of chars. [70]

In 2005, Cetin and co-workers analyzed the properties of radiata pine char. Chars were prepared at different pressures, temperatures and heating rates. They

reported that pyrolysis conditions had a significant impact on the morphology of chars. They observed formation of smooth surfaces and bigger cavities with an increase in pyrolysis pressure. The global gasification reactivities measured using TGA were observed to increase with a decrease in operating pressure and increase in heating rate. They suggested that increase in char reactivity at higher heating rates could be due to an increase in the total surface area. However, they observed a decreased micropore network at greater heating rates. [71] We can conclude from both the above works that high heating rates and low pressure generally ensure better reactivity.

2.3.2 Significance of char crystallinity

Lu and co-workers used a DTF to prepare different chars. An atmosphere of 99% nitrogen was ensured during pyrolysis. 1% oxygen was used for combustion of volatiles released during pyrolysis. They suggest that this could ensure non contamination of char particles with volatiles/soot. They also prepared chars at low heating rates in order to compare it with DTF chars. DTF chars were prepared at 1173 K, 1473 K and 1773 K. They used very low residence times of less than 1s. The low heating rate char was prepared at 1473 K for 30 minutes. Reactivity of chars was measured in a fixed bed reactor. Nitrogen and oxygen gas mixtures was used for estimation of reactivity. The chars were structurally characterized using quantitative X-ray diffraction (QXRD) and high resolution TEM (HRTEM). They observed that char structures become more ordered with a decrease in heating rate and an increase in pyrolysis temperature. They also suggest that amorphous carbon is more reactive than crystalline carbon during combustion. A decrease in reactivity of the chars was observed with an increase in ordering. [72]

Lu et al. in 2000, reported on the characteristics of pulverized coal chars obtained in a DTF at different temperatures. They prepared char samples at 900°C, 1200°C and 1500°C. The residence time for the experiments was about 1s. All the experiments were conducted at atmospheric pressure and slightly oxidizing atmo-

sphere (1% oxygen). The chars were removed of mineral matter chemically and X-ray diffraction was used to study the structure of chars. Other techniques used for char characterization were field emission SEM (FESEM) and focused ion beam miller (FIB). They observed that chars obtained at higher temperatures are more condensed and ordered. They could also observe a variation in char structure depending on the type of coal used. [73]

Zhang and co-workers studied the effect of pyrolysis conditions on the properties of coal char. They used a horizontal tube furnace with a flow of 99.99% nitrogen and variable temperature to prepare the chars. The reactivity of the chars was measured in a TGA using air as the reactive gas. The reactivity of chars was measured at lower temperatures. They observed a decrease in reactivity with an increase in intensity of pyrolysis. They could not observe a very good correlation between the surface area and char reactivity. More reactive chars were observed to more sensitive to pyrolysis conditions. They concluded that the decrease in reactivity of chars could be due to an increase in turbostratic carbon at severe pyrolysis conditions. [74] From the work of researchers reported in these paragraphs we can observe that the reactivity decreases due to increase in crystallinity at higher temperatures.

2.3.3 Significance of active surface area

In the year 1963, Laine discussed the significance of active surface area in reactions between carbon and oxygen. Total surface area was estimated using nitrogen BET and the active surface area was estimated from the oxygen complex formed when the samples were exposed to oxygen for 24 hours at 300°C. He observed that rate constants estimated from measurement of active surface area were fairly constant. However, rate constants calculated from BET surface area varied significantly with conversion. [75]

A highly cited work on the significance of carbon active sites during gasifica-

tion has been reported by Radovi and co-workers. They used lignite coal which had been removed of inorganic constituents using HCl and HF. Slow pyrolysis was carried out in a horizontal tube furnace at temperatures between 975 K and 1475 K in nitrogen atmosphere with residence times about one hour. Fast pyrolysis experiments were conducted at 1275K in an entrained flow furnace with residence times between 0.3 s and 5 min. Reactivity with air was studied using a TGA. Oxygen chemisorption capacity and carbon dioxide physical adsorption capacity of the chars was estimated. They observed a decrease in the active surface area (ASA) with heat treatment. This could be estimated from the reduction in oxygen chemisorption capacity, as well as, an increase in ordering. Total surface area (TSA) values were estimated by assuming that micro-pore volume of chars are approximately equal to the BET monolayer capacity. However, they observed that TSA was unable to provide an accurate estimation of reactivity. They observed that oxygen chemisorption capacity was a good indicator of the number of carbon active sites. They finally concluded that active sites are lost with an increase in severity of pyrolysis. [76]

An extensive work on char gasification and influence of surface area has also been reported by Lizzio and co-workers. The chars were prepared from different coals at low heating rates in nitrogen atmosphere at a temperature of 900C. Reactivity of the char samples was measured in a differential flow fixed bed reactor. The char samples were preheated to 900°C before being gasified with carbon dioxide. Reactive surface area (RSA) of the char samples was estimated after a specific conversion level. They observed that RSA normalized gasification rates remained constant through the entire range of conversion. They suggested that active surface area of chars are not always proportional to the reactive surface area and hence might not be used for prediction of reactivity. [77] Work of researchers described above suggest that TSA is not a suitable parameter for estimating the reactivity. However, Adschiri and co-workers suggested a relationship between the estimated BET surface area and carbon dioxide reactivity of coal chars. They measured the surface area of chars at different conversion levels and observed that the rate of con-

version per unit surface area estimated using BET remained more or less constant at conversion levels higher than 40%. [78]

The importance of active surface area of chars has also been identified by Khan. He studied the reactivity of chars prepared under mild pyrolysis conditions using TGA. He suggests that intrinsic reactivity of chars is governed by char active surface area and the catalytic properties of impurities. He further categorizes the char gas interactions into different steps. Initially the gas diffuses to the reaction sites. This is followed by chemisorption of the gas into the reaction site which is followed by reaction and subsequent desorption of the products. Finally the product gases are transported from the surface of carbon to atmosphere. He also suggests that the active sites could be imperfections in the carbon crystalline structure. He observed that the amount and rate of oxygen chemisorption are influenced by the sorption temperature. This could suggest that sites with different sorption energies are utilized. He suggests that BET surface area estimated with carbon dioxide and nitrogen are not good for prediction of intrinsic reactivity. He observed a great variation in intrinsic rate constant estimated using BET area. However, the variation in estimated reactivity was significantly lower using measured active surface area (ASA). Finally, he concludes that measured ASA could provide a good approximation of the actual ASA. He also noted that pressure, temperature and parallel gasification could influence the actual ASA. [79]

Guerrero and co-workers characterized chars obtained from pyrolysis of eucalyptus and estimated their reactivity. Pyrolysis of eucalyptus was carried out at different heating rates and temperatures. Surface area and pore volume of the char particles were estimated by carbon dioxide adsorption. They also estimated the reactivity of the chars. Morphology of the chars was investigated using SEM. They observed that chars prepared at higher heating rates had a higher reactivity. The higher reactivity could be attributed to greater surface area, and higher content of oxygen and hydrogen giving rise to more active sites. [80]

It can be observed clearly from work of researchers compiled in this paragraph that active surface area estimated using chemisorption provides a better estimation of the char gas reactivity.

2.4 Brief review of work on gasification kinetics

Estimation of gasification kinetics is a highly researched area. Very complex models involving active surface area and taking into consideration the effect of adsorption and desorption have been proposed by researchers. In this section simple mathematical models that are used for estimation of gasification kinetics are presented.

A recent work by Ollero et al. on the CO₂ gasification kinetics of olive residue considers two kinetic models viz. nth order model and Langmuir-Hinshelwood model. The olive char samples were gasified in a TGA at elevated temperatures. They itemized the overall reaction into the following steps:

- $C_f + CO_2 \xrightarrow{k_1} C(O) + CO$
- $C(O) + CO \xrightarrow{k_2} C_f + CO_2$
- $C(O) \xrightarrow{k_3} CO + C_f$

Where C(O) represents a carbon-oxygen complex and C_f represents an active site. The Langmuir-Hinshelwood kinetic expression was expressed as Eqn.2.1, where C_T represents the total number of active sites in char at any instant. When CO concentrations are neglected the equations are reduced to an nth order form (Eqn.2.2).

$$r = \frac{k_1 C_T P_{CO_2}}{1 + (k_2/k_3) P_{CO} + (k_1/k_3) P_{CO_2}} \quad (2.1)$$

$$r = k C_T P_{CO_2}^n \quad (2.2)$$

$$r_{percent\ conv.} = k P_{CO_2}^n \quad (2.3)$$

They reported that reactivity depended on percent conversion, along with the reaction temperature and gas concentration and correlated the total number of active sites to the degree of conversion. Eqn.2.2 could be reduced to Eqn.2.3 for a particular conversion level. [81] Lee et al., studied the gasification kinetics of coal pyrolyzed in a fluidized bed reactor. They estimated combustion and steam gasification kinetics of coal chars using a shrinking core model. The kinetic parameters were obtained using Eqn.2.4, where, $X = (w-w_{ash})/(w_0- w_{ash})$. [82]

$$\frac{dX}{dt} = ke^{-E/RT} P^n (1 - X)^{2/3} \quad (2.4)$$

Hurt et al. have effectively classified char oxygen combustion reactivity models into four basic classes. The first type is the Global power law model where rate of reaction can be expressed in a simple form ($r = kP^n_{oxygen}$). The second type is the Langmuir-Hinshelwood (LH) type of kinetic expression. Limitations of these two models have been described elaborately. The nth order model is only applicable over narrow ranges of temperature/pressure. The LH expression is widely employed by researchers, however, it is not able to explain variations over wide ranges. Moreover, it does not take order of reaction into account. The other two types are the three step semi global and the enhanced three step semi global which consider the reaction of oxygen complex. [83]

Various char conversion models for solid fuels have been summarized in the PhD dissertation by Tremel. The observed reactivity (r_{obs}) [g/g.s] can be related to the intrinsic reactivity (r_i)[g/m²s] for certain conditions using Eqn.2.5, where s is the available or specific surface area of char, depending on the operating conditions.

$$r_{obs} = sr_i \quad (2.5)$$

The nth order rate model is discussed. He suggested that nth order rate model does not take into account the decrease in impact of partial pressure at higher operating pressures. Moreover, the model does not consider the effect of adsorption of products on the rate of reaction. The LH model and the Langmuir-Hinshelwood-

Hougen-Watson (LHHW) model which take adsorption and desorption into account are discussed in detail. The form of LH model has been described earlier. The LHHW model for CO₂ adsorption on carbon active site, followed by formation of carbon oxygen complex and subsequent desorption of CO from the char surface was described using Eqn.2.6, where $k_{CO_2} = k_{desorption} \times K_{CO_2}$. K_{CO_2} is the rate constant for formation of surface complex and $k_{desorption}$ is the rate constant for desorption of CO from the surface complex. In this model the number of active sites required for adsorption of one gas molecule is considered to be 1.

$$r_{C,CO_2} = \frac{k_{CO_2} P_{CO_2}}{1 + K_{CO_2} P_{CO_2} + \sum K_j P_j} \quad (2.6)$$

Subsequently, the work of various researchers relating conversion with reaction rate has been discussed. Models considering mass transfer limitations at various operating conditions, pore diffusion, molecular diffusion, Knudsen diffusion and thermal deactivation have been compiled, which are beyond the scope of this work. [84] Another highly cited work by Laurendeau, on heterogeneous kinetics of coal char gasification and combustion effectively compiles various available surface models and particle reaction models [85].

2.5 Review of work on pyrolysis of asphaltenes

Researchers have primarily studied the thermal decomposition of asphaltenes at low heating rates. The behaviour of asphaltenes during low heating rate pyrolysis could be helpful in better understanding of the fast pyrolysis process in the entrained flow reactor. In this section the works of different researchers on pyrolysis behaviour of asphaltenes has been discussed.

In the year 1978, Moschopedis and co-workers reported on the thermal decomposition of Athabasca asphaltenes. They pyrolyzed the asphaltenes sample at temperatures between 200°C and 600°C in a conventional tube furnace with a flow of dry nitrogen. A heating rate of 5°C/min was used and the sample was maintained at the pyrolysis temperature for one and half hours. Composition of gaseous products

was estimated simultaneously. They observed a wide variety of products ranging from very light hydrocarbons to benzene insoluble high molecular weight hydrocarbons. They also reported a remarkable difference in product nature and composition beyond 350°C. They observed evolution of methane, carbon monoxide, carbon dioxide and ethane at temperatures lower than 300°C. Higher paraffin hydrocarbons and hydrogen sulfide were produced at higher temperatures suggesting severe degradation. They suggested that at temperatures lower than 350°C peripheral groups could be eliminated, while, at higher temperatures asphaltene molecule would be severely degraded. [86]

A year later, Rubinstein and co-workers reported their findings relating thermal decomposition of asphaltenes with their geochemical nature of origin. Pyrolysis was carried out in sealed glass vials at temperatures around 300°C for 72 hours under vacuum. Subsequently, the products were cooled at -60°C and extracted with n-pentane and benzene after being pulverized. This was followed by gravimetric analysis of the products. They observed that pyrolysis of asphaltenes produces significant quantities of products bearing properties similar to that of crude oil. They also reported that biodegradation does not have a significant impact on the nature of pyrolysed products. [87]

Later, Behar and co-workers published their work on characterization of asphaltenes from different sources using chromatography and pyrolysis. Pyrolysis experiments were conducted in a horizontal micro furnace with 1 μ g 1 mg of n-heptane precipitated asphaltenes samples. A flow of inert carrier gas (Ar or He) was maintained. Temperatures of 450°C and 550°C were maintained during pyrolysis. The products were analyzed using different chromatographic techniques. They observed higher percentage of n-alkenes in the products obtained at 550°C. However, the fraction of longer n-alkenes was less suggesting secondary cracking at higher temperatures. They also observed that the yield of pyrolysed products decreases with a decrease in H/C ratio of the asphaltenes and a zero product yield was predicted for H/C ratio less than 0.5. Asphaltenes with lower sulfur content (<

2%) were observed to produce more saturated hydrocarbons on pyrolysis than sulfur rich asphaltenes. They could also conclude that asphaltenes were formed from less severe thermal degradation of kerogen compared to other fractions of crude oil. [88]

Savage and co-workers pyrolysed asphaltenes between 350°C and 565°C for times varying between 5 min and 150 min in batch tubing bomb reactors. The products were subsequently analyzed by gas chromatography (GC) or a combination of GC and mass spectrometry (GC/MS). The yield of pyrolysis products was significantly less at 350°C and primarily comprised of light gases (H_2S , CO_2 , CH_4 , C_2H_6 , C_3H_8 , $n\text{-C}_4\text{H}_{10}$), maltenes and unreacted asphaltenes. No coke was formed at this temperature. At 400°C, formation of coke was observed along with products obtained at 350°C. H_2S and light hydrocarbons were the major products up to 450°C along with coke. They could conclude from near constant yields of carbon dioxide and hydrogen sulfide at lower temperatures that sulfur and oxygen atoms could be attached as peripheral functional groups to the condensed aromatic ring. They also observed n-alkanes in near constant yields at lower temperatures suggesting their presence in equal proportions attached to the condensed structure. Larger hydrocarbons obtained at higher temperatures were observed to be unsaturated. Finally, they could classify the pyrolysis process into two steps consisting of primary reactions involving formation of coke, maltenes and gas; and secondary reactions involving degradation of maltenes and reactions between asphaltene core and produced gases. [89]

In 1997, Calemma and Rausa reported on the thermal decomposition behaviour of asphaltenes using TGA and Py/GC/MS. They observed that activation energies and reaction orders increased with an increase in aromatic carbon content of asphaltenes. They could classify the pyrolysis process into three steps viz. initial scission of aliphatic side chains attached to aromatic rings; scission of aliphatic bridges between aromatic or naphthenic units; and aromatization of existing structures. [90]

Later in 2003, Gray tried to explain pyrolysis and coking behavior of asphaltenes through their molecular structures. He pointed out that thermal cracking of asphaltenes generated a wide variety of products with different boiling points, molecular weights and functional groups. He also stated that the yield of solid residue during pyrolysis could suggest the quantity of aromatic carbon in asphaltenes. Finally, he concluded that asphaltene molecule could consist of different aromatic groups connected by bridges and attached to various aliphatic groups. He suggested that this model could explain pyrolysis behaviour of asphaltenes more precisely. [23]

Chapter 3

Experimental Section

3.1 Feed Preparation

Asphaltenes samples were obtained from the deasphalting unit of Nexen Energy ULC. Long Lake upgrader project based near Fort McMurray in northern Alberta. Bitumen is extracted using steam assisted gravity drainage (SAGD) and the rejected carbon stream from bitumen is used to generate steam for the SAGD process [18]. Naphtha was used in this facility for precipitation of asphaltenes. Asphaltenes samples were received in barrels from Nexen Energy ULC. Asphaltenes were dark brown to black solids at room temperature with a smooth and shiny texture. Solid feeding of asphaltenes to the drop tube furnace (DTF) was chosen in order to avoid inherent problems associated with liquid feeding viz. in-efficient lab scale atomization and coke formation at localized hotspots preventing consistent feeding.

Initially, some difficulty was encountered during the preparation of specific cut sizes of pulverized asphaltenes. Dry grinding and slurry grinding of asphaltenes was carried out in Retsch Planetary Ball Mill PM 100. The slurry grinding process involved using asphaltenes and deionized water (ratio of 2:3) and grinding at speeds of 450 rpm for 10 minutes. The prepared slurry was then vacuum dried (approx. 6 psia pressure) at 65°C for a day. This was followed by vacuum drying at 70°C for another 24 hours. However, after such elongated periods of vacuum drying, the feed was not completely dry and required further drying. Subsequently, the feed was manually ground and sieved to different cut sizes. However, the observed pro-

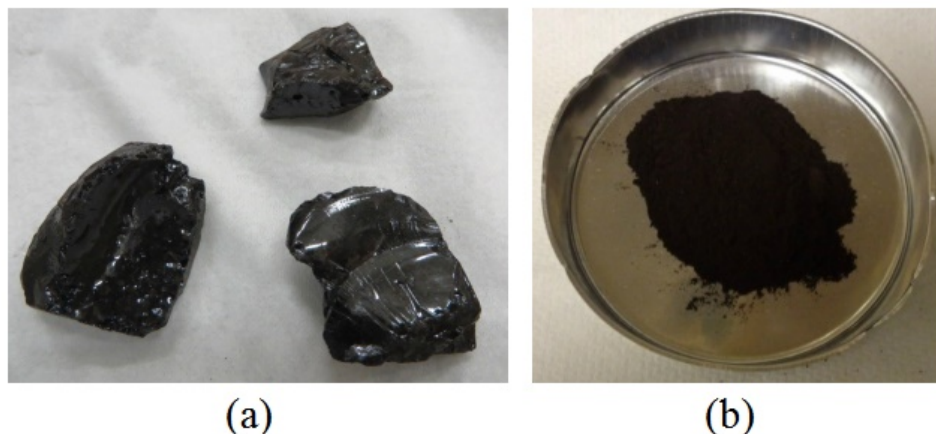


Figure 3.1: Asphaltenes feed (a) raw asphaltenes (b) crushed asphaltenes

portion of feed particles, with cut sizes less than $150\ \mu\text{m}$ was considerably less. This process was discarded since it proved to be uneconomical and ineffective. After much trial and error, intermittent dry grinding at low rpm for shorter duration proved to be the most convenient method for grinding asphaltenes. Pulverized asphaltenes were sieved to various cut sizes. Cut size between $150\text{-}212\ \mu\text{m}$ was primarily considered for most of the experiments. Repeatability studies were conducted with different particle sizes viz. $<53\ \mu\text{m}$, $53\text{-}106\ \mu\text{m}$ and $106\text{-}150\ \mu\text{m}$. The images of raw asphaltenes and pulverized asphaltenes are shown in Fig. 3.1.

3.2 Char Preparation

Pyrolysis experiments were carried out in an atmospheric entrained flow drop tube furnace. The drop tube furnace (DTF) consists of a Mullite tube (65 mm inner diameter and 153 cm height) which is electrically heated with molybdenum disilicide (Moly-D 33) heating elements. Three PID temperature controllers (Omron E5CK) located at the middle, bottom and top of the DTF control temperature along the length of the tube. They can be controlled using LabView interface on the associated computer. The DTF was calibrated periodically using a quarter inch calibrated type K thermocouple (additional details in Appendix). Gas flow rates (nitrogen 99.998% and air) were controlled using high precision mass flow controllers (Aal-

borg instruments). Pressure in the furnace was maintained slightly above 1 atm using vacuum pumps. The feeding system consists of a *screw feeder* (Schenck AccuRate volumetric feeder) and a *feeder probe*.

The feeder probe (Fig. 3.2(a)) was custom designed for feeding solid pulverized asphaltenes and it consists of an annular tube with cooling water, from a refrigerated circulator, passed through the annulus. A single whole 3/8 inch tube was used as the inner tube, in order to avoid any accumulation of asphaltenes, which could result due to introduction of heterogeneity because of fittings etc. Lower portion of the feeder probe, closer to the furnace, was cooled externally with air. This arrangement restricted melting and sticking of asphaltenes to the inner walls of the feeding tube. The feeder probe was cleaned with tetrahydrofuran (THF) (99.97%) and acetone after each experiment, in order to remove any asphaltenes and chars, sticking to the inner walls of the tube. The header, of the feeder probe has ports for measuring absolute pressure and for feeding nitrogen. Nitrogen flows through the annular part and helps in entrainment of the asphaltenes particles. During the experiment, a constant flow of nitrogen was maintained in the screw feeder, in order to support effective feeding.

Nominal residence time was calculated, considering complete entrainment and ideal gas law. More accurate estimation of residence time, has been obtained using mathematical models (using COMSOL Multiphysics®), discussed in Appendix). The feeding system was volumetrically calibrated before each experiment; however the real amount of feed to the DTF, was estimated by weighing the feeder before and after each experiment. Similar feed rates were maintained for each experiment. Amount of asphaltenes fed into the system was restricted due to overloading of soot in the cascade impactor (Dekati impactor Filter Stage). Pyrolysed products were partly collected in an air-cooled collection probe (Fig. 3.2(b)). The cooled stream, further passed through a cyclone (Dekati Cyclone) where char particles larger than 10 μm were separated from flue gas and soot. Chars collected from the collection probe and cyclone showed similar characteristics. Total weight of char collected in

Table 3.1: Operating conditions at which char samples were collected

Sample Name	Nominal Temperature of DTF (°C)	Nominal Residence Time (s)
800 °C Char	800	8.4
1000 °C Char	1000	8.4
1200 °C Char	1200	8.4
1400 °C Char	1400	8.4
11.8 s Char	1200	11.8
8.4 s Char	1200	8.4
6.5 s Char	1200	6.5
4.9 s Char	1200	4.9

the collection probe, as well as, cyclone was considered for estimating the yield of chars. The char samples were weighed using Mettler Toledo XS 105 balance and were stored in air-tight containers to prevent oxidation.

The flue gas carrying soot particles, passed through the cascade impactor, where soot particles were collected. An alternative arrangement consisting of a bag filter was also used to strip the flue gas of particulate matter. The experimental setup is shown schematically in Fig. 3.3. Experiments on coal and oil sand coke have been successfully conducted earlier on the same setup with slight modifications [17,91]. Pyrolysis experiments were conducted at different nominal temperatures of the DTF viz. 800°C, 1000°C, 1200°C, 1400°C. The drop tube furnace was heated slowly (max. 100°C/h) and maintained at the desired temperature for sufficient time before any experiment. A continuous flow of air was maintained during the heating process. Subsequently, flow of air to the DTF was substituted, with a flow of nitrogen, in order to purge the system. Nominal residence time of the particles was varied by varying the flow rate of nitrogen. The flow rate of nitrogen was typically varied between 5 SLPM and 12 SLPM. Table 3.1 shows the operating conditions at which chars were collected. The sample names indicated in this table have been used throughout this work.

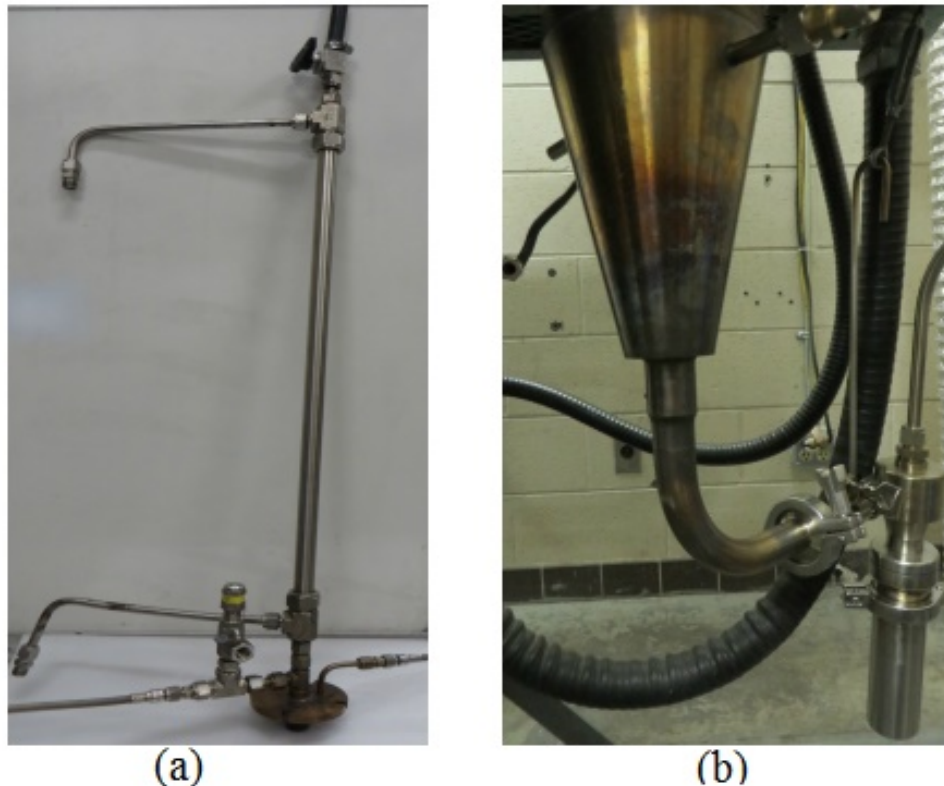


Figure 3.2: (a) Feeder probe for feeding solid asphaltenes (b) Collection probe and cyclone

3.3 Characterization of asphaltenes and chars

Properties of asphaltenes and its chars were studied using extensive characterization techniques. The experimental procedures followed have been discussed briefly in the following paragraphs.

Proximate analysis of asphaltenes was carried out in accordance with ASTM D7582 for coke [92]. About 1 g of asphaltenes (150-212 μm cut size) was weighed and transferred into one of the crucibles previously placed in the carousel of LECO 701 Thermogravimetric Analyzer. The LECO 701 TGA has a balance resolution of 0.0001 g. It can achieve temperatures up to 1000°C. Moreover, it can handle up to 19 samples at once and is much more convenient for proximate analysis than conventional techniques involving muffle furnace and analytical balance. It had been

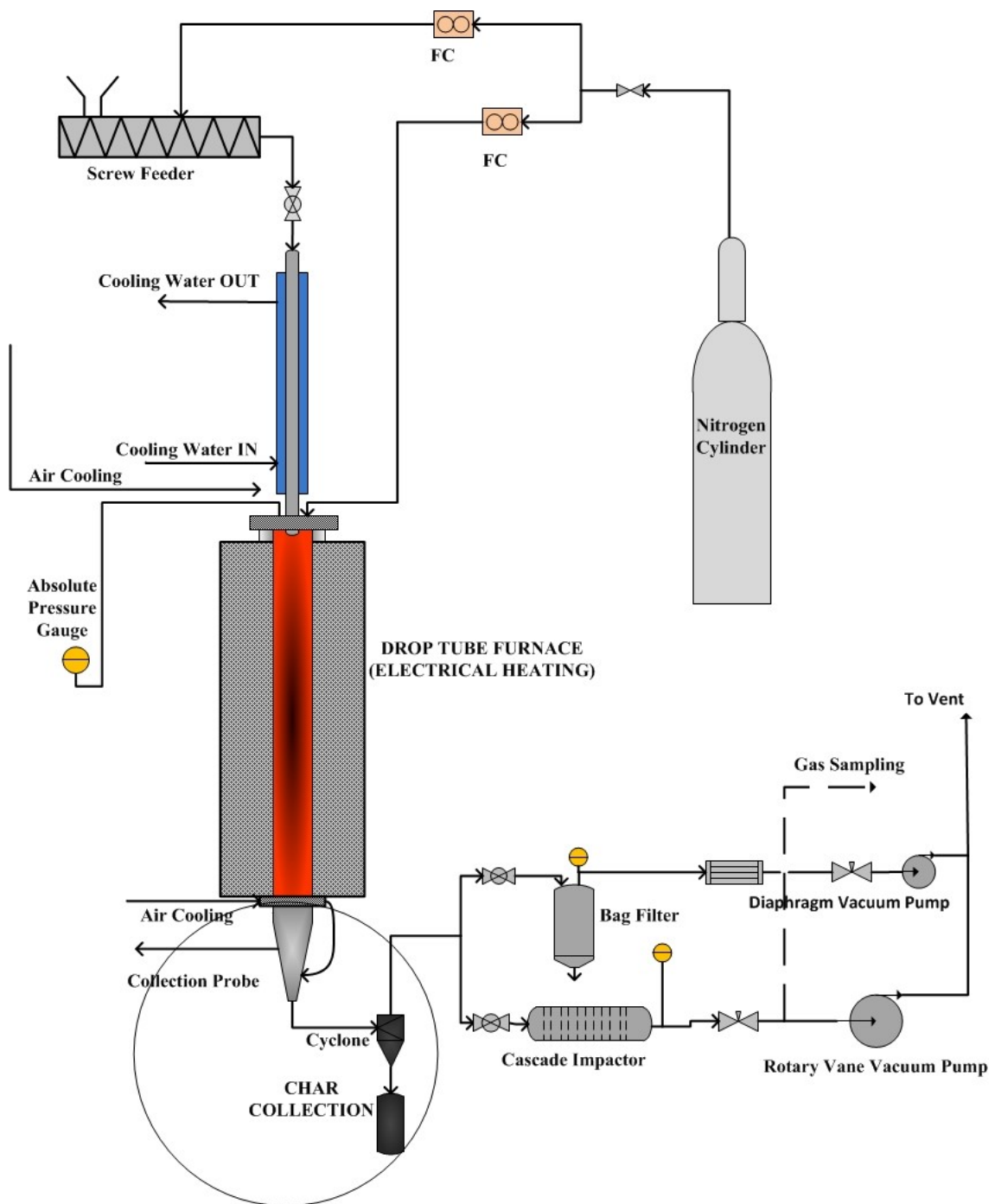


Figure 3.3: Schematic diagram of the entrained flow pyrolysis setup

pre-programmed with the standard procedure described in ASTM D7582 for coke. Moisture, volatile and ash content were estimated simultaneously for three different samples of asphaltenes and the average value has been reported. Ultimate analysis of asphaltenes and its chars was conducted in Carlo Erba EA 1108 Elemental Analyzer with about 1 mg of sample.

Experimental run time in the DTF was reduced in order to avoid overloading of soot in the cascade impactor. This prevented collection of large quantities of chars. Hence, micro thermogravimetric analysis of chars was conducted for estimation of fixed carbon and volatile matter. TA Instruments SDT Q600 was used for this purpose. SDT Q600 features a horizontal balance and furnace with a balance resolution of 0.1 μg . Nitrogen (99.999%) and air cylinders from Praxair were connected to the primary ports of the TGA. Pyrolysis of the chars was conducted at different heating rates (between 2°C/min and 50°C/min) in a flow of nitrogen (100 ml/min). Alumina crucibles were used in all the experiments.

Surface morphology of asphaltenes chars was studied using Hitachi S-2700 Scanning Electron Microscopy (SEM) equipped with PGT (Princeton Gamma-Tech) IMIX digital imaging system and PGT PRISM IG (Intrinsic Germanium) detector for energy dispersive X-ray analysis (EDX). The SEM is also equipped with a GW Electronics System 47 four quadrant solid state Backscattered Electron Detector. Char samples were placed on carbon conductive tapes fixed to SEM specimen stubs. Steps were taken to ensure uniform distribution of chars on the tapes. Subsequently the samples were coated with carbon. In some cases carbon coating was avoided, but it affected the quality of the images. Extensive SEM/ EDX analysis was used to identify the morphology, as well as, content of mineral matter in chars. In order to study the cross section of chars, polished pellets of chars embedded in epoxy were prepared. Char samples were uniformly dispersed in West System 105 epoxy resin and West System 205 fast hardener mixed in constant proportions. Hardened pellets were initially polished, using BuehlerMet 2 abrasive paper of increasingly finer grades, in a polisher. The semi-polished pellets were further polished using alumina

polishing suspension. Subsequently, the polished pellets were analyzed using SEM.

Infrared spectrum of chars and powdered asphaltenes was recorded using ABB MB 3000 FTIR Spectrometer (detector gain 81, ZnSe beam splitter material). The IR transmittance spectra were obtained with a 4 cm^{-1} resolution between 400 and 4000 cm^{-1} and blank calibration was performed before each run, in order to ensure accuracy. Steps were also taken to ensure similar quantities of sample during each run. X-ray diffraction of powdered asphaltenes and chars was carried out in Rigaku Ultima IV X-ray Diffractometer (focussing beam, Cu tube, 40 kV , $2\theta = 10\text{-}110^\circ$, $2^\circ/\text{min}$. scan speed). X-ray fluorescence analysis of asphaltenes and chars was conducted in Ametek EDAX Orbis PC Energy Dispersive Instrument (Rh tube, 40 kV , $750\ \mu\text{A}$). Inductively Coupled Plasma Mass Spectrometry (ICP-MS) was conducted in a Thermo Scientific iCAP Q ICP-MS. 50 mg of sample was digested in 3 ml of Nitric Acid in a microwave digester. After digestion the contents were transferred into a 100 ml standard flask and diluted with nano-pure water. The final solution was filtered and 49.5 ml of $1\%\text{HNO}_3$ was mixed with 0.5 ml of the sample, which was analyzed.

3.4 Experiments for estimation of gasification reactivity and kinetics of chars

Global gasification reactivity of char samples was estimated using TA Instruments SDT Q600 Simultaneous TGA/DSC with $3\text{-}5\text{ mg}$ of char samples. The char samples were initially dried at $110\text{ }^\circ\text{C}$ for 5 minutes in nitrogen (99.999% purity) flow. Subsequently, they were heated to the gasification temperature, (heating rate of $50\text{ }^\circ\text{C}/\text{min}$) which was maintained for 15 minutes . Alumina crucibles were used in all the experiments. Reactive gases were introduced through the reactive gas port which could be opened and closed using a solenoid valve. The solenoid valve can be controlled using the program defined for the TGA. Flow of CO_2 (99.999% purity) was controlled externally using a calibrated mass flow controller. It was mixed

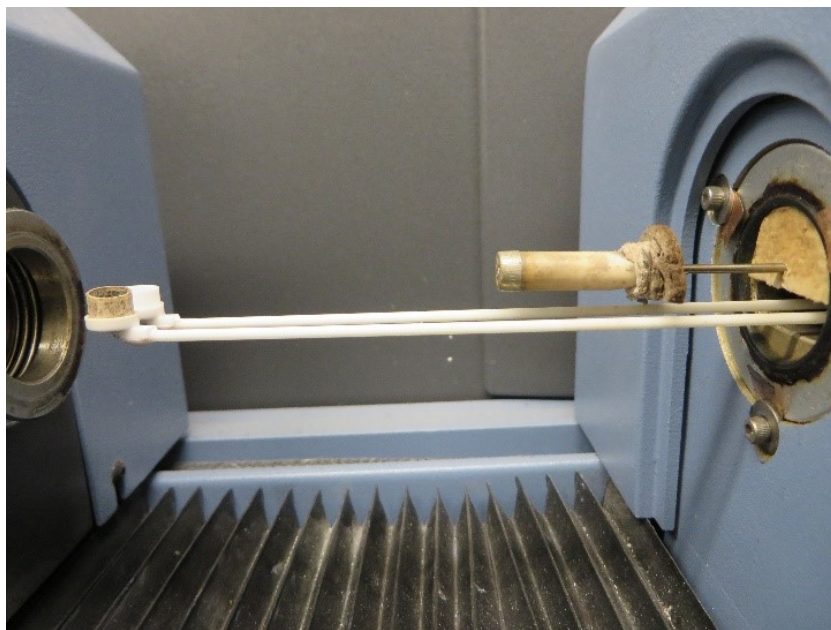


Figure 3.4: Diffuser arrangement in TA Instruments SDT Q600 TGA

with nitrogen (99.999% purity) in different proportions and introduced through the reactive gas port.

Char steam interactions were studied by introducing steam using a syringe pump and diffuser (described elsewhere [91]) arrangement shown in Fig. 3.4. A programmable PHD 4400 syringe pump, filled with deionized (DI) water was used to introduce DI water, at different flow rates, into the diffuser, through the reactive gas port. Sufficient flow rate of nitrogen was maintained, in order to ensure proper diffusion. Very high flow rates of DI water was avoided, as it could lead to condensation of water vapor in the furnace. The concentration of steam entering the TGA was controlled by varying the flow rate of DI water and nitrogen. Experiments were conducted for about an hour, or until significant portion of the char sample was gasified. Subsequently, the TGA furnace was purged with high flow rates of nitrogen, in order to remove any existing moisture in the system. Experiments were repeated to obtain a consistent reading.

In order to compare the reactivity values of different chars, 20% steam-N₂ mix-

ture and 100% CO₂ were chosen, as they demonstrated comparable reactivity with chars. Reactivity of different chars was compared at 950°C. Gasification kinetic parameters were estimated for 1000°C char. 4-5 mg of char sample was reacted with varying concentration of steam (10%, 20%, 30% and 33%) and CO₂ (10%, 25%, 50%, 75% and 100%) at different temperatures (800°C, 850°C, 900°C, 925°C, 950°C and 1000°C) in order to estimate the kinetic parameters.

3.5 Experiments for estimation of pyrolysis kinetics of asphaltenes

Decomposition kinetics for asphaltenes was estimated using ASTM E1641 [93], with minor deviations. Sample weights were kept higher than the prescribed weights owing to the presence of large quantities of volatile matter in asphaltenes. Heating rates between 2 °C/min and 10 °C/min were used for pyrolysis. A higher heating rate of 15 °C/min was used in order to identify the changes occurring at higher heating rates. Flow rate of 50 ml/min of nitrogen (99.999% purity) was maintained during all the pyrolysis experiments. The asphaltenes samples were heated from room temperature to 900°C at the heating rates described above and the decomposition curves were recorded. Most of the decomposition occurred between 350-450 °C. The calculations could not fit into the standard procedure described in ASTM E1641. Therefore, extensive linear regression was performed in order to obtain the kinetic parameters. The calculations have been presented in later sections.

Chapter 4

Results and Discussions

4.1 Characterization of asphaltenes

In this section results obtained from SEM analysis; proximate and ultimate analysis; and thermal characterization have been discussed. The physical appearance of raw and pulverized asphaltenes has been presented in the previous chapter. Proximate and ultimate analysis of asphaltenes has been shown in Table 4.1. It can be clearly identified from the table that asphaltenes have very limited quantity of ash, and significant quantity of sulfur. Moreover, asphaltenes have large amount of volatile matter (63 %). Presence of limited quantity of ash in asphaltenes, hampered accurate quantitative estimation using conventional techniques viz. X-ray fluorescence and energy dispersive X-ray (EDX). However, EDX mapping was used to obtain a qualitative idea on the nature of minerals present in asphaltenes. A homogeneous distribution of sulfur can be observed from the mapping. It is known that Albertan

Table 4.1: Proximate and ultimate analysis of asphaltenes

Species	wt.(%)
Moisture	0.1
Ash	0.6
Volatile	63.0
Fixed carbon	36.3
C	82.68
H	8.34
S	7.75
N	1.20
O*	0.03

* by difference

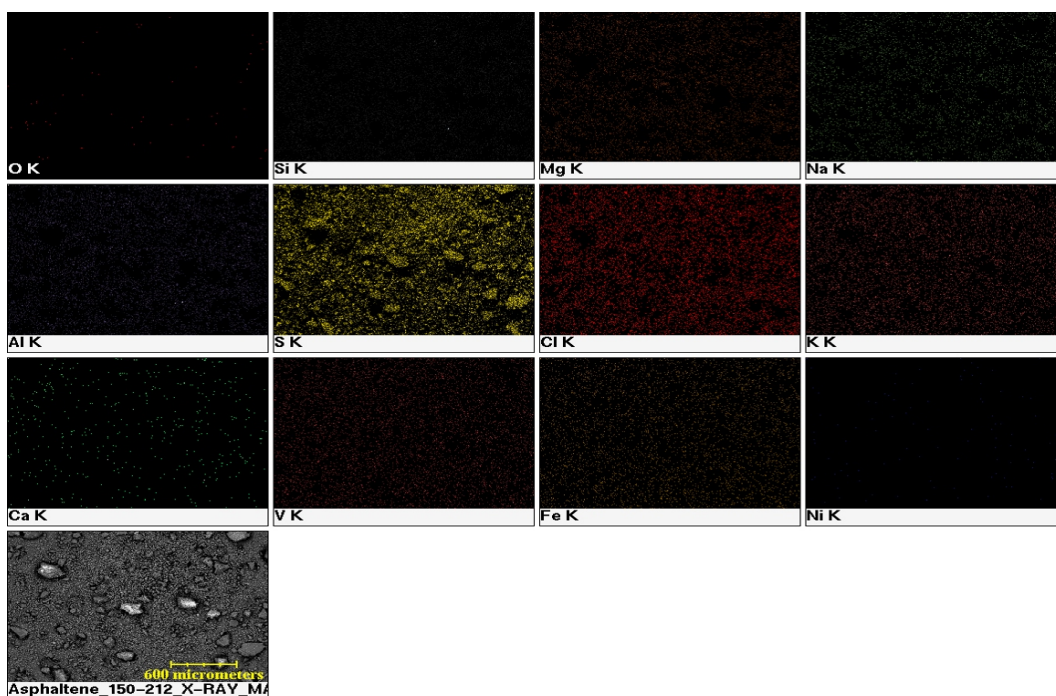


Figure 4.1: EDX mapping of asphaltenes

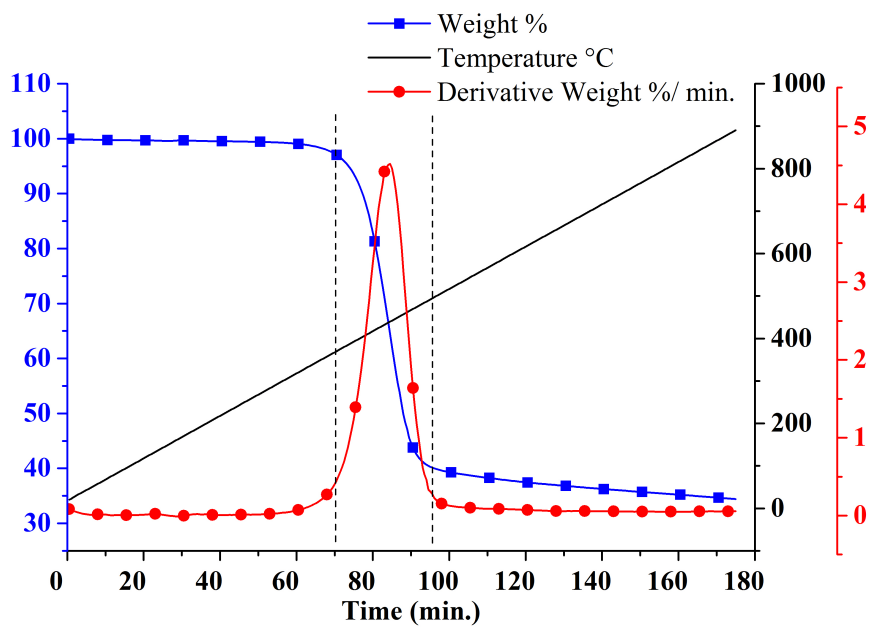


Figure 4.2: TGA and DTG curves for asphaltenes in inert atmosphere (heating rate 10 °C/min)

asphaltenes are rich in sulfur, which is present in aromatic and aliphatic forms (7:3 ratio by weight) [14, 94]. Therefore, the observed sulfur could be aliphatic or aromatic in nature. Researchers have shown that trace metals - vanadium and nickel are present in abundant quantity in petroleum, in porphyrinic and non-porphyrinic structures, which exhibit similar physical and chemical stabilities [56, 57]. An uniform distribution of minute quantities of V and Ni can also be observed from the mapping. EDX mapping could also reveal the presence of discrete minute quantities of aluminosilicates/clay, iron oxides and silica in the asphaltenes. In later sections, Fourier transform infrared spectroscopy (FTIR), X-ray diffraction (XRD), inductively coupled plasma mass spectrometry (ICP-MS) analyses of asphaltenes, have been discussed along with that of chars.

Thermogravimetric analysis of asphaltenes (Fig. 4.2) was carried out in order to get a better understanding of the thermal decomposition process. Maximum weight loss region for asphaltenes was observed between 350 °C and 500 °C. This result is in accordance with other thermal decomposition studies on asphaltenes obtained from nearby regions in northern Alberta and Saskatchewan [86, 95–97]. Thermal decomposition below 350 °C is negligible and could be due to loss of minor peripheral groups. Previous researchers have reported that the volume of produced H₂S and heavier hydrocarbons increases rapidly beyond 350 °C suggesting actual onset of pyrolysis [86].

4.2 Yield and composition of chars

4.2.1 Yield of chars

Yield and quality of pyrolysed products vary significantly with heating rate, final temperature and residence time at temperature [70, 98–100]. Yield of chars from DTF experiments was significantly lower than the fixed carbon content of asphaltenes. This can be explained as higher heating rates overcome mass transfer limitations resulting in better pyrolysis [100, 101]. Observed trend in yield of chars

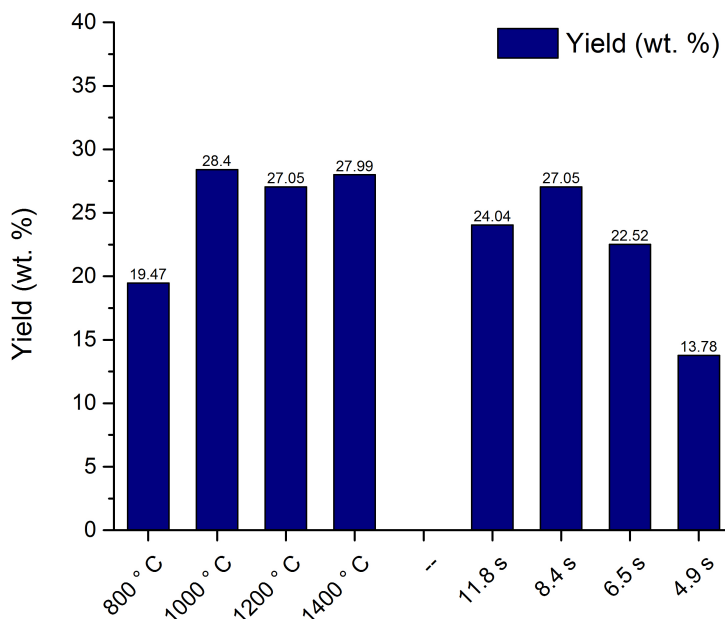


Figure 4.3: Yield of asphaltene chars prepared in the DTF at varying operating conditions

can be accounted to practical limitations of the cyclone separator. 800 °C char was significantly lighter than other chars which resulted in char particles being carried over to the initial stages of the cascade impactor. Fig. 4.3 shows the yield of chars prepared in the DTF at varying operating conditions.

$$Yield(wt.\%) = \frac{wt.of\ char}{wt.of\ asphaltene\ fed} \times 100\% \quad (4.1)$$

4.2.2 Proximate and ultimate analysis of chars

Content of volatile matter in chars obtained at different operating temperatures decreased from 32.99 wt.% in 800 °C Char to 6.45 wt.% in 1400 °C char. Asphaltene and its chars have very limited quantity of ash. A specific trend could not be identified for the content of ash in char; however chars had higher content of ash than raw asphaltene (0.60 wt.% in asphaltene to 2.18 wt.% in 1400 °C char). Table 4.2 shows the ultimate analysis of asphaltene chars prepared in the DTF at vary-

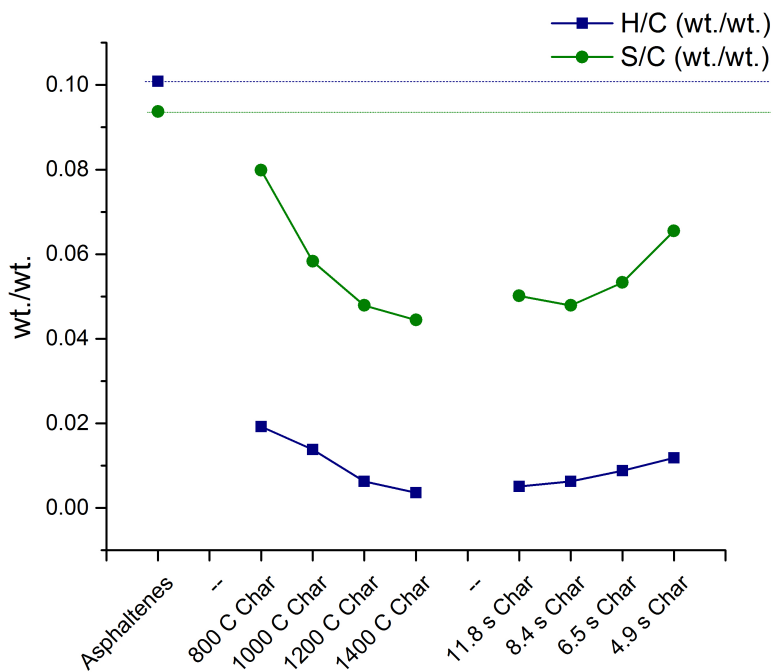


Figure 4.4: H/C ratio (wt. /wt.) and S/C ratio (wt./wt.) of asphaltenes chars prepared in the DTF at varying operating conditions

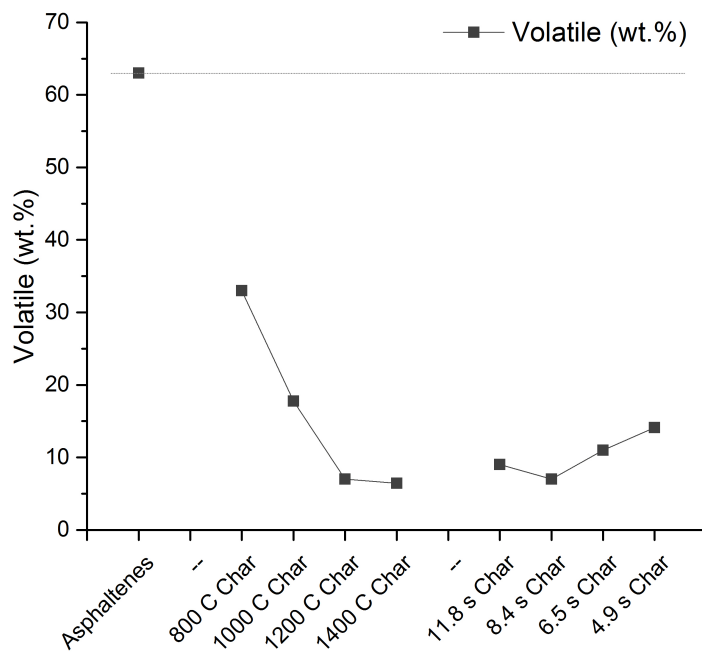


Figure 4.5: Content of volatile matter in asphaltenes chars prepared in the DTF at varying operating conditions

Table 4.2: Ultimate analysis of asphaltenes chars prepared in the DTF at varying operating conditions

Item	C(wt.%)	H(wt.%)	S(wt.%)	N(wt.%)	O*wt.(%)
800°C Char	84.40	1.62	6.74	1.90	5.34
1000°C Char	90.04	1.24	5.25	1.44	2.03
1200°C Char	92.50	0.58	4.43	1.06	1.43
1400°C Char	94.25	0.34	4.19	0.79	0.43
11.8 s Char	92.37	0.47	4.63	0.9	1.63
8.4 s Char	92.50	0.58	4.43	1.06	1.43
6.5 s Char	92.12	0.81	4.91	1.08	1.08
4.9 s Char	88.68	1.05	5.81	1.32	3.14

* by difference

ing operating conditions. Fig. 4.4 shows the variation in H/C ratio and S/C ratio of chars. Fig. 4.5 shows the variation in content of volatile matter of chars. H/C ratio of chars shows a greater rate of variation at lower temperatures (below 1000 °C) which could represent de-alkylation and subsequent polymerization. This is followed by a slower rate of decrease which could signify cyclization and aromatization. At very high temperatures (1200 - 1400 °C) the decrease in H/C ratio is the slowest and could be due to condensation and peri-condensation of aromatic rings. [22] Slight variation in carbon content of chars is observed at this temperature.

Initial decrease in content of sulfur is rapid. It could be due to loss of alkyl sulfur with low C-S bond dissociation energy [21]. Values of S/C and H/C are comparable for asphaltenes. However, H/C value for chars is sufficiently lower than S/C values. It can be clearly seen that a fixed proportion of sulfur does not disappear even at such extreme conditions. This sulfur could be the aromatic sulfur present in asphaltenes. It can also be identified from the ultimate analysis data that sulfur content of chars obtained at higher temperatures is about half that of raw asphaltenes. Content of heteroatoms also tends to decrease for chars obtained at higher temperatures. The content of volatile matter and heteroatoms, as well as, H/C ratio of char increase with a decrease in residence time, though the effect is much less prominent.

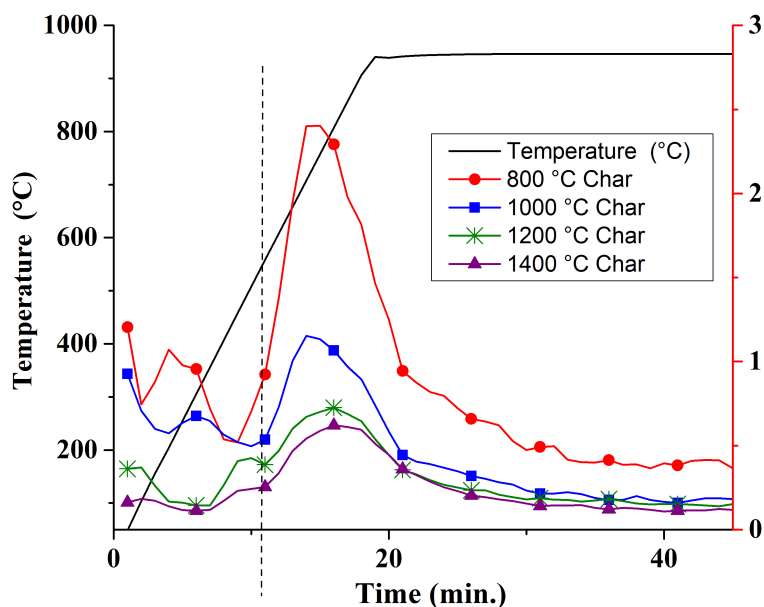


Figure 4.6: DTG curves for asphaltene chars in inert atmosphere (heating rate 50 °C/min)

4.2.3 Thermal analysis of chars

Chars were pyrolysed in a TGA at different heating rates in order to identify the origin of remaining volatile matter in chars. Fig. 4.6 shows the differential of the mass loss curves for chars collected at different operating temperatures in the DTF. A higher heating rate was used to obtain a better resolution. Two peaks can be clearly identified. These peaks were not observed when the heating rate was reduced to 10 °C/min or lower. These peaks can explain the origin of volatile matter in chars. Most of the volatile matter in chars occurs due to incomplete de-volatilization (larger peak) and some due to re-condensation (smaller peak).

4.2.4 Determination of functional groups in chars

Fig. 4.7 represents the Fourier transform infrared (IR) spectra of asphaltene and its chars (wave number range 600 cm^{-1} to 4000 cm^{-1}). The IR spectra can be interpreted to identify various functional groups [102]. Absorbance peaks (or trans-

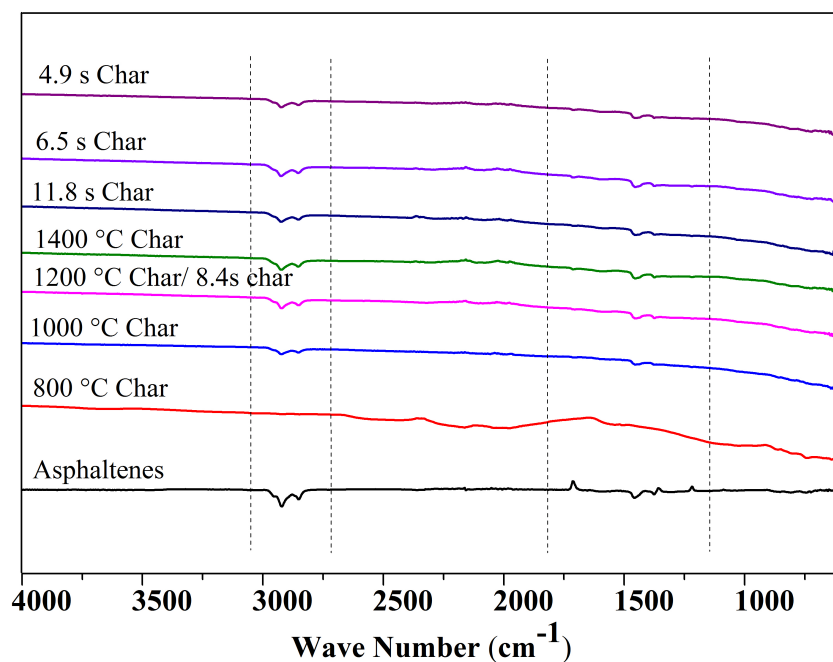


Figure 4.7: FTIR spectra of asphaltenes and its chars

mittance dips) for asphaltenes can be identified as aliphatic CH ($3000-2700\text{ cm}^{-1}$), -OH (carboxylic acids $3300-2500\text{ cm}^{-1}$), aromatic CH ($3100-3000\text{ cm}^{-1}$), CH_2 - and CH- (wag $1350-1150\text{ cm}^{-1}$), $\text{CH}_2\text{-S}$ (wag 1250 cm^{-1}), C=O carbonyl group ($1900-1550\text{ cm}^{-1}$) and aromatic in-ring CH ($1400-1600\text{ cm}^{-1}$) stretching. Carbonyl groups (C=O) typically exhibit a strong spectra, but the peaks exhibited between $1550-1900\text{ cm}^{-1}$ are rather weak. Therefore, the possibility of occurrence of OH (carboxylic acid group) in $2500-3300\text{ cm}^{-1}$ is very less. The peaks around $2700-3000\text{ cm}^{-1}$ can be primarily attributed to aliphatic -CH and some aromatic -CH. $\text{CH}_2\text{-S}$ which is observed around 1250 cm^{-1} in asphaltenes IR spectra seems to be negligible in char. Most of the remaining sulfur in char should be aromatic or thiophenic Sulfur. Aromatic in-ring stretching is exhibited in char samples ($1400-1600\text{ cm}^{-1}$), as well as, asphaltenes but an increase in aromaticity could not be clearly ascertained from FTIR data. In order to confirm gradual onset of aromatic condensation at higher temperatures X-ray diffraction (XRD) pattern of asphaltenes and its chars was studied.

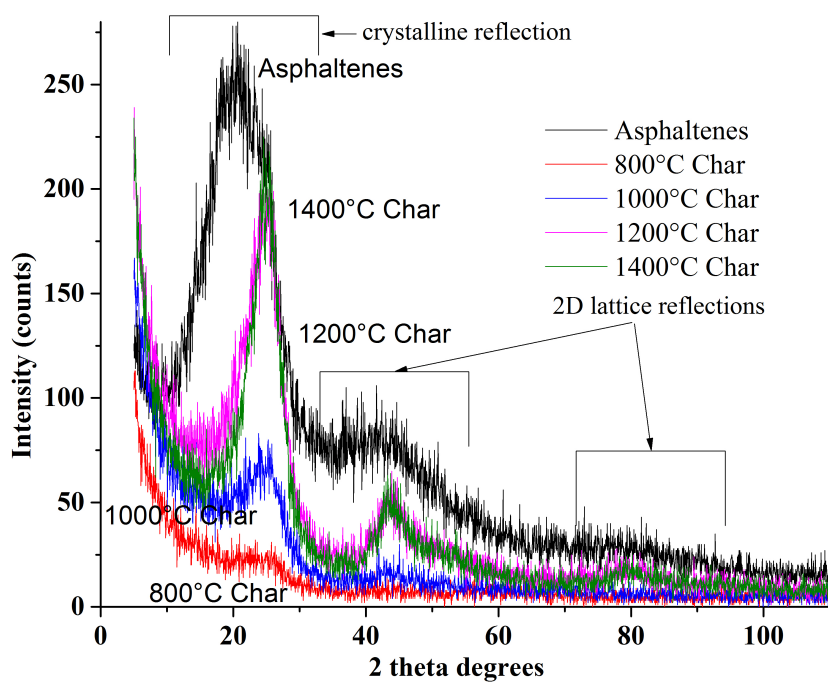


Figure 4.8: X-ray diffraction pattern of asphaltenes and its chars obtained at different operating temperatures

4.2.5 X-ray diffraction pattern of chars

Fig. 4.8 represents X-ray diffraction patterns for asphaltenes and its chars obtained at different operating temperatures. XRD is used extensively for determining the presence of crystalline salts [103]. Asphaltenes and its chars have very limited quantity of ash which could not be identified from the XRD pattern. The XRD pattern for chars is strikingly similar to patterns from carbon black [104] or coal [105]. A qualitative estimation of amorphous and crystalline carbon could be obtained from the observed intensity curves. One strong crystalline reflection (002) and two 2-dimensional lattice reflections (10) and (11) could be identified. The XRD pattern can be explained by the presence of short range crystalline carbon (intermediate between amorphous carbon and graphite) or turbostratic structure, and significant amount of amorphous carbon which accounts for the background intensity [105]. Asphaltenes tend to have more crystalline phase than chars obtained from the DTF at lower temperatures. Chars obtained at higher operating temperatures tend to exhibit higher ordering or graphitization. This could be due to condensation and peri-

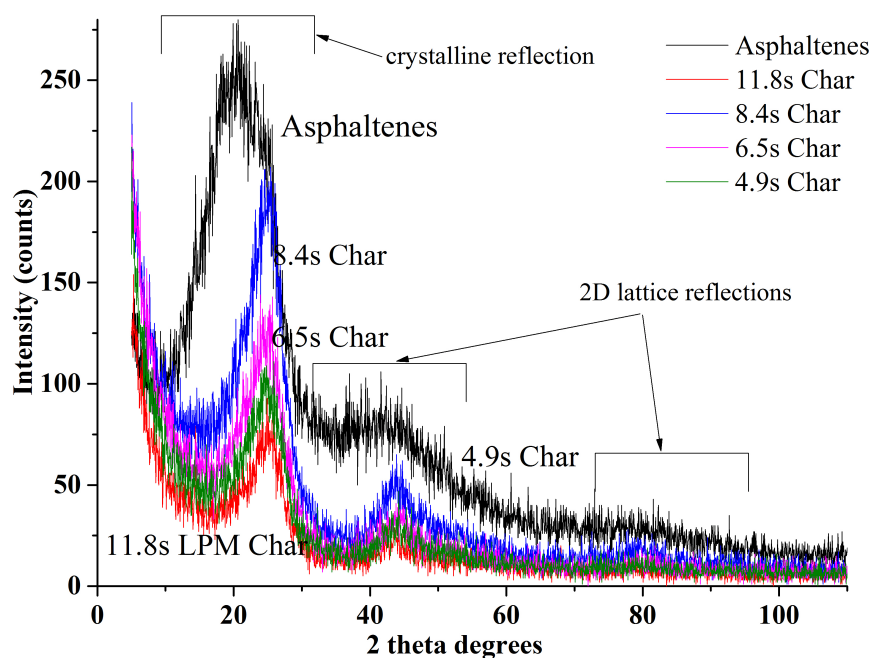


Figure 4.9: X-ray diffraction pattern of asphaltenes and its chars obtained at different residence times

condensation of aromatic rings at higher temperatures. Similar behavior has been reported in literature for coal, petroleum coke and activated carbon [72, 105–108]. Fig. 4.9 represents X-ray diffraction patterns for asphaltenes and its chars obtained at different residence times. Residence time had a much lesser effect on graphitization than temperature.

4.2.6 Mineral matter in chars

High concentration of carbon coupled with very low concentration of ash prevented accurate quantitative estimation of mineral matter in char by conventional analytical techniques like X-ray fluorescence (XRF) and energy dispersive X-ray (EDX). However, EDX mapping (Fig. 4.10) was used to obtain a qualitative idea about the nature of minerals present in char. EDX mapping of chars obtained at different temperatures could not reveal significant variation in mineral matter. Aluminium, silicon and iron were observed as discrete particles of aluminosilicates or clay and

Table 4.3: Content of vanadium and nickel in asphaltenes and its chars

Sample Name	vanadium (ppmw)	nickel (ppmw)
Asphaltenes	1763.4	671.32
800 °C	2858.78	1119.90
1000 °C Char	4225.55	1577.04
1200 °C Char	3022.95	1143.84
1400 °C Char	2565.78	991.47
11.8 s Char	3938.05	1575.32
8.4 s Char	3022.95	1143.84
6.5 s Char	3489.69	1304.56
4.9 s Char	3614.51	1392.78

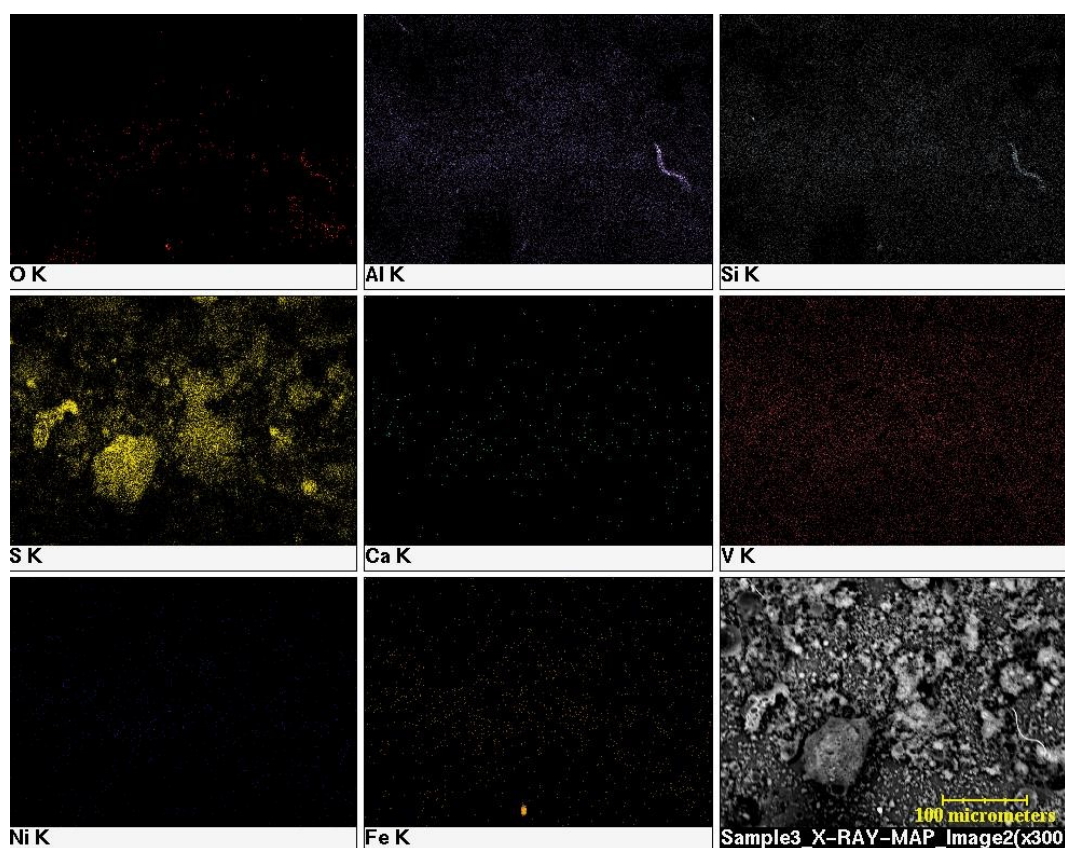


Figure 4.10: EDX Mapping of 1200 °C Char (300X magnification)

iron oxides. Sulfur was observed evenly distributed in the char (slightly more concentration observed in bigger sized char particles). EDX mapping of chars revealed negligible concentrations of V and Ni distributed uniformly throughout. No surface evolution of V and Ni was detected in the chars even at such extreme operating conditions. Inductively coupled plasma mass spectrometry (ICP-MS) was carried

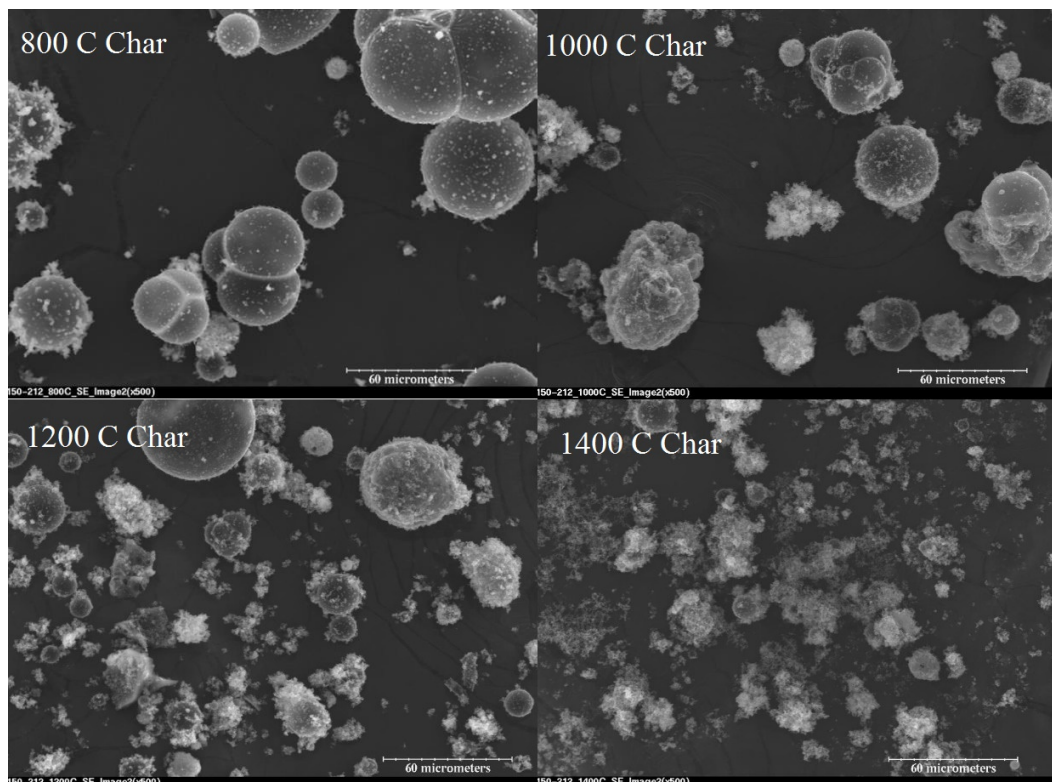


Figure 4.11: SE SEM image of chars obtained at different operating temperatures (similar magnifications 500X)

out to obtain a better estimate of the concentration of trace metals. Table 4.3 shows the concentration of V and Ni in asphaltenes and its chars. It was observed that V and Ni tend to accumulate completely in chars.

4.3 Morphological changes in chars

Morphology of chars has significant influence on char gasification reactivity [71, 109]. Char collected from the DTF at 800 °C was extremely light and slightly sticky to touch. Individual char particles could be perceived as *small inflated balloons* to the naked eyes. Chars collected at higher temperatures from the DTF were finer and had higher bulk densities. They were also significantly less stickier than 800 °C char. Fig. 4.11 shows the SEM images of chars collected at different operating temperatures. SEM images of chars collected at different residence times(Fig.4.12)

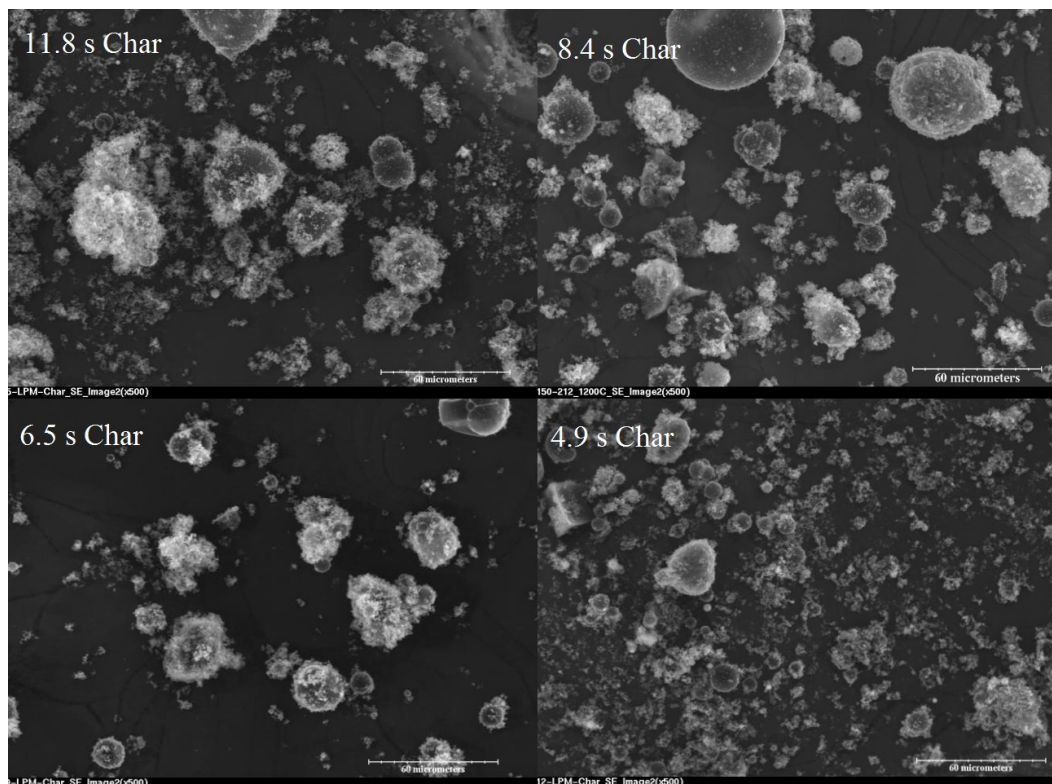


Figure 4.12: SE SEM image of chars obtained at different residence times (similar magnifications 500X)

could not reveal any significant variation in morphology. Diameter of individual char particles tends to decrease with an increase in operating temperature. Chars obtained at higher operating temperatures have considerable amount of fragmented particles.

SEM of char cross-section (Fig.4.13(a)) could reveal that individual char particles are completely hollow (or cenospheres [110]) and have porous walls. Surface of char particles was primarily smooth and could be due to initial rapid melting of asphaltenes [70]. The hollow vesicular structure could have resulted from rapid evolution of gases during pyrolysis [111]. Soot is deposited in minute quantities on the surface of char particles. (White dots observed in SEM image (Fig.4.13(b)) of char surface have a structure similar to that of soot identified at very high magnification) Similar studies have also shown that the diameter of asphaltenes cenospheres decreases with temperature and thickness of external cenosphere wall, as well as,

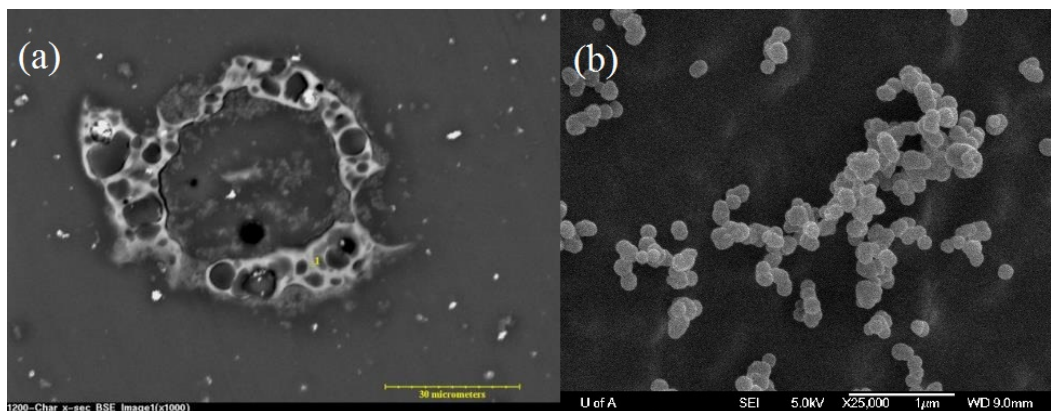


Figure 4.13: (a) cross section BSE SEM of 1200°C char (1000X) (b) SE SEM of soot on surface of char (25,000X)

bulk density increases with an increase in temperature [110].

4.4 Reactivity of chars

Global gasification reactivity, for atmospheric gasification of chars was studied using thermogravimetry. Differential of the weight loss curves can provide an accurate estimation of the instantaneous apparent reactivities [g/g.s]. Differential of the weight loss curves for char-CO₂ and char-steam, at 950 °C, reactions have been plotted in Fig. 4.14. The curves have been smoothed using SavitzkyGolay filter (polynomial of order three). Reactivity of steam with chars was observed to be significantly higher than CO₂. N₂-20% steam- char reactivity was comparable to 100% CO₂-char reactivity. Gasifying agents of similar reactivity were chosen in order to effectively identify and conclude any observable trend in the reactivity of the chars. Chars obtained at higher operating temperatures exhibited lower reactivity, than chars obtained at lower temperatures. The same trend in apparent reactivity was observed for both char-20% steam and char-100% CO₂. Moreover, the effect of residence time on reactivity was easily identifiable. Chars obtained at shorter residence times exhibited higher reactivity. Asphaltenes, unlike coal have very limited inorganic matter which could catalytically affect gasification reactions. The decrease in reactivity for chars obtained at higher temperatures and longer residence times

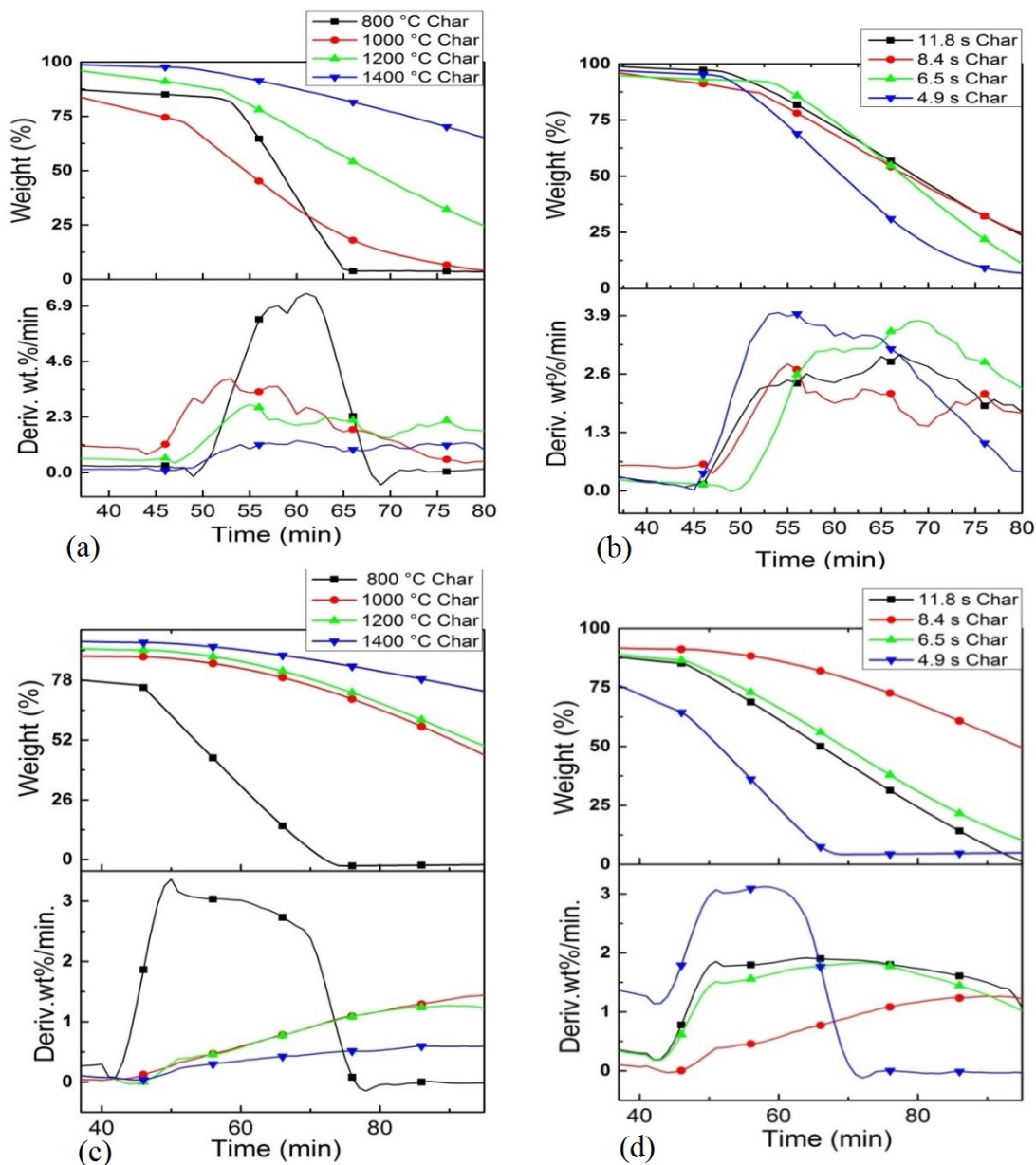


Figure 4.14: TGA and DTG curves for global char gasification reactivity (a) Chars obtained at different operating temperatures with 20% steam (b) Chars obtained at different residence times with 20% steam (c) Chars obtained at different operating temperatures with 100% CO₂ (d) Chars obtained at different residence times with 100% CO₂

can be attributed to observed increase in aromaticity and graphitization from X-ray diffraction studies. Observed loss in reactivity of coal and petroleum coke chars, due to ordering of carbon structure and annealing at higher temperature and longer carbonization time has been suggested by researchers [72, 107, 108, 112]. Chars obtained at higher temperatures and longer residence times have lower concentration of heteroatoms. Researchers have also suggested the loss in reactivity due to the reduction in content of heteroatoms [80]. Chars obtained at higher temperatures have more observable macro-porosity. Increase in macro-porosity coupled with an increase in skeletal structure and decrease in micro-porosity at higher temperatures has been observed for other carbonaceous chars [107, 109, 113]. Stronger role of micro-porosity in determining char reactivity has also been reported for uncatalyzed carbon gasification reactions [114].

4.5 Kinetics of asphaltenes pyrolysis

Researchers have reported that pyrolysis reactions are faster than heterogeneous char gas interactions [10]. Since, estimation of actual rate of asphaltenes pyrolysis at entrained flow conditions, is quite challenging, pyrolysis experiments were conducted at lower heating rates in a TGA for estimation of the kinetic expression. This kinetic expression could help in predicting the actual rate with some degree of accuracy. Asphaltenes were pyrolyzed at different heating rates viz. 2°C/min, 5°C/min, 10°C/min, 7°C/min and 15°C/min to the final temperature of 900°C in a flow of 50 ml/min nitrogen (99.999% purity) . It can be observed from the mass loss curves (Fig. 4.15) that most of the decomposition occurs between 350°C and 450°C. Standard calculation procedure using numerical integration constants, described in ASTM E1641, could not fit the data generated for pyrolysis of asphaltenes. Therefore, extensive regression techniques were used to obtain the kinetic parameters.

Assuming, first order decomposition of asphaltenes:

$$-r = k[C] \quad (4.2)$$

$$-\frac{d[C]}{dt} = k[C] \quad (4.3)$$

Integrating Eqn. 4.3

$$\int \frac{d[C]}{[C]} = - \int k \cdot dt \quad (4.4)$$

When $\Delta t \rightarrow 0$ Eqn. 4.4 can be approximated to (where X represents the %conversion)

$$\ln \frac{X_2}{X_1} = k\Delta t \quad (4.5)$$

Values of k obtained from Eqn. 4.5 were substituted in the Arrhenius Equation (Eqn. 4.6) in order to estimate the activation energy (E_a) and the pre-exponential factor (A)

$$k = Ae^{\frac{-E_a}{RT}} [1/s] \quad (4.6)$$

Taking natural logarithm of both sides, this equation reduces to the form

$$\ln(k) = \ln(A) - \frac{E_a}{RT} \quad (4.7)$$

Fig. 4.16 shows that the assumption (of first order irreversible decomposition) holds good within the temperature range 350°C and 425°C. The kinetic expression can be described by Eqn. 4.8. At very high heating rates, mass transfer limitations are overcome [100, 101]. Therefore, rate of pyrolysis could be much faster, with lower activation energy and greater pre-exponential factor, in the entrained flow drop tube furnace experiments.

$$k[s^{-1}] = 1.46 \times 10^8 [s^{-1}] e^{\frac{-150.170 \text{ kJ/mol}}{RT}} \quad (4.8)$$

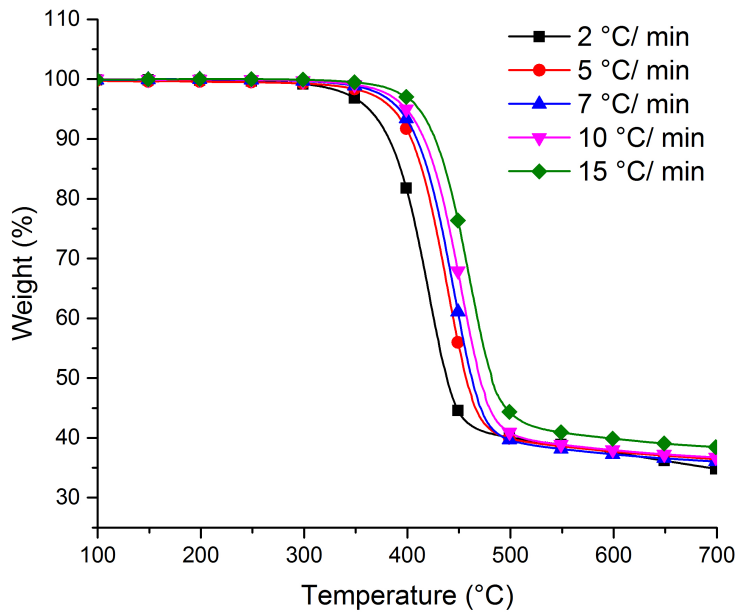


Figure 4.15: Mass loss curves for pulverized asphaltenes at different heating rates

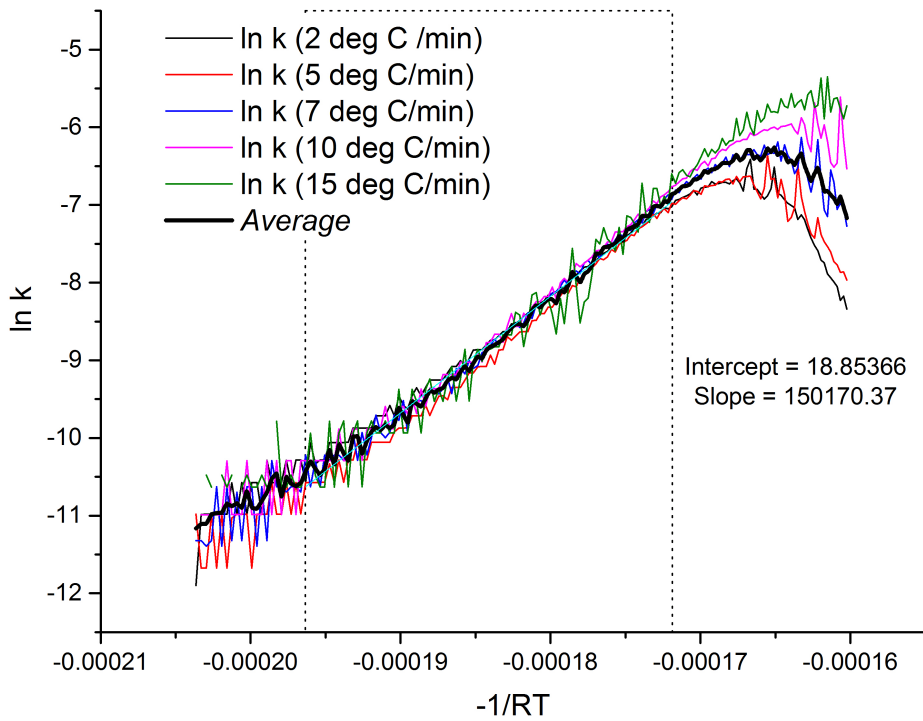


Figure 4.16: $\ln k$ vs $-1/RT$ for pyrolysis at different heating rates

4.6 Estimation of char gasification kinetics

The significance of heterogeneous char gas reactions has been discussed in sufficient detail in earlier sections of this work. Boudouard reaction and water gas shift reaction are the major char gas reactions in gasification process and they are endothermic in nature [10]. Researchers have described the rate of char gas interactions using different definitions. The simplest way of describing the reaction rate is by relating it to the mass of char. This rate is often described as *apparent reaction rate* or *global reaction rate* and has the units [g/g.s]. Another way of describing the reactivity of chars is by relating it to the surface area of chars. This is known as *intrinsic reactivity* and has the units [g/m².s]. [84] Estimation of total surface area of asphaltene chars by mercury porosimetry and N₂ BET could not yield reliable results. Kinetic model of the form ($r_{gas}=kP^n_{gas}$) [81, 83, 84, 115] was used to estimate the kinetic parameters for char CO₂ and char steam interactions at elevated temperatures between 800°C and 1000°C using a TGA with varying concentrations of gas at atmospheric pressure. The rate of reaction at temperatures below 800°C was observed to be extremely slow. The limitations of this model have been discussed earlier. A comparable solution procedure has been described in literature [82, 115]. The kinetic parameters were estimated for char obtained from the DTF at 1000°C.

4.6.1 Char CO₂ gasification kinetics

Instantaneous observed rate of gasification can be estimated using Eqn. 4.9

$$r_{inst.} = \frac{-1}{m - m_{ash}} \left(\frac{\Delta m}{\Delta t} \right) [g/g.s] \quad (4.9)$$

Since, the content of ash in asphaltene chars is significantly less, the above equation reduces to the form

$$r_{inst.} = \frac{-1}{m} \left(\frac{\Delta m}{\Delta t} \right) [g/g.s] \quad (4.10)$$

The global power law kinetic model for char CO₂ reaction is shown in Eqn.

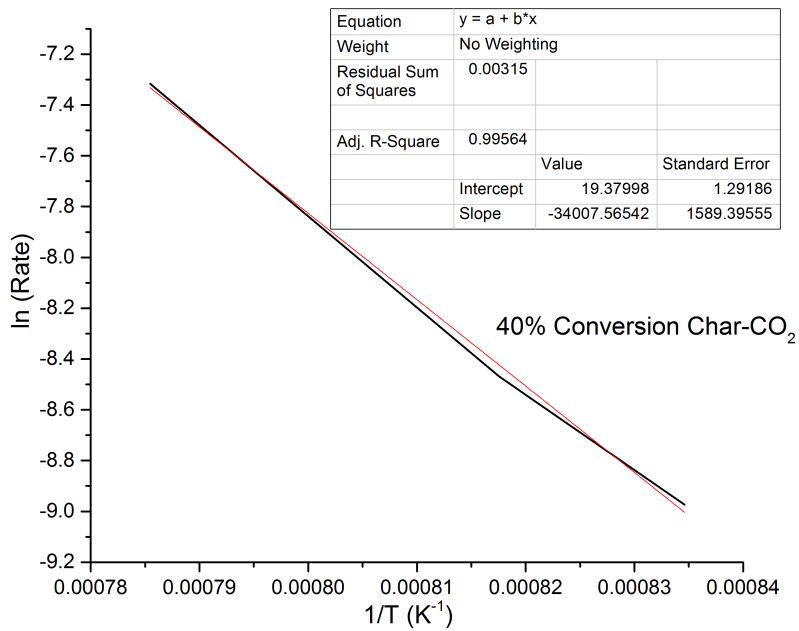


Figure 4.17: Plot of $\ln(r)$ vs $1/T$ for 1000°C char 100% CO₂ interaction at 40% conversion

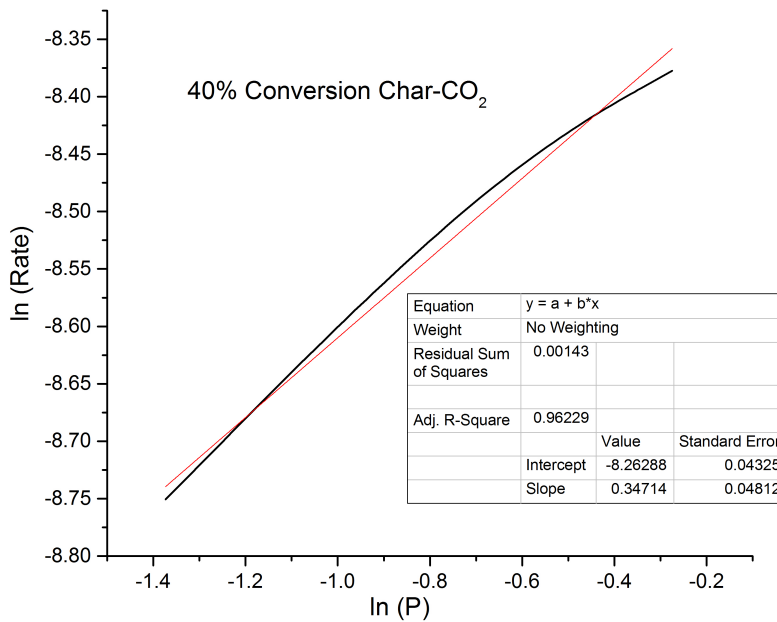


Figure 4.18: Plot of $\ln(r)$ vs $\ln(P)$ for 1000°C char CO₂ interaction at 950°C and 40% conversion

Table 4.4: Values of $\ln nP + \ln A$ and $-E_a/R$ for different conversion levels of 1000°C Char CO₂ interaction

Conversion(%)	Intercept ($\ln nP + \ln A$)	Slope ($-E_a/R$)
20	19.43616	-34619.23871
25	18.66054	-33458.4352
30	19.74823	-34635.77698
40	19.37998	-34007.56542
Average	19.3062275	-34180.25408

Table 4.5: Values of n and $\ln A - E_a/RT$ for different conversion levels for 1000°C Char CO₂ interaction

Conversion(%)	Slope (n)	Intercept ($\ln A - E_a/RT$)
20	0.39445	-8.7623
30	0.35734	-8.43885
40	0.34714	-8.26288
Average	0.36631	-8.48801

4.11. E_a represents the activation energy in J/mol, R is the universal gas constant in J/mol-K, A is the pre-exponential factor and P is the partial pressure in bar.

$$r = Ae^{-\frac{E_a}{RT}} P_{CO_2}^n [g/g.s] \quad (4.11)$$

Taking natural logarithm of both sides, this equation reduces to the form

$$\ln(r) = \ln(A) - \frac{E_a}{RT} + n \ln(P_{CO_2}) \quad (4.12)$$

The total number of active sites in char is related to % conversion [81, 84], therefore, the rate for a particular conversion level for different concentrations of reacting gas and temperature was considered. Kinetic parameters were estimated for char conversion levels below 40%. Fig.4.17 and Fig.4.18 were plotted for 40% conversion of chars. Averages (Table 4.4 and 4.5) were estimated in order to reduce error. The global kinetic expression for 1000°C char CO₂ interaction is shown in Eqn. 4.13:

$$r[g/g.s] = 2.8 \times 10^8 e^{-\frac{284.175 \text{ kJ/mol}}{RT}} P_{CO_2}^{0.37} \quad (4.13)$$

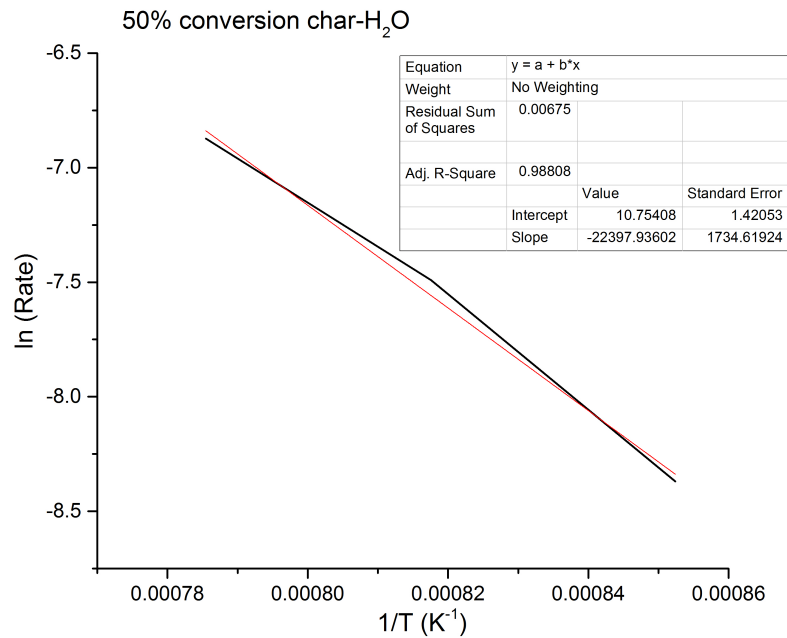


Figure 4.19: Plot of ln(r) vs 1/T for 1000°C char 20% steam interaction at 50% conversion

4.6.2 Char steam gasification kinetics

Kinetic parameters for char steam interaction were estimated using a similar procedure. However, greater variation was observed at different conversion levels. This variation tends to reduce at higher conversion levels. Fig.4.19 and Fig.4.20 were plotted for 50% conversion of chars. The global kinetic expression for 1000°C char steam interaction at 50% conversion level is shown in Eqn. 4.14 :

$$r[g/g.s] = 1.32 \times 10^5 e^{\frac{-186.216 \text{ kJ/mol}}{RT}} P_{H_2O}^{0.65} \quad (4.14)$$

4.6.3 Comparison between pyrolysis and gasification kinetics

Table 4.6 shows a comparison between pyrolysis and gasification kinetics. 1000°C temperature and 1 bar pressure is considered for the comparison. It can be clearly seen from the table that pyrolysis reactions are much faster than gasification reactions. It can also be observed that char-CO₂ reactions are faster than char-H₂O interactions. At such temperatures, pyrolysis and gasification reactions are expected

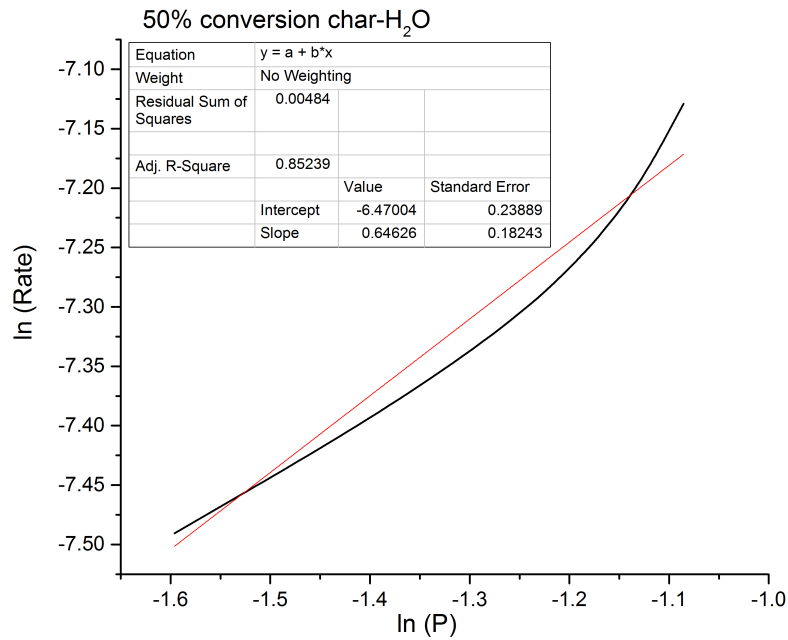


Figure 4.20: Plot of $\ln(r)$ vs $\ln(P)$ for 1000°C char steam interaction at 950°C and 50% conversion

Table 4.6: Comparison between pyrolysis kinetics and gasification kinetics

Reaction	Activation Energy (E_a)	Rate Constant (k)
Pyrolysis	150.170 kJ/mol	100.68 s ⁻¹
char-CO ₂	284.175 kJ/mol	6.13 X 10 ⁻⁴ s ⁻¹ bar ^{-0.37}
char-H ₂ O	186.216 kJ/mol	3.02 X 10 ⁻³ s ⁻¹ bar ^{-0.65}

to proceed simultaneously [10]. The importance of char-gas interactions, already discussed in earlier sections is substantiated by this comparison.

Chapter 5

Conclusions and Recommendations for Future Research

5.1 Conclusions

Operating temperature and residence time affect the morphology, structure and reactivity of asphaltenes chars obtained from rapid pyrolysis in an entrained flow reactor. Following conclusions can be drawn from the results of the present study:

- Chars obtained at higher operating temperatures exhibited higher fragmentation, graphitization, aromaticity and macro-porosity. Global gasification reactivity, H/C ratio, nominal particle size, volatile matter and content of heteroatoms decreased for chars obtained at higher temperatures. Decrease in apparent gasification reactivity could be due to greater ordering of carbon structure and/or reduction in micro-porosity at higher temperatures leading to reduction in active surface area of chars. The decrease in content of heteroatoms in chars obtained at higher temperatures could also explain the loss in reactivity.
- Residence time at a given operating temperature (between 5-12 s) had less distinct effect on char characteristics and reactivity. Global gasification reactivity, H/C ratio and content of volatiles and heteroatoms reduced for chars collected at higher residence times. Changes in aromaticity, graphitization

and morphology were minimal. Thermal deactivation at increased carbonization times could explain loss in gasification reactivity.

- Vanadium and nickel present in raw asphaltenes, tend to accumulate in chars. However, their effect on the reactivity of chars was not observed. Evolution of V and Ni during pyrolysis was not observed, and they continue to exist as organometallic structures evenly distributed throughout. Asphaltenes and its chars have limited quantity of mineral matter (clay, iron oxides, silica) in discrete quantities.
- Sulfur in asphaltenes exists in both aromatic and aliphatic forms, however, sulfur present in char exists primarily in the aromatic form. Aliphatic sulfur is primarily lost during pyrolysis. Values of S/C and H/C are comparable for asphaltenes, however, these values are very different for chars. This observation, as well as, FTIR spectra of asphaltenes and its chars corroborates the fact that aromatic sulfur is not lost even at extreme conditions.
- Cross section SEM of char particles revealed a hollow structure (cenospheres) with porous walls. Some soot particles were observed on the surface of chars. The remaining volatile matter in chars can be primarily attributed to incomplete de-volatilization (and part re-condensation).
- Char CO₂ reactions were observed to be slower than char H₂O reactions at gasification temperatures. The reactivity of chars with 20% steam-N₂ mixture was comparable to the reactivity of chars with 100% CO₂. This behaviour was observed for chars prepared at different operating conditions.
- Char CO₂ interactions could be expressed in the form of n^{th} order rate equation at lower conversions. Effect of conversion on the rate of gasification was prominent for char H₂O interactions. Moreover, the effect of steam partial pressure ($n=0.65$) on reactivity was observed to be higher than CO₂ partial pressure ($n=0.37$). Gasification reactions were observed to be extremely slow at temperatures below 800°C for both steam and CO₂.

- Pyrolysis of asphaltenes was observed to be at least 5-6 orders of magnitude higher than atmospheric gasification reactions. This observation substantiates the importance of char-gas interactions in gasification process. The actual rate of pyrolysis in the drop tube furnace is expected to be much higher than predicted from the kinetic expression, as mass transfer limitations are overcome at extremely high heating rates. The yield of chars from pyrolysis in the drop tube furnace, were observed to be lower than the fixed carbon content of asphaltenes, suggesting better pyrolysis at very high heating rates.
- The mathematical model for flow of particles in the drop tube furnace could highlight the significance of density and particle size on the residence time. Residence time of particles was observed to increase significantly below particle sizes of $75\mu\text{m}$.

5.2 Recommendations for Future Research

The present work addressed certain areas, however, leaving room for much more. Some of the areas that need to be explored are suggested below:

- The significance of active surface area (ASA), total surface area (TSA) in explaining the reactivity of chars has been suggested by many researchers [75–77]. However, in the present study ASA, TSA and porosity were not estimated. Rate models should be estimated considering TSA and ASA separately. Applicability of the rate expression considering TSA should be studied over different ranges of temperature, partial pressure, as well as, conversion. The influence of pore structure, thermal deactivation and mass transfer limitations should be taken into account while proposing the model [84]. Conventionally, char gasification rates are estimated using TGA, however, it involves cooling and subsequent re-heating of chars, which could have significant effect on the actual gasification rate. Moreover, in an actual gasification process in an entrained flow reactor, pyrolysis and gasification reactions occur simul-

taneously, which could affect the rate of gasification [10]. Notable amount of work could be done on the above area.

- In the present work, chars were prepared at atmospheric pressure and gasification kinetics was also estimated at the same pressure. Researchers, have reported that operating pressure affects the quality and reactivity of chars [70]. Moreover, industrial entrained flow gasifiers are usually operated at higher pressures [10]. Experimental setup which can operate at higher pressures needs to be designed. The gasification reactivity of chars could be estimated using high pressure thermogravimetry.
- The composition of gaseous products formed during pyrolysis was not studied in the present work. Composition of the products could help in understanding the pyrolysis process better. Moreover, a comparison of the products obtained during fast and slow pyrolysis could help in explaining the behaviour of functional groups and heteroatoms in asphaltenes and chars.

References

- [1] US EIA. International energy outlook 2013. *US Energy Information Administration*, 2013.
- [2] CIA Factbook. The world factbook. *See also: <https://www.cia.gov/library/publications/the-world-factbook>*, 2014.
- [3] Report CAPP. Crude oil forecast, markets and transportation. Technical report, Canadian Association of Petroleum Producers, 2013.
- [4] Norbert Berkowitz and James G. Speight. The oil sands of alberta. *Fuel*, 54(3):138–149, 1975.
- [5] I Rubinstein, OP Strausz, C Spyckerelle, RJ Crawford, and DWS Westlake. The origin of the oil sand bitumens of alberta: a chemical and a microbiological simulation study. *Geochimica et Cosmochimica Acta*, 41(9):1341–1353, 1977.
- [6] Otto P Strausz and Elizabeth M Lown. *The chemistry of Alberta oil sands, bitumens and heavy oils*. Alberta Energy Research Institute Calgary, 2003.
- [7] Keng H. Chung, Chunming Xu, Yunxiang Hu, and Renan Wang. Supercritical fluid extraction reveals resid properties. *Oil and Gas Journal*, 95(3):66–69, 1997.
- [8] Richard F. Meyer and Emil D. Attanasi. Heavy oil and natural bitumen-strategic petroleum resources. *World*, 434:650.7, 2003.
- [9] James G. Speight. *The chemistry and technology of petroleum*. CRC press, 2014.

- [10] C. Higman and M. Van der Burgt. Gasification processes. *Gasification. 2nd ed.* Burlington: Gulf Professional Publishing, 2008.
- [11] LD Smoot and PJ Smith. Coal combustion and gasification, 1985.
- [12] Kamran Akbarzadeh, Hussein Alboudwarej, William Y. Svrcek, and Harvey W. Yarranton. A generalized regular solution model for asphaltene precipitation from n-alkane diluted heavy oils and bitumens. *Fluid Phase Equilibria*, 232(1):159–170, 2005.
- [13] Richard P. Dutta, William C. McCaffrey, Murray R. Gray, and Karlis Muehlenbachs. Thermal cracking of athabasca bitumen: influence of steam on reaction chemistry. *Energy and Fuels*, 14(3):671–676, 2000.
- [14] M. Siskin, SR Kelemen, CP Eppig, LD Brown, and M. Afeworki. Asphaltene molecular structure and chemical influences on the morphology of coke produced in delayed coking. *Energy and Fuels*, 20(3):1227–1234, 2006.
- [15] Eric Y. Sheu. Petroleum asphaltene properties, characterization, and issues. *Energy and Fuels*, 16(1):74–82, 2002.
- [16] Edward Furimsky. Gasification of oil sand coke: Review. *Fuel Processing Technology*, 56(3):263–290, 1998.
- [17] Farshid Vejahati, Hassan Katalambula, and Rajender Gupta. Entrained-flow gasification of oil sand coke with coal: Assessment of operating variables and blending ratio via response surface methodology. *Energy and Fuels*, 26(1):219–232, 2011.
- [18] Rich Kerr, John Birdgeneau, Bob Batt, Peter Yang, Gary Nieuwenburg, Phil Rettger, Jim Arnold, and Yoram Bronicki. The long lake project-the first field integration of sagd and upgrading. In *SPE International Thermal Operations and Heavy Oil Symposium and International Horizontal Well Technology Conference*. Society of Petroleum Engineers, 2002.

- [19] Arash Karimi, Kuangnan Qian, William N. Olmstead, Howard Freund, Cathleen Yung, and Murray R. Gray. Quantitative evidence for bridged structures in asphaltenes by thin film pyrolysis. *Energy and Fuels*, 25(8):3581–3589, 2011.
- [20] Samina Rahmani, William C. McCaffrey, Heather D. Dettman, and Murray R. Gray. Coking kinetics of asphaltenes as a function of chemical structure. *Energy and Fuels*, 17(4):1048–1056, 2003.
- [21] Yingxian Zhao, Murray R. Gray, and Keng H. Chung. Molar kinetics and selectivity in cracking of athabasca asphaltenes. *Energy and Fuels*, 15(3):751–755, 2001.
- [22] Yingxian Zhao, Feng Wei, and Ying Yu. Effects of reaction time and temperature on carbonization in asphaltene pyrolysis. *Journal of Petroleum Science and Engineering*, 74(1):20–25, 2010.
- [23] Murray R. Gray. Consistency of asphaltene chemical structures with pyrolysis and coking behavior. *Energy and Fuels*, 17(6):1566–1569, 2003.
- [24] American Society for Testing and Materials (ASTM). Astm d6560-12, standard test method for determination of asphaltenes (heptane insolubles) in crude petroleum and petroleum products. 2012.
- [25] David L. Mitchell and James G. Speight. The solubility of asphaltenes in hydrocarbon solvents. *Fuel*, 52(2):149–152, 1973.
- [26] JB Boussingault. Memoire sur la composition des bitumens. In *Annales de Chimie et de Physique*, volume 64, page 141, 1837.
- [27] Otto P. Strausz, Manuel Torres, Elizabeth M. Lown, Imre Safarik, and Juan Murgich. Equipartitioning of precipitant solubles between the solution phase and precipitated asphaltene in the precipitation of asphaltene. *Energy and Fuels*, 20(5):2013–2021, 2006.

- [28] J. Marcusson. Asphalt und kohle. *Angewandte Chemie*, 32(28):113–115, 1919.
- [29] OG Strieter. National bureau of standards j. *Research*, 26:415, 1941.
- [30] Kosta J. Leontaritis and G. Ali Mansoori. Asphaltene deposition: a survey of field experiences and research approaches. *Journal of Petroleum Science and Engineering*, 1(3):229–239, 8 1988.
- [31] Sai R. Panuganti, Mohammad Tavakkoli, Francisco M. Vargas, Doris L. Gonzalez, and Walter G. Chapman. Saft model for upstream asphaltene applications. *Fluid Phase Equilibria*, 359(0):2–16, 12/15 2013.
- [32] Sebastiano Corraera and Daniel Merino-Garcia. Simplifying the thermodynamic modeling of asphaltenes in upstream operations. *Energy and Fuels*, 21(3):1243–1247, 2007.
- [33] Irena Gawel, Dagmara Bociarska, and Piotr Biskupski. Effect of asphaltenes on hydroprocessing of heavy oils and residua. *Applied Catalysis A: General*, 295(1):89–94, 10/13 2005.
- [34] James G. Speight and Speros E. Moschopedis. On the molecular nature of petroleum asphaltenes. *Chemistry of asphaltenes*, 195:1–15, 1981.
- [35] JT Miller, RB Fisher, P. Thiyagarajan, RE Winans, and JE Hunt. Sub-fractionation and characterization of mayan asphaltene. *Energy and Fuels*, 12(6):1290–1298, 1998.
- [36] ROBERT B. Long. Concept of asphaltenes. *Am.Chem.Soc., Div.Pet.Chem., Prepr.:(United States)*, 24(CONF-790917-(Vol. 24)(No. 4)), 1979.
- [37] Simon I. Andersen and Kulbir S. Birdi. Aggregation of asphaltenes as determined by calorimetry. *Journal of colloid and interface science*, 142(2):497–502, 1991.
- [38] Eric Y. Sheu, Dave A. Storm, and Maureen M. De Tar. Asphaltenes in polar solvents. *Journal of Non-Crystalline Solids*, 131:341–347, 1991.

- [39] F. J. Nellensteyn. In *Proc. World Petroleum Congress*, volume 2, page 616, 1933.
- [40] J. P. Pfeiffer and RNJ Saal. Asphaltic bitumen as colloid system. *The Journal of physical chemistry*, 44(2):139, 1940.
- [41] Otto P. Strausz, Thomas W. Mojelsky, and Elizabeth M. Lown. The molecular structure of asphaltene: an unfolding story. *Fuel*, 71(12):1355–1363, 1992.
- [42] Teh F. Yen, J. G. Erdman, and Sidney S. Pollack. Investigation of the structure of petroleum asphaltenes by x-ray diffraction. *Analytical Chemistry*, 33(11):1587–1594, 1961.
- [43] John P. Dickie and Teh F. Yen. Macrostructures of the asphaltic fractions by various instrumental methods. *Analytical Chemistry*, 39(14):1847–1852, 1967.
- [44] T. Ignasiak, AV Kemp-Jones, and OP Strausz. The molecular structure of athabasca asphaltene. cleavage of the carbon-sulfur bonds by radical ion electron transfer reactions. *The Journal of organic chemistry*, 42(2):312–320, 1977.
- [45] Otto P. Strausz, Thomas W. Mojelsky, Farhad Faraji, Elizabeth M. Lown, and Ping'an Peng. Additional structural details on athabasca asphaltene and their ramifications. *Energy and Fuels*, 13(2):207–227, 1999.
- [46] Henning Groenzin and Oliver C. Mullins. Molecular size and structure of asphaltenes from various sources. *Energy and Fuels*, 14(3):677–684, 2000.
- [47] Jeff M. Sheremata, Murray R. Gray, Heather D. Dettman, and William C. McCaffrey. Quantitative molecular representation and sequential optimization of athabasca asphaltenes. *Energy and Fuels*, 18(5):1377–1384, 2004.
- [48] Oliver C. Mullins. The modified yen model. *Energy and Fuels*, 24(4):2179–2207, 2010.

- [49] JD Payzant, DS Montgomery, and OP Strausz. The identification of homologous series of benzo [b] thiophenes, thiophenes, thiolanes and thianes possessing a linear carbon framework in the pyrolysis oil of athabasca asphaltene. *Aostr J.Res*, 4:117–131, 1988.
- [50] Geoffrey S. Waldo, Oliver C. Mullins, James E. Penner-Hahn, and S. P. Cramer. Determination of the chemical environment of sulphur in petroleum asphaltenes by x-ray absorption spectroscopy. *Fuel*, 71(1):53–57, 1 1992.
- [51] Masoud Kasrai, G. M. Bancroft, Roger W. Brunner, Ralph G. Jonasson, James R. Brown, Kim H. Tan, and Xinghong Feng. Sulphur speciation in bitumens and asphaltenes by x-ray absorption fine structure spectroscopy. *Geochimica et Cosmochimica Acta*, 58(13):2865–2872, 1994.
- [52] Z. Frakman, TM Ignasiak, EM Lown, and OP Strausz. Oxygen compounds in athabasca asphaltene. *Energy and Fuels*, 4(3):263–270, 1990.
- [53] Teresa Ignasiak, Otto P. Strausz, and Douglas S. Montgomery. Oxygen distribution and hydrogen bonding in athabasca asphaltene. *Fuel*, 56(4):359–365, 10 1977.
- [54] Sudipa Mitra-Kirtley, Oliver C. Mullins, Jan Van Elp, Simon J. George, Jie Chen, and Stephen P. Cramer. Determination of the nitrogen chemical structures in petroleum asphaltenes using xanes spectroscopy. *Journal of the American Chemical Society*, 115(1):252–258, 1993.
- [55] TF Yen, LJ Boucher, JP Dickie, EC Tynan, and GB Vaughan. Vanadium complexes and porphyrins in asphaltenes. *J.Inst.Petrol*, 55(542):87–99, 1969.
- [56] JT Miller, RB Fisher, AMJ Van der Eerden, and DC Koningsberger. Structural determination by xafs spectroscopy of non-porphyrin nickel and vanadium in maya residuum, hydrocracked residuum, and toluene-insoluble solid. *Energy and Fuels*, 13(3):719–727, 1999.

- [57] C. D. Pearson and John B. Green. Comparison of processing characteristics of mayan and wilmington heavy residues: 2. characterization of vanadium and nickel complexes in acid-base-neutral fractions. *Fuel*, 68(4):465–474, 1989.
- [58] Pacific SFA. Sfa pacific gasification database. Technical report, Mountain View: SFA Pacific Inc., 2001.
- [59] Gnter Bauer, Volker Gther, Hans Hess, Andreas Otto, Oskar Roidl, Heinz Roller, and S. Sattelberger. Vanadium and vanadium compounds. *Ullmans Encyclopedia of Industrial Chemistry*, 1996.
- [60] Werner Soyez. Slag-related risks in partial oxidation plants. In *AIChE Ammonia Safety Symposium, Denver*, 1988.
- [61] MS Crowley. Hydrogen-silica reactions in refractories. *AMERICAN CERAMIC SOCIETY BULLETIN*, 46(7):679–, 1967.
- [62] Masami Ashizawa, Saburo Hara, Kazuhiro Kidoguchi, and Jun Inumaru. Gasification characteristics of extra-heavy oil in a research-scale gasifier. *Energy*, 30(1112):2194–2205, 0 2005.
- [63] Edward Furimsky. Gasification reactivities of cokes derived from athabasca bitumen. *Fuel Processing Technology*, 11(2):167–182, 10 1985.
- [64] A. P. Watkinson, Gordon Cheng, and David P. C. Fung. Gasification of oil sand coke. *Fuel*, 68(1):4–10, 1 1989.
- [65] D. Scott and A. Carpenter. Advanced power systems and coal quality. In *Fuel and Energy Abstracts*, volume 37. Elsevier Science, 1996.
- [66] K. Chung, L. Janke, R. Dureau, and E. Furimsky. Leachability of cokes from syncrude stockpiles. *Environmental Science and Engineering*, pages 50–53, 1996.

- [67] A. Palmer and E. Furimsky. Steam gasification of balmer coal in the presence of lignite ash. *Fuel science and technology international*, 4(4):433–446, 1986.
- [68] S. Nourouzi-Lavasani, F. Larachi, and M. Benali. Energy and hydrogen co-production from (athabasca bitumen) coke gasification with co2 capture. *Industrial and Engineering Chemistry Research*, 47(18):7118–7129, 2008.
- [69] Arash Karimi, Natalia Semagina, and Murray R. Gray. Kinetics of catalytic steam gasification of bitumen coke. *Fuel*, 90(3):1285–1291, 3 2011.
- [70] E. Cetin, B. Moghtaderi, R. Gupta, and TF Wall. Influence of pyrolysis conditions on the structure and gasification reactivity of biomass chars. *Fuel*, 83(16):2139–2150, 2004.
- [71] E. Cetin, R. Gupta, and B. Moghtaderi. Effect of pyrolysis pressure and heating rate on radiata pine char structure and apparent gasification reactivity. *Fuel*, 84(10):1328–1334, 2005.
- [72] Liming Lu, Chunhua Kong, Veena Sahajwalla, and David Harris. Char structural ordering during pyrolysis and combustion and its influence on char reactivity. *Fuel*, 81(9):1215–1225, 2002.
- [73] Liming Lu, Veena Sahajwalla, and David Harris. Characteristics of chars prepared from various pulverized coals at different temperatures using drop-tube furnace. *Energy and Fuels*, 14(4):869–876, 2000.
- [74] Shou-Yu Zhang, Jun-Fu Lu, Jian-Sheng Zhang, and Guang-Xi Yue. Effect of pyrolysis intensity on the reactivity of coal char. *Energy and Fuels*, 22(5):3213–3221, 2008.
- [75] NR Laine, FJ Vastola, and PL Walker Jr. The importance of active surface area in the carbon-oxygen reaction1, 2. *The Journal of physical chemistry*, 67(10):2030–2034, 1963.

- [76] Ljubia R. Radovi, Philip L. Walker Jr, and Robert G. Jenkins. Importance of carbon active sites in the gasification of coal chars. *Fuel*, 62(7):849–856, 1983.
- [77] Anthony A. Lizzio, Hong Jiang, and Ljubisa R. Radovic. On the kinetics of carbon (char) gasification: reconciling models with experiments. *Carbon*, 28(1):7–19, 1990.
- [78] Tadafumi Adschiri and Takehiko Furusawa. Relation between CO_2 -reactivity of coal char and bet surface area. *Fuel*, 65(7):927–931, 1986.
- [79] M. R. Khan. Significance of char active surface area for appraising the reactivity of low-and high-temperature chars. *Fuel*, 66(12):1626–1634, 1987.
- [80] M. Guerrero, M. P. Ruiz, M. U. Alzueta, R. Bilbao, and A. Millera. Pyrolysis of eucalyptus at different heating rates: studies of char characterization and oxidative reactivity. *Journal of Analytical and Applied Pyrolysis*, 74(12):307–314, 8 2005.
- [81] P Ollero, A Serrera, R Arjona, and S Alcantarilla. The CO_2 gasification kinetics of olive residue. *Biomass and Bioenergy*, 24(2):151–161, 2003.
- [82] Jong Min Lee, Yong Jeon Kim, Woon Jae Lee, and Sang Done Kim. Coal-gasification kinetics derived from pyrolysis in a fluidized-bed reactor. *Energy*, 23(6):475–488, 1998.
- [83] Robert H Hurt and Joseph M Calo. Semi-global intrinsic kinetics for char combustion modeling. *Combustion and flame*, 125(3):1138–1149, 2001.
- [84] Alexander Tremel. *Reaction Kinetics of Solid Fuels during Entrained Flow Gasification*. PhD thesis, Technische Universität München, 2012.
- [85] Normand M Laurendeau. Heterogeneous kinetics of coal char gasification and combustion. *Progress in energy and combustion science*, 4(4):221–270, 1978.

- [86] Speros E. Moschopedis, Sat Parkash, and James G. Speight. Thermal decomposition of asphaltenes. *Fuel*, 57(7):431–434, 7 1978.
- [87] I. Rubinstein, C. Spyckerelle, and O. P. Strausz. Pyrolysis of asphaltenes: a source of geochemical information. *Geochimica et Cosmochimica Acta*, 43(1):1–6, 1 1979.
- [88] F. Behar and R. Pelet. Characterization of asphaltenes by pyrolysis and chromatography. *Journal of Analytical and Applied Pyrolysis*, 7(12):121–135, 11 1984.
- [89] Phillip E. Savage, Michael T. Klein, and Simon G. Kukes. Asphaltene reaction pathways. 1. thermolysis. *Industrial and Engineering Chemistry Process Design and Development*, 24(4):1169–1174, 1985.
- [90] V. Calemma and R. Rausa. Thermal decomposition behaviour and structural characteristics of asphaltenes. *Journal of Analytical and Applied Pyrolysis*, 40(4):569–584, 5 1997.
- [91] Farshid Vejahati. *Entrained Flow Gasification of Oil Sand Coke*. PhD thesis, University of Alberta, 2012.
- [92] American Society for Testing and Standard Materials (ASTM). D7582-12. *Standard Test Methods for Proximate Analysis of Coal and Coke by Macro Thermogravimetric Analysis*, 2012.
- [93] ASTM International. Astm e1641-07: Standard test method for decomposition kinetics by thermogravimetry. 2007.
- [94] Glen Brons and Jimmy M. Yu. Solvent deasphalting effects on whole cold lake bitumen. *Energy and Fuels*, 9(4):641–647, 1995.
- [95] J. G. Speight. Thermal cracking of athabasca bitumen, athabasca asphaltenes, and athabasca deasphalted heavy oil. *Fuel*, 49(2):134–145, 4 1970.

- [96] Aprameya Ambalae, Nader Mahinpey, and Norman Freitag. Thermogravimetric studies on pyrolysis and combustion behavior of a heavy oil and its asphaltenes. *Energy and Fuels*, 20(2):560–565, 2006.
- [97] I. Rubinstein and O. P. Strausz. Thermal treatment of the athabasca oil sand bitumen and its component parts. *Geochimica et Cosmochimica Acta*, 43(12):1887–1893, 12 1979.
- [98] Jon Gibbins-Matham and Rafael Kandiyoti. Coal pyrolysis yields from fast and slow heating in a wire-mesh apparatus with a gas sweep. *Energy and Fuels*, 2(4):505–511, 1988.
- [99] F. Mermoud, S. Salvador, L. Van de Steene, and F. Golfier. Influence of the pyrolysis heating rate on the steam gasification rate of large wood char particles. *Fuel*, 85(10):1473–1482, 2006.
- [100] Ozlem Onay and O. M. Kockar. Slow, fast and flash pyrolysis of rapeseed. *Renewable Energy*, 28(15):2417–2433, 2003.
- [101] Ozlem Onay. Influence of pyrolysis temperature and heating rate on the production of bio-oil and char from safflower seed by pyrolysis, using a well-swept fixed-bed reactor. *Fuel Processing Technology*, 88(5):523–531, 5 2007.
- [102] Norman B. Colthup, Lawrence H. Daly, and Stephen E. Wiberley. *Introduction to infrared and Raman spectroscopy*. Elsevier, 1990.
- [103] Bertram E. Warren. *X-ray Diffraction*. Courier Dover Publications, 1969.
- [104] J. Biscoe and BE Warren. An xray study of carbon black. *Journal of Applied Physics*, 13(6):364–371, 2004.
- [105] L. Lu, V. Sahajwalla, C. Kong, and D. Harris. Quantitative x-ray diffraction analysis and its application to various coals. *Carbon*, 39(12):1821–1833, 2001.

- [106] Jinggeng Zhao, Liuxiang Yang, Fengying Li, Richeng Yu, and Changqing Jin. Structural evolution in the graphitization process of activated carbon by high-pressure sintering. *Carbon*, 47(3):744–751, 2009.
- [107] Osvalda Senneca, Piero Salatino, and Sabato Masi. Microstructural changes and loss of gasification reactivity of chars upon heat treatment. *Fuel*, 77(13):1483–1493, 1998.
- [108] O. Senneca, P. Russo, P. Salatino, and S. Masi. The relevance of thermal annealing to the evolution of coal char gasification reactivity. *Carbon*, 35(1):141–151, 1997.
- [109] Jianglong Yu, John A. Lucas, and Terry F. Wall. Formation of the structure of chars during devolatilization of pulverized coal and its thermoproperties: a review. *Progress in energy and combustion science*, 33(2):135–170, 2007.
- [110] N. Bomo, J. Lahaye, G. Prado, and G. Claus. Formation of cenospheres during pyrolysis of residual fuel oils. *Symposium (International) on Combustion*, 20(1):903–911, 1985.
- [111] Ramesh K. Sharma, Jan B. Wooten, Vicki L. Baliga, Xuehao Lin, W. Geoffrey Chan, and Mohammad R. Hajaligol. Characterization of chars from pyrolysis of lignin. *Fuel*, 83(11):1469–1482, 2004.
- [112] EM Suuberg. *Thermally induced changes in reactivity of carbons*, pages 269–305. Fundamental issues in control of carbon gasification reactivity. Springer, 1991.
- [113] H-Y Cai, A. Megaritis, R. Messenbck, M. Dix, DR Dugwell, and R. Kandiyoti. Pyrolysis of coal maceral concentrates under pf-combustion conditions (i): changes in volatile release and char combustibility as a function of rank. *Fuel*, 77(12):1273–1282, 1998.
- [114] RH Hurt, AF Sarofim, and JP Longwell. Role of microporous surface area in uncatalyzed carbon gasification. *Energy and Fuels*, 5(2):290–299, 1991.

- [115] Behnam Berahman. A preliminary study on pyrolysis and gasification of asphaltenes and coal-asphaltene slurry in entrained flow reactor. Master's thesis, University of Alberta, 2012.
- [116] AB Comsol. Particle tracing module users guide. *Version: May*, 2013.
- [117] Ronald W Breault. Gasification processes old and new: a basic review of the major technologies. *Energies*, 3(2):216–240, 2010.

Appendix

A-1 Mathematical modeling of the DTF

A-1.1 Steady state temperature and velocity profile of the DTF

Nominal residence time of asphaltenes in the drop tube furnace was estimated assuming complete entrainment and ideal gas law. It is speculated that, most of the asphaltenes are pyrolyzed in the initial section (topmost section) of the drop tube furnace. The density and nominal diameter of the pyrolyzed particles could vary significantly based on the extent of pyrolysis. This makes accurate estimation of residence time, quite challenging. In order to obtain a preliminary estimation of the variation in residence time, a mathematical model of the drop tube furnace was formulated using COMSOL Multiphysics® Version 4.3b. 2 Dimensional axisymmetric model of the drop tube was prepared with dimensions similar to the original

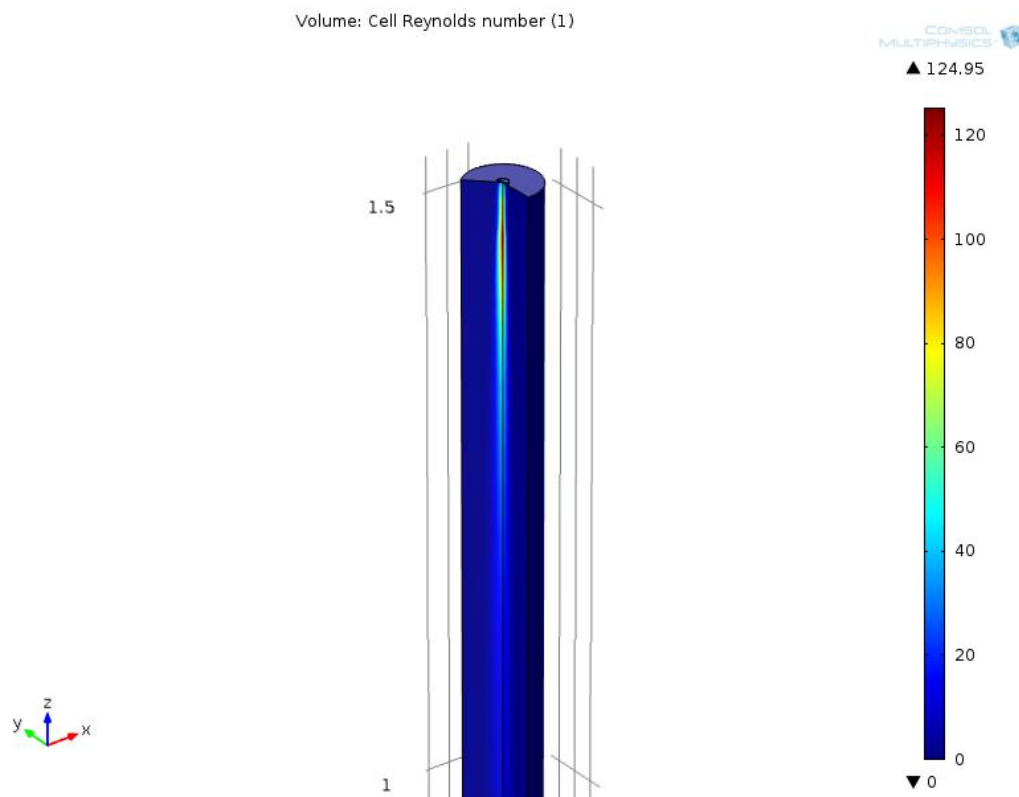


Figure A-1: Reynolds number for 7 SLPM flow of nitrogen and wall temperature of 1200°C in the DTF

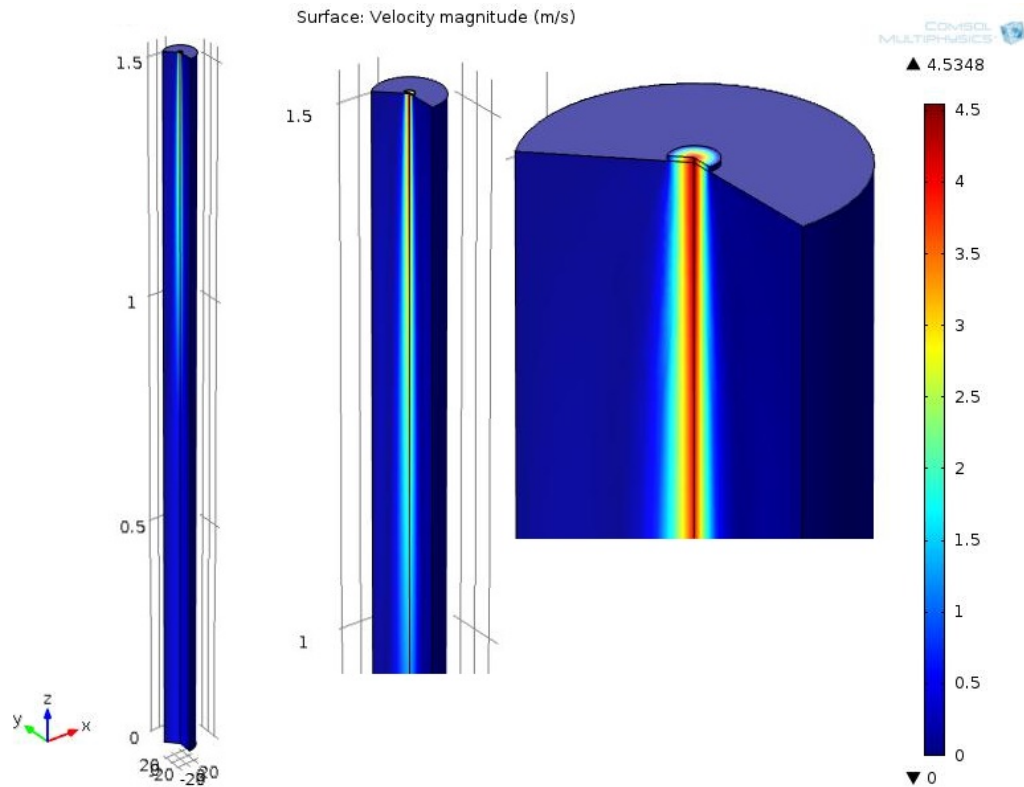


Figure A-2: Steady state velocity profile for 7 SLPM flow of nitrogen and wall temperature of 1200°C in the DTF

experimental setup. The entire DTF model including the nozzle was meshed using physics controlled triangular mesh. Using materials browser, nitrogen was added to the entire model. A volumetric flow of 7 SLPM of nitrogen was specified at the inlet of the nozzle. Temperatures of the inlet and DTF wall were set at 298.15 K and 1473.15 K (1200°C) respectively. A slight vacuum (0.01 atm) was applied to the outlet of the drop tube. A stationary, steady state single phase laminar flow model with heat transfer in fluids was considered for modeling the velocity and temperature profiles of the DTF. Values of Reynolds number (Re) obtained from the flow model confirm that the flow is laminar (Fig. A-1). It can be seen from Fig. A-1 that the maximum value of Re occurs, just after the nozzle. The velocity profile (Fig. A-2) shows that maximum gas flow velocity of 4.5 m/s is attained just after the nozzle. Temperature profile of the DTF is shown in Fig. A-3.

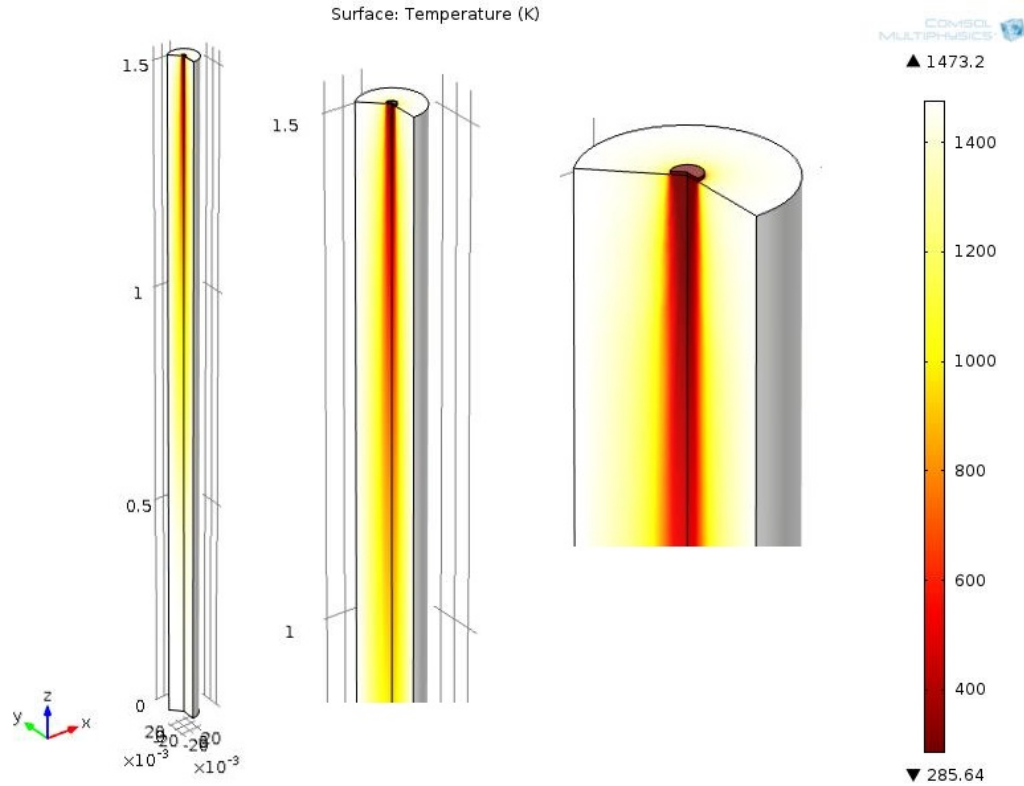


Figure A-3: Steady state temperature profile for 7 SLPM flow of nitrogen and wall temperature of 1200°C in the DTF

A-1.2 Estimation of residence time of particles in the DTF

Particle tracing module of COMSOL Multiphysics® was used to trace the path of flow of particles in the drop tube. The influence of *drag forces*, *gravity forces* and *thermophoretic forces* on the particles was considered. The total force on a particle can be represented by Eqn. A-1 [116].

$$\frac{d}{dt}(mv) = F_D + F_G + F_{Ext} \quad (\text{A-1})$$

Where m is the mass of the particle, v is the velocity of the particle, F_D is the drag force acting on the particle, F_G is the gravitational force and F_{Ext} is any other force like thermophoretic force, Brownian force etc. acting on the particle. The drag force, F_D can be expanded into Eqn. A-2, where τ represents the velocity response time for the particle and u represents the velocity of the fluid. [116]

$$F_D = \frac{1}{\tau}m(u - v) \quad (\text{A-2})$$

Stokes law is not applicable for particles with Reynolds number (relative value) greater than 1. Schiller-Naumann method is applicable in such cases. According to Schiller-Naumann method, the velocity response time for the particle can be represented as Eqn. A-3. [116]

$$\tau = \frac{4\rho_p d^2}{3\mu C_D Re} \quad (\text{A-3})$$

$$C_D = \frac{24}{Re}(1 + 0.15Re^{0.637}) \quad (\text{A-4})$$

$$Re = \frac{\rho[u - v]d}{\mu} \quad (\text{A-5})$$

In the above equations ρ_p is the density of the particle, ρ is the density of the fluid, Re is the relative Reynolds number, μ is the viscosity of the fluid and d is the diameter of the particle. The gravity force, F_G can be expanded into Eqn. A-6, where g is the acceleration due to gravity. [116]

$$F_G = mg \frac{\rho_p - \rho}{\rho_p} \quad (\text{A-6})$$

Thermophoretic force results due to temperature gradient in the fluid. Due to thermophoretic forces, particles tend to move from hotter to colder regions. It can be represented as Eqn. A-7, where k_f and k_p are the thermal conductivities of the fluid and particle respectively. C is a constant with value equal to 1.17. [116]

$$F_{Ext} = \frac{6\pi d \mu^2 C (k_f/k_p) \nabla T}{\rho(2(k_f/k_p) + 1)T} \quad (\text{A-7})$$

The significance of particle size and density in deciding the residence time can be realized from equations described above. Velocity field and other properties

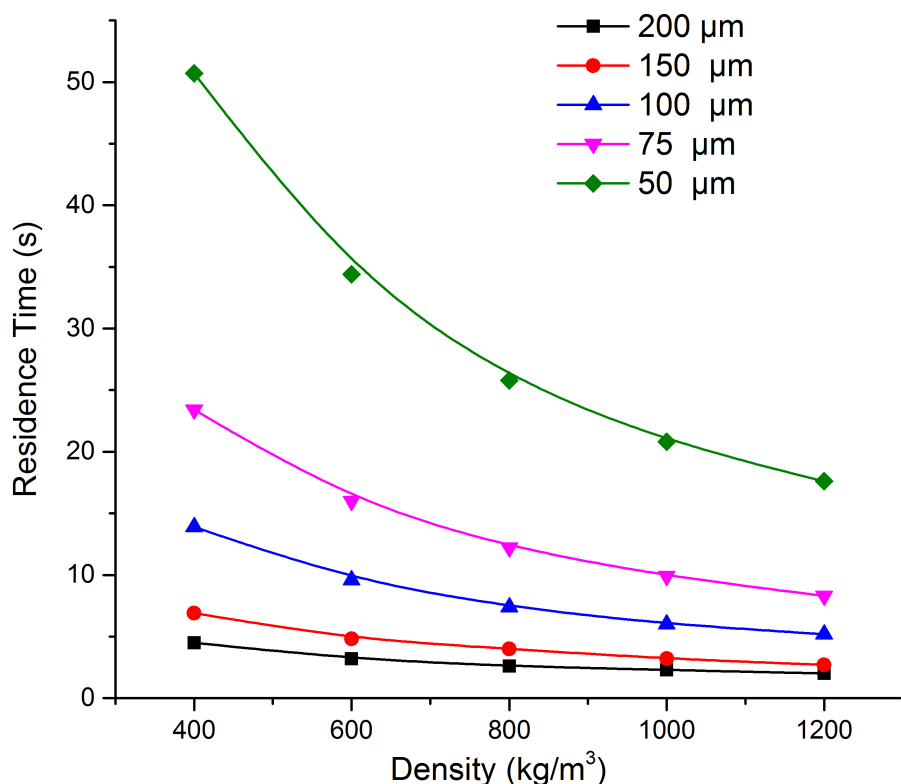


Figure A-4: Variation of residence time with particle size and density for 7 SLPM flow of nitrogen and 1200°C temperature in the DTF

estimated for 7 SLPM flow of nitrogen and 1200°C wall temperature, were considered for the background fluid. Particles were released at intervals of 0.1 s. The value of turbulent kinetic energy was retained as 0. In absence of accurate thermal conductivity data for intermediate products, the default value of particle thermal conductivity viz. 1 W/m-K was retained. Moreover, production of gaseous components during pyrolysis was neglected. Subsequently, particle size and particle density values were varied and the time required by the particles to completely traverse the length of the tube was estimated. The variation of residence time with particle size and density for 7 SLPM flow of nitrogen and 1200°C wall temperature in the DTF has been plotted in Fig. A-4. Particles larger than 200 μm have residence times lower than 8 s even at very low densities of 200kg/m³. Particles less than 75 μm tend to have much longer residence times and show much greater variation with decrease in particle density. The existing model can be used to predict



Figure A-5: Experimental setup for calibrating the DTF

the residence times for different wall temperatures, as well. In actual condition particles tend to have a decreasing density and particle size as they traverse the length of the DTF. Therefore, particles should require longer times in order to traverse the bottom section of the drop tube.

A-2 Calibration of the drop tube furnace

A 1/4 inch type K thermocouple (Super OMEGACLAD XL probe) calibrated for 600, 800 and 1250 °C was used to calibrate the drop tube furnace (DTF). Different lengths were marked on the thermocouple, and a circular disc (made of alumina clay) was fixed near the end of the probe, so as to prevent any contact with the DTF wall. Co-current flow of air was maintained during the calibration, using vacuum pumps. The DTF was calibrated for set temperatures of 800°C and 1000°C. The experimental setup for calibration has been shown in Fig. A-5. Variation of tem-

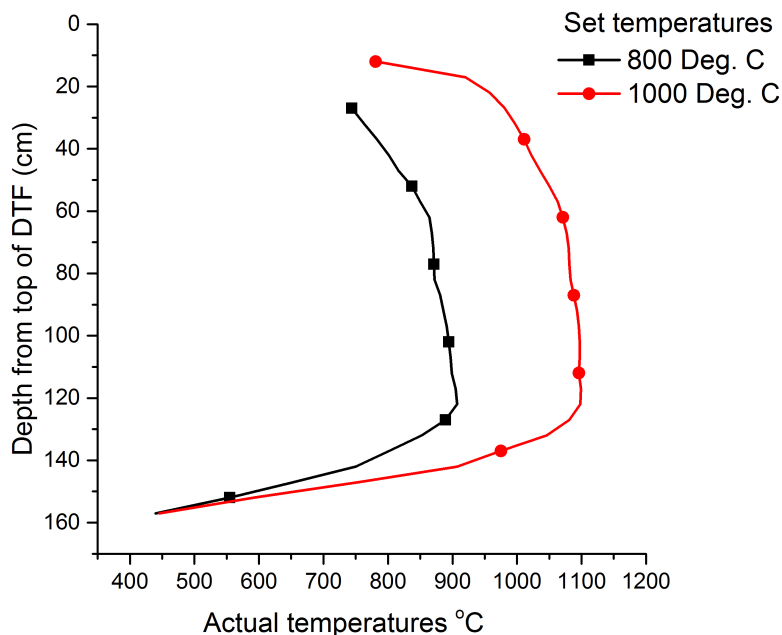


Figure A-6: Variation of temperature along the length of the DTF

perature along the length of the tube is shown in Fig. A-6.

A-3 Additional Experiments

A-3.1 Preliminary study on the effect of feed size on char quality

Asphaltenes were pulverized and sieved to particle sizes of $<53 \mu\text{m}$, $53\text{-}106 \mu\text{m}$, $106\text{-}150 \mu\text{m}$ and $150\text{-}212 \mu\text{m}$. Chars were prepared using the experimental procedure described in earlier sections. All the experiments were conducted at $1200 \text{ }^\circ\text{C}$ nominal temperature and nominal residence time of 8.4s. Fig. A-7 shows the SEM images of chars prepared from varying feed sizes of asphaltenes. Nominal size of chars obtained from finer sized asphaltenes feed, tends to be lower, however the variation is not significant. Volatile matter content of chars (Fig. A-8) did not vary significantly with variation in size of feed particles. Feed size of $150\text{-}212 \mu\text{m}$ was selected for most of the experiments based on standard feed size data for entrained

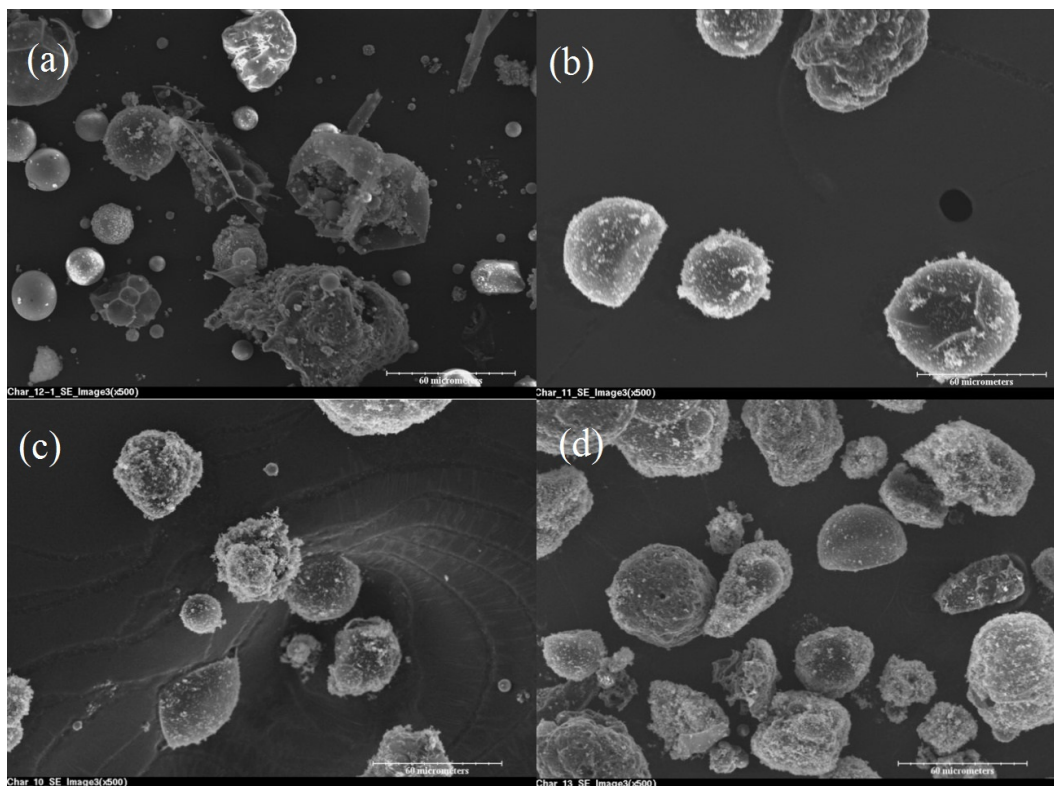


Figure A-7: Secondary electron SEM image of asphaltenes chars prepared with different feed sizes at 500X magnification a) $<53 \mu\text{m}$ b) $53-106 \mu\text{m}$ c) $106-150 \mu\text{m}$ and d) $150-212 \mu\text{m}$

flow gasification of solid fuels described in literature [10, 117].

A-3.2 Test for repeatability

Asphaltenes were pulverized and sieved to cut sizes between 106 and $150 \mu\text{m}$. Chars were prepared using the experimental procedure described in earlier sections. Three sets of experiments were conducted at $1200 \text{ }^\circ\text{C}$ nominal temperature and nominal residence time of 8.4s . Yield of chars from each experiment was found to be around 25% confirming repeatability (Table. A-1). SEM images of chars also confirmed the similarity in structure.

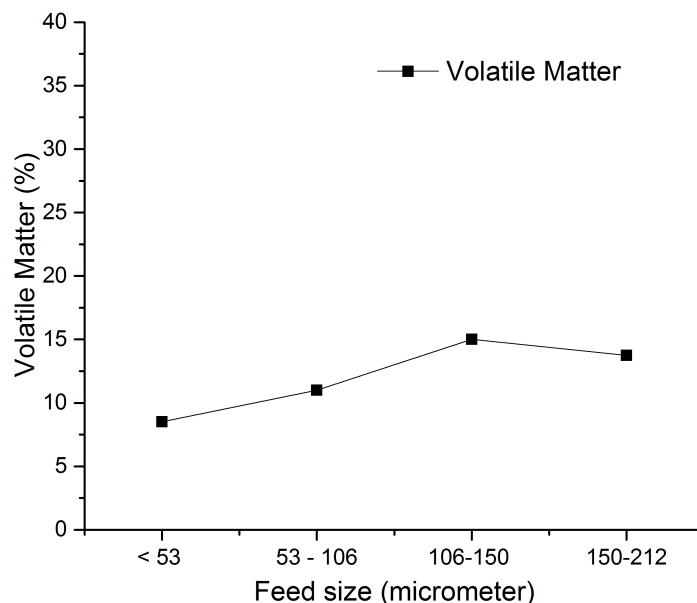


Figure A-8: Percentage of volatile matter in chars obtained from different feed sizes of asphaltenes

Table A-1: Test for repeatability

Experiment Serial No.	% Yield
1	24.83
2	23.35
3	25.02

A-3.3 Preliminary studies on char surface area and particle size distribution

Surface area of chars was estimated using N₂ BET (Brunauer-Emmett-Teller) experiments conducted in Quantachrome Autosorb IQ. About 160 mg of chars sample was outgassed at 200°C for 15 hours. The bath temperature was controlled at 77.35 K by filling liquid nitrogen in the Dewar flask. Analysis was performed at different values of relative pressure. Estimation of data for single points required appreciably longer times than conventional zeolite samples. (Fig. A-9) shows a typical adsorption isotherm generated for 1400°C chars. Negative values of adsorbed nitrogen were reported at lower relative pressures. Similarly, negative values were also

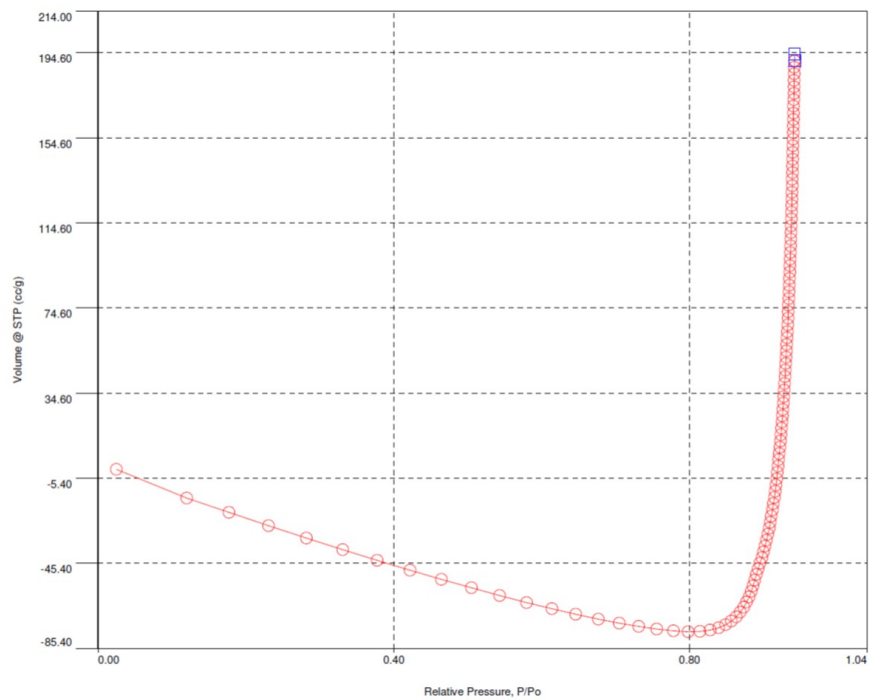


Figure A-9: N₂ adsorption isotherm for 1400°C char

Table A-2: Pore diameter of char samples using low pressure mercury porosimetry

Char Sample	Pore diameter (μm)
800°C Char	63
1000 °C Char	35
1200 °C Char	5
1400 °C Char	10

reported for other chars outgassed for 8 hours. Evolution of lighter components during adsorption could be one of the possible causes behind this observation. In the future, experiments would be conducted with prolonged outgassing times and with CO₂, instead of N₂. Char porosity measurements were also conducted using a Quantachrome Poremaster mercury porosimeter in low pressure mode. Table. A-2 shows the estimated pore diameter of chars, with a variation in operating temperature of the DTF. A decrease in pore diameter was observed, with an increase in operating temperature. However, the results could not explain the hollow cenospheric structure of chars. Estimation of particle size distribution of chars using Malvern Mastersizer 3000E, could not yield any result, as char particles were extremely light and floated on the surface of deionized water, preventing proper circulation.